

TECHNISCHE UNIVERSITÄT MÜNCHEN

Lehrstuhl für Technische Chemie II

SYNTHESIS AND APPLICATION OF SOLID BASE CATALYSTS

Manuela C. I. Bezen

Vollständiger Ausdruck der von der Fakultät für Chemie der Technischen Universität
München zur Erlangung des akademischen Grades eines
Doktors der Naturwissenschaften (Dr.rer.nat.)
genehmigten Dissertation.

Vorsitzender:

Univ.-Prof. Dr. K.-O. Hinrichsen

Prüfer der Dissertation:

1. Univ.-Prof. Dr. J. A. Lercher

2. Univ.-Prof. Dr. K Köhler

Die Dissertation wurde am 02.06.2010 bei der technischen Universität München
eingereicht und durch die Fakultät für Chemie am 21.09.2010 angenommen.

„Ein Optimist ist ein Mensch, der ein Dutzend Austern bestellt, in der Hoffnung, sie mit der Perle, die er darin findet, bezahlen zu können.“

(Theodor Fontane, 1819 - 1898)

Acknowledgements

Finally after three and a half years, I get the chance to thank all the people supporting me and being on my side during the time doing my PhD, what was for sure not always easy (for me and them).

First, I want to thank you Johannes for giving me the opportunity to work on a very interesting, diversified and challenging topic. Thank you for having always nice advices and helping ideas when I was struggling (not only with my work but also with myself). I want to thank you for giving me the opportunity to manage an own industrial project, which gave me a lot of experience and pleased me a lot, travel and present my research during national and international conferences.

I want to express my gratitude to PD Thomas Müller (supervising me in the 1st year of my project), PD Cornelia Bretkopf (supervising me in the last year of my PhD) and PD Andreas Jentys who helped me during the whole time with any question (especially on IR-spectroscopy) I had and always made sure that I learn something from our talks. Especially I want to thank you Conny for supporting me during good and bad times, helping me writing the thesis and publications and motivating me to finish the thesis. For the latter part I also want to thank you Andy.

The author gratefully thanks Dr. Hans-Christian Rath, Dr. Thomas Kruppa and Dr. Thorsten Löhl for fruitful discussions during the cooperation in the first two years of my PhD thesis. I want thank you Mr. Hermann for caring out and analyzing the ethoxylation reactions.

I want to thank all my nice colleagues, especially Richard Knapp, Tobias Förster, Ana Hrabar, Monica Pop, Sonja Wyrzgol, Daniela Hartmann, Yanzhe Yu and Chen Zao for a memorable and great time.

Thank you Xaver (Hecht) measuring N₂-chemisorptions and doing everything making my setups running, Andreas (Marx), making my computer and electronics working, Martin (Neukamm) for AAS measurements and organization for chemicals.

Thank you Helen (Lemmermöhle) for making sure that our personally and financial stuff is fine, Steffi (Meier) for making impossible appointments with Johannes

possible and Katharina (Thies) doing all organisations, because without you great ladies nothing will be running.

Last but not least I want to mention and give very lot of thanks to my husband, parents, brothers and my grandfather as well as to my friends always supporting me, not only during the time of my PhD thesis, but also during my whole life. Thanks to them that they are so proud of me and give me always new motivation for going on and doing my way on my best.

List of Abbreviations

[A]	Concentration of substance A
AAS	Atomic absorption spectroscopy
aq.	Aqueous
B	Magnetic field
BET	Brunauer-Emmet-Teller
°C	Degree Celsius
c	Concentration
cm ⁻¹	Wavenumbers
cm ³	Cubic centimeter
E _a	Activation energy
F _{He}	Helium-flow
FHWHM	Full width at half maximum
FID	Flame ionization detector
g	Gramm
g _l	Nuclear gravimetric factor
GC	Gas chromatography
h	Hour
H _B	Full width at half maximum
IR	Infrared spectroscopy
K	Kelvin (273.15 K = 0 °C)
k _(i)	Rate constant of substance i
k ₀	Pre-exponential factor
M	1 Molar
MAS	Magic angle spinning
MS	Mass spectrometry
MFC	Mass flow controller
m ²	Square meter
mA	Milliampere
mL	Milliliter
mbar	Millibar

mm	Millimeter
m	Milli (10^{-3})
min	Minute
mol	Mol
n_A	Amount of substance A
NMR	Nuclear magnetic resonance
nm	Nano meter
pyd	pyridine
ppm	Parts per million
R	Ideal gas constant ($= 8.314\ 471(15)\ \text{J}\cdot\text{K}^{-1}\cdot\text{mol}^{-1}$)
$r_{(i)}$	Rate of formation of substance i
RT	Room temperature
S	Selectivity
s	Second
sox.	Soxhlet
T	Temperature
T_r	Temperature of reaction
T	Tesla
TEM	Transmission electron microscopy
TGA	Thermo-gravimetric analysis
TPD	Temperature programmed desorption
TPO	Temperature programmed oxidation
TOF	Turn over frequency
UV	Ultra violet
wt.-%	Weight percent
XRD	X-ray diffraction
XPS	X-ray photoelectron spectroscopy

Greek letters

λ	wavelength
ν_A	Stoichiometric factor of substance A
τ	Residence time
δ	Chemical shift
μ	Micro (10^{-6})
μ_N	Nuclear magnetron

Chemical compounds

AgNO_3	Silver nitrate
Al	Aluminum
Al_2O_3	Alumina
Al^{IV}	Tetrahedral aluminum
Al^{VI}	Octahedral aluminum
$\text{Al}(\text{NO}_3)_3 \cdot 9\text{H}_2\text{O}$	Aluminum nitrate nonahydrate
Au	Gold
CN	Cyanide
CO	Carbon monoxide
CeO	Ceria
$\text{CeO}(\text{CO}_3)_2 \cdot x\text{H}_2\text{O}$	Cerium carbonate hydrate
$\text{CeO}(\text{NO}_3)_2 \cdot 6\text{H}_2\text{O}$	Cerium nitrate hexahydrate
CO_2	Carbon dioxide
F	Fluorine
$\text{HAuCl}_4 \cdot 3\text{H}_2\text{O}$	Gold (III) chloride hydrate
HCN	Hydrogen cyanide
H_2O	Water
He	Helium
M	Metal
MeOH	Methanol
Mg	Magnesium

MgO	Magnesia
$\text{Mg}_6\text{Al}_2\text{CO}_3(\text{OH})_{16}\cdot\text{H}_2\text{O}$	Hydrotalcite (natural mineral)
$\text{Mg}(\text{NO}_3)_2\cdot 6\text{H}_2\text{O}$	Magnesium nitrate hexahydrate
$\text{Mg}_x(\text{Al})\text{O}$	Magnesium aluminum mixed oxide
MgZnAl	Magnesium zinc aluminum mixed oxide
MNO	Metal nitrosyl
N_2	Nitrogen
Na	Sodium
NaBH_4	Sodium borohydrate
NaHCO_3	Sodium bicarbonat
NaOH	Sodium hydroxide
NH_4F	Ammonium fluoride
NO_3	Nitrate
O_2	Oxygen
-OCH ₃	methoxy
-OCHO	formate
SiC	Silicon carbide
Zn	Zinc
ZnO	Zinc oxide
$\text{Zn}(\text{NO}_3)_2\cdot 6\text{H}_2\text{O}$	Zinc nitrate hexahydrate

CHAPTER 1 SOLID BASE CATALYSIS	1
1.1 Introduction.....	2
1.2 Conversion of propan-2-ol	4
1.2.1 Differentiation of acid and basic sites.....	4
1.2.2 Reaction mechanism	5
1.3 Kinetics of propan-2-ol conversion.....	8
1.3.1 Activity	8
1.3.2 Parallel reactions.....	9
1.4 Condensation of 1,2-epoxy-octane with hexanol	12
1.5 Scope of the thesis	13
1.6 References	15
CHAPTER 2 EXPERIMENTAL	16
2.1 Characterization techniques	17
2.2 Catalytic tests	23
2.2.1 Conversion of propan-2-ol.....	23
2.2.2 Hydrogenation of acetone	24
2.2.3 Condensation of 1,2-epoxy-octane with hexanol.....	25
2.3 References	26
CHAPTER 3 MAGNESIUM/ALUMINUM MIXED OXIDES.....	27
3.1 Introduction	28
3.2 Experimental	29
3.2.1 Preparation	29
3.2.2 Characterization techniques	31
3.2.2.1 Textural analysis	31
3.2.2.2 Infrared spectroscopy.....	31
3.2.3 Catalytic tests.....	32

3.3	Results	32
3.3.1	Textural analysis of Mg/Al mixed oxides	32
3.3.2	XRD analysis of Mg/Al mixed oxides	33
3.3.3	^{27}Al MAS-NMR spectroscopy of Mg/Al mixed oxides	36
3.3.4	Infrared spectroscopy of adsorbed pyridine on Mg/Al mixed oxides	36
3.3.5	Infrared spectroscopy of adsorbed CO_2 on Mg/Al mixed oxides	38
3.3.6	Infrared spectroscopy of adsorbed propan-2-ol on Mg/Al mixed oxides	40
3.3.7	Kinetics of propan-2-ol conversion	42
3.3.7.1	Influence of Mg/Al ratio	42
3.3.7.2	Influence of calcination temperature	44
3.3.7.3	Influence of sodium content	47
3.3.7.4	Reproducibility	49
3.4	Discussion	51
3.5	Conclusions	54
3.6	References	56
CHAPTER 4 ZINC MODIFIED MAGNESIUM/ALUMINUM MIXED OXIDES		59
4.1	Introduction	60
4.2	Experimental	61
4.2.1	Zinc modified Mg/Al mixed oxides	61
4.2.2	Characterization	62
4.2.3	Catalytic tests	64
4.3	Results	64
4.3.1	Textural analysis	64
4.3.2	XRD analysis	65
4.3.3	^{27}Al MAS-NMR spectroscopy	66
4.3.4	Acid and base properties determined by NH_3 - and CO_2 -TPD	67
4.3.5	Kinetics of elimination reactions of propan-2-ol	68
4.3.6	Application in the condensation of 1,2-epoxy-octane with hexanol	69

4.4	Discussion	70
4.5	Conclusions	73
4.6	References	74
CHAPTER 5 FLUORINE MODIFIED MAGNESIUM/ALUMINUM MIXED OXIDES ...		76
5.1	Introduction	77
5.2	Experimental	78
5.2.1	Materials	78
5.2.1.1	Mg/Al mixed oxide precursors	78
5.2.1.2	Fluorinated Mg/Al mixed oxides	79
5.2.2	Characterization	79
5.2.3	Catalytic experiments.....	80
5.3	Results	81
5.3.1	Textural analysis	81
5.3.2	XRD analysis	83
5.3.3	²⁷ Al- MAS NMR spectroscopy	85
5.3.4	¹⁹ F- MAS NMR spectroscopy of fluorine modified Mg/Al mixed oxides ...	86
5.3.5	Base properties determined by TPD of CO ₂	88
5.3.6	Kinetics of elimination reactions of propan-2-ol	89
5.3.7	Catalytic condensation of 1,2-epoxy-octane with hexanol	92
5.4	Discussion	93
5.5	Conclusions	97
5.6	References	99
CHAPTER 6 AU SUPPORTED ON CERIA		101
6.1	Introduction	102
6.2	Experimental	105
6.2.1	Preparation	105
6.2.1.1	Ceria.....	105

6.2.1.2	Ceria-urea.....	106
6.2.1.3	Au/Ceria.....	106
6.2.2	Characterization Techniques.....	107
6.2.2.1	Bulk techniques.....	107
6.2.2.2	Surface techniques	108
6.2.2.3	Infrared spectroscopy.....	108
6.2.3	Catalytic tests.....	109
6.2.3.1	Conversion of propan-2-ol.....	109
6.2.3.2	Hydrogenation of acetone.....	109
6.3	Results	110
6.3.1	Characterization	110
6.3.2	Thermal stability of urea modified and Au supported ceria	119
6.3.3	Infrared spectroscopy of adsorbed methanol	124
6.3.3.1	Ceria - influence of modification with urea and gold	124
6.3.3.2	Ceria - influence of Au deposition method	126
6.3.4	Infrared spectroscopy of adsorbed propan-2-ol	129
6.3.4.1	Adsorption of propan-2-ol on commercial ceria and modified ceria..	129
6.3.4.2	Adsorption of propan-2-ol on ceria (N100) and Au/ceria (N100)	131
6.3.5	Infrared spectroscopy of adsorbed pyridine.....	132
6.3.6	Acid-base properties determined by NH ₃ - and CO ₂ -TPD	135
6.3.6.1	Ceria and Au/ceria samples obtained by commercial ceria	136
6.3.6.2	Ceria and Au/ceria samples obtained by self-prepared ceria.....	137
6.3.6.3	Ceria and Au modified ceria via DPu and NaOH method	140
6.3.7	Conversion of propan-2-ol as catalytic test for acid-base centers	141
6.3.7.1	Influence of Au	141
6.3.7.2	Influence of activation conditions.....	143
6.3.7.3	Influence of ceria support	144
6.3.7.4	Influence of deposition-precipitation agent	146
6.3.7.5	Formation of by-products	149
6.4	Discussion.....	150

6.5	Conclusions.....	154
6.6	References.....	156
CHAPTER 7 SUMMARY		160
CURRICULUM VITAE.....		165
LIST OF PUBLICATIONS.....		166
LIST OF PRESENTATIONS.....		167

Chapter 1

Solid base catalysis

1.1 Introduction

The driving force of many chemical reactions is an acid-base exchange. Arrhenius^[1] gave a definition in 1887 and described bases as OH^- donor materials as for instance metal hydroxides. Only 46 years later Brønsted^[2] extended the definition of Arrhenius and postulated that bases are materials which have the possibility to accept H^+ . Due to the definition of Brønsted a base can be anionic or neutral. In the same year Lewis^[3] defined an aqueous independent acid base theory, wherein bases acts as electron pair donor materials.^[4]

Tanabe^[5] reviewed industrial applications of solid acid-base catalysis and was cited more than 300 times. In total 127 acid, base and acid-base bifunctional catalysts used in chemical processes were found, however, only 10 of them were base solids. Thus there is a strong demand on research of solid base materials also if the number of publications was certainly increased over the last 10 years.

Iglesia^[6] reviewed the importance of bifunctional acid-base catalysis and described the need of acid-base pairs in stabilizing intermediates in many different reactions. In general, a catalyst is denoted acidic when the first reaction step is initiated by an acid site, in contrast a base catalyzed reaction is initiated by interaction of the acidic site of the reactant with the basic site of the catalyst.^[7]

One of the latest applications of solid base materials is the use for environmental prevention and pollution by limiting noxious effects. Busca^[4] reviewed the convenient advances in solid base catalysis for industrial and environmental chemistry of commercial processes.

Table 1-1. Catalytic systems used as solid base catalysts reported by Hattori.^[7]

<i>Catalyst system</i>	<i>Example</i>
<i>Single component metal oxides</i>	Alkaline Earth oxides Alkali metal oxides Rare earth oxides Thorium oxide Zirconia Zinc oxide Titania
<i>Zeolites</i>	Alkali ion-exchanged zeolites Alkali ion-added zeolites
<i>Supported alkali metal ions</i>	on alumina on silica on alkaline earth oxide Metals and hydroxides on alumina
<i>Clay minerals</i>	Hydrotalcite Chrystolite Sepiolite
<i>Non-oxides</i>	KF supported on alumina Lanthanide imide and nitride on zeolite

Hattori^[7-9] reviewed the generation, characterization and catalytic behavior of solid base catalysts and listed 5 different types of solid materials acting as basic catalysts which are listed in Table 1-1. He explained the formation of basic sites for instance of magnesia due to calcination and the dependence of basic site types on the pre-treatment temperature. Water, CO₂ and in some cases oxygen will be removed from the surface by heating. Depending on the type of reaction different calcination temperatures are beneficial. For example, in the 1-butene isomerization a calcination temperature of already 530 °C leads to the most active catalyst, whereas the 1,3- butadiene hydrogenation owes a MgO catalyst pre-treated at high 1050 °C as most active one.^[9]

Many organic reactions in the fine chemical synthesis are base catalyzed. Examples which use heterogeneous basic catalysts are given in Figure 1-1.^[8]

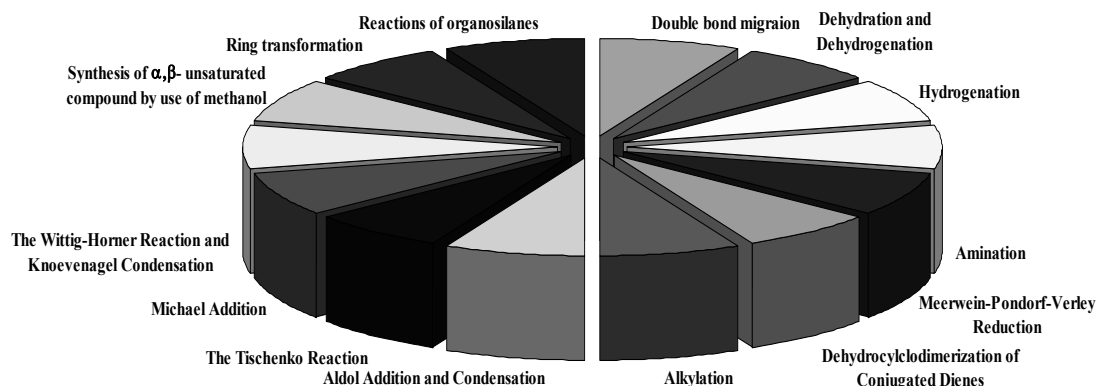


Figure 1-1. Overview of heterogeneous base catalyzed reactions given by Hattori.^[8]

1.2 Conversion of propan-2-ol

1.2.1 Differentiation of acid and basic sites

The conversion of propan-2-ol is well known as test reaction to determine acidic and basic properties of materials in heterogeneous catalysis.^[10] Characteristic main products are acetone and propene. Nevertheless, the detailed reaction mechanism of acetone and propene as well as di-*iso*-propylether formation is still under discussion. An overview of reaction pathways was given by Gervasini et. al.^[11] According to this, propan-2-ol is converted to propene by dehydration. Dehydrogenation of propan-2-ol generates acetone. By condensation of two alcohol molecules di-*iso*-propylether occurs. Depending on constitution and strength of active sites, several elimination reactions are discussed. For instance an E₁-, E_{1cb}- or an E₂- mechanism. The E₁-mechanism is described as a uni-molecular reaction.^[12] A detailed discussion for the formation of acetone, propene and di-*iso*-propylether over various active sites on oxidic surfaces is given in the next section.

1.2.2 Reaction mechanism

Depending on the kind and distribution of acid-base sites, there are different reaction mechanisms described in literature by different authors, which will be explained more detailed in the following part.

The formation of acetone described by Waugh^[13] (Figure 1-2) can be classified as an E_{1cb} -mechanism. The reaction is induced by very strong basic sites such as oxygen atoms in the oxide or mixed metal oxide lattice. In the first reaction step a proton is separated from the OH-group of the alcohol molecule and adsorbed on a surface oxygen atom. In the second step, α -hydrogen elimination of the alkoxide intermediate follows and leads to acetone and hydrogen.

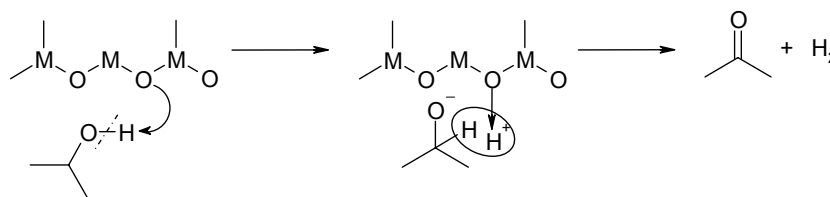


Figure 1-2. Formation of acetone over strong basic sites via an E_{1cb} -mechanism.

Propene is formed on strong Lewis-acidic sites via an E_1 -mechanism. The oxygen atom of the alcohol molecule adsorbs on the metal site of the mixed oxide catalyst surface and a secondary carbenium ion is formed. Due to the β -hydrogen elimination of the carbenium ion, propene and water are formed. This mechanism was established by Noller^[14] (Figure 1-3).

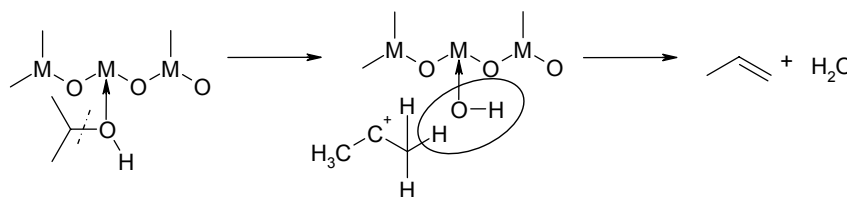


Figure 1-3. Formation of propene over Lewis-acidic sites via an E_1 -mechanism.

However, there are two other different reaction pathways which lead to propene. The first one is dehydration of propan-2-ol via an E_2 -mechanism. The alcohol molecule adsorbs on

two sites on the catalyst surface. The OH-group is adsorbed on the metal site. One of the hydrogen atoms of the methyl-groups is adsorbed on an oxygen atom of the mixed oxide. In a following step, water is split off, and simultaneously propene is formed over a concerted process (Figure 1-4).

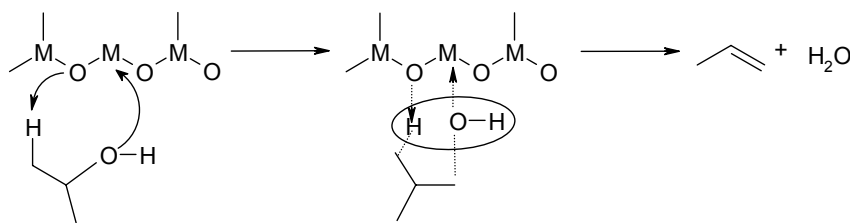


Figure 1-4. Formation of propene over acidic and basic sites via an E_2 -mechanism.

Via an E_{1cb} -mechanism, a carbanion is formed as conjugated base on very strong basic sites and a proton is split off from one of the methyl-groups. In the second step, the OH-group of the carbanion adsorbs on metal sites of the mixed oxide with weak Lewis-acid strength. Dehydration generates propene (Figure 1-5).

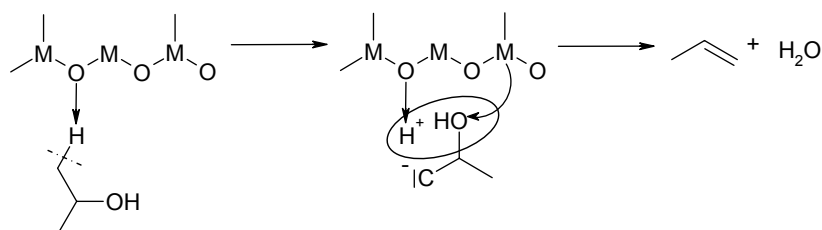


Figure 1-5. Formation of propene over basic sites and acidic sites via an E_{1cb} -mechanism.

Condensation of propan-2-ol opens a possible side reaction leading to di-*iso*-propylether. The reaction mechanism can be classified as a E_2 -elimination. In the first step, two propan-2-ol molecules are co-adsorbed on different sites of the metal oxide catalyst surface. One of the molecules adsorbs at an oxygen atom, while the other one is adsorbed at the metal site. In the second step, the condensation to di-*iso*-propylether takes place due to formation of water (Figure 1-6). The di-*iso*-propylether formation via an E_2 -mechanism is described in detail by Blaszkowski and van Santen.^[15]

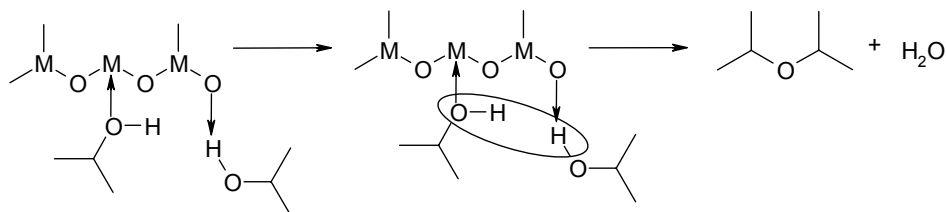


Figure 1-6. Formation of di-*iso*-propylether over acidic and basic sites via an E₂-mechanism.

In summary, there are four different types of reaction pathways depending on the strength and constitution of active surface sites given in Table 1-2.

Table 1-2. Product formation depending on strength and constitution of active surface sites

<i>Active sites</i>	<i>Mechanism</i>	<i>Intermediate</i>	<i>Product</i>
Strong basic	E _{1cb}	Alkoxide	Acetone
Strong acid	E ₁	Carbenium-ion	Propene
Acidic/(basic)	E ₂	1 adsorbed species	Propene
Acidic/(basic)	E ₂	2 adsorbed species	di- <i>iso</i> -Propylether
Strong basic/ weak acidic	E _{1cb}	Carbanion	Propene

Further the formation of propene occurs involving redox reactions after a reverse Mars van Krevelen mechanism wherein the first step includes the oxidation of the catalyst (see Figure 1-7).^[16] The last step is the reverse oxidation of the metal oxide by water.

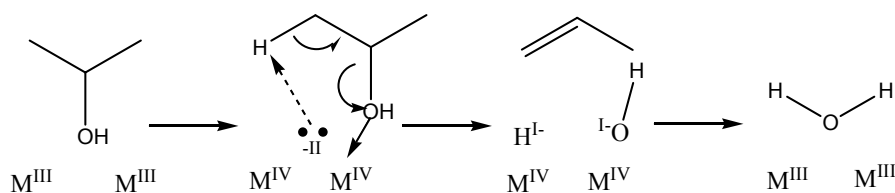


Figure 1-7. Redox model of propene formation after a reverse Mars van Krevelen mechanism.

During the conversion of propan-2-ol, various secondary products can be formed. Possible reaction pathways are described by Haffad.^[16] He explored the transformation of propan-2-ol over simple metal oxides, e.g., titania, zirconia and ceria.

The formation of C₆-alkenes occurs via different reaction pathways. They can be formed either by a cationic dimerization of propene, requiring acidic sites or starting from

the ether (di-*iso*-propylether) giving an oxonium-ion, then a carbene followed by a Wittig-type rearrangement to an alkoxide and last the desorption of C₆-alkenes occurs (Figure 1-8).

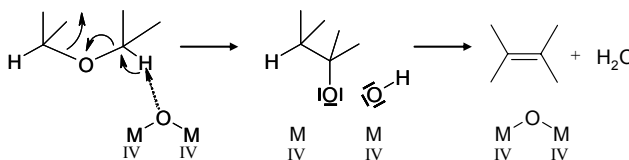


Figure 1-8. Dehydration of di-*iso*-propylether.^[16]

A third possibility is the reductive coupling of acetone, which requires strongly reduced surface sites.

C₆-Dienes occur over metal surface reduction by propene. Two propene molecules react with surface oxygen under the formation of water and C₆-diene. An oxygen vacancy remains on the oxide surface. Thus, this kind of reaction requires high oxygen mobility, which was observed for high surface area ceria.

Additionally, formation of C₆-dienes appear via reductive coupling of two acetone molecules over acid sites.

Acetone condensation over basic sites leads to *ketonic species*. In the first reaction step, an aldol is formed which is dehydrated to mesityl oxide. The latter product can be hydrogenated to *iso*-butyl-methylketone (Figure 1-9).

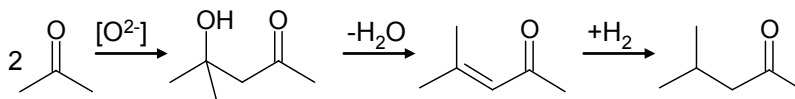


Figure 1-9. Reductive coupling of acetone followed by the formation of ketones.

1.3 Kinetics of propan-2-ol conversion

1.3.1 Activity

In general the suitability of a catalyst for a chemical process depends on its activity, selectivity and stability. The activity is determined by the reaction rate defined as

r . The rate is calculated via the concentration of the substrate, the volume or mass of the catalyst and time of reaction (Eq.1).

$$r = \frac{\text{converted amount of substrate}}{\text{volume or mass} \cdot \text{time}} (\text{mol} \cdot \text{g}^{-1} \cdot \text{s}^{-1}) \quad (1)$$

The catalytic activity can be further expressed by the activation energy E_a . The Arrhenius equation describes the temperature dependence of the rate constant for a reaction. Herein k_0 is defined as pre-exponential factor and R as gas constant (Eq. 2).

$$k = k_0 e^{-(E_a / RT)} \quad (2)$$

The specific activity for a catalytic center, e.g. a metal in supported catalysts, in a special reaction can be defined as *turn over frequency (TOF)*. The TOF is determined by the number of molecular reactions per unit time (Eq. 3).

$$TOF = \frac{\text{volumetric rate of reaction}}{\text{number of centers / volume}} (\text{time}^{-1}) \quad (3)$$

The selectivity S_P (Eq. 4) of a reaction gives the ratio of the products related to the starting material. The selectivity depends on the course and the stoichiometry of a reaction. In case of heterogeneous catalysis the interplay of size and shape of pores and products plays a crucial role, too.

$$S = \frac{n_P |v_A|}{(n_{A,0} - n_A) |v_A|} (\text{mol / mol or \%}) \quad (4)$$

1.3.2 Parallel reactions

Characteristic for parallel reaction is that the reactant A (propan-2-ol) can be converted simultaneously to the products B (propene) and C (acetone) (Figure 1-10).

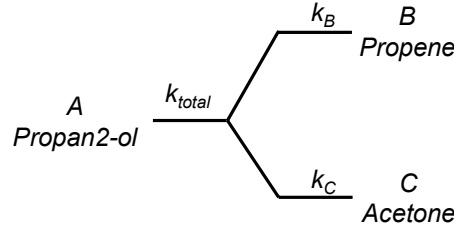


Figure 1-10. Progress of parallel reaction

The rate constant k_{total} (propan-2-ol) (Eq. 5) describes the sum of the single rate constants k_B (propene) and k_C (acetone) related to the formation of the products B and C.

$$k_{total} = k_b + k_c \quad (5)$$

For both parts of the parallel reaction scheme a first order reaction is proposed. Therefore the total rate equation for the conversion of reactant A can be expressed as in equation (Eq. 6). Due to transformation (Eq. 7) and after integration (Eq. 8), wherein A_0 is the start concentration of reactant A and τ describes the residence time, equation (9) gives the term for the total rate constant.

$$\frac{d[\text{propan} - 2 - \text{ol}]}{dt} = -k_{\text{propan-2-ol}} \cdot [\text{propan} - 2 - \text{ol}] \quad (6)$$

$$\frac{d[\text{propan} - 2 - \text{ol}]}{[\text{propan} - 2 - \text{ol}]} = -k_{\text{propan-2-ol}} \cdot dt \quad \int_{t=0}^t dt = t \quad (7)$$

$$\ln[\text{propan} - 2 - \text{ol}] - \ln[\text{propan} - 2 - \text{ol}]_0 = -k_{\text{propan-2-ol}} \cdot t \quad (8)$$

$$k_{\text{propan-2-ol}} = (k_{\text{propene}} + k_{\text{acetone}}) = -\frac{\ln \frac{[\text{propan} - 2 - \text{ol}]}{[\text{propan} - 2 - \text{ol}]_0}}{t} \quad (9)$$

With term (10) it is possible to determine the rate constant k_{total} via the residence time τ and the concentration ratio of the reactant before $[A_0]$ and after $[A]$ the reaction.

The rates of the formation of the products B (10) and C (11) are described in the following equations.

$$\frac{d[\text{propene}]}{dt} = k_{\text{propene}} \cdot [\text{propan-2-ol}] \quad (10)$$

$$\frac{d[\text{acetone}]}{dt} = k_{\text{acetone}} \cdot [\text{propan-2-ol}] \quad (11)$$

The rate constants k_B and k_C will be calculated via the ratio y (Eq. 12).

$$y = \frac{k_{\text{propene}}}{k_{\text{acetone}}} = \frac{S_{\text{propene}}}{S_{\text{acetone}}} \quad (12)$$

Therefore one will make use of the selectivity of the parallel reaction. The selectivity is defined as (Eq. 13).

$$S_{\text{propene}} = \frac{k_{\text{propene}}}{k_{\text{propene}} + k_{\text{acetone}}} \text{ and } S_{\text{acetone}} = \frac{k_{\text{acetone}}}{k_{\text{propene}} + k_{\text{acetone}}} \quad (13)$$

Due to transpose of (Eq. 9) and combination of (Eq. 12) and (13) the rate constants k_B and k_C are determined by equations (Eq. 14) and (Eq. 15).

$$k_{\text{propene}} = k_{\text{propan-2-ol}} - \frac{k_{\text{propene}}}{y} \Rightarrow k_{\text{propene}} = \frac{k_{\text{propan-2-ol}}}{(1 + \frac{1}{y})} \quad (14)$$

$$k_{\text{acetone}} = k_{\text{propan-2-ol}} - \frac{y}{k_{\text{acetone}}} \Rightarrow k_{\text{acetone}} = \frac{k_{\text{propan-2-ol}}}{(1 + y)} \quad (15)$$

1.4 Condensation of 1,2-epoxy-octane with hexanol

Reactions of epoxides occur under basic or acidic conditions. Ring opening reactions of epoxides are useful tools in organic synthesis of allylic and aliphatic compounds.^[17] However, this type of reaction can also serve as probe for application in the synthesis of ethoxylates. Ethoxylates are one of the most important nonionic surfactants and are widely used in the manufacturing of a great variety of products.^[18]

The condensation of 1,2-epoxy-octane (1) is a nucleophilic substitution wherein hexanol (2) acts as the nucleophile and attacks the epoxide which act as electrophile thus 1-hexyloxy)decan-2-ol (3) is formed (see Figure 1-11).

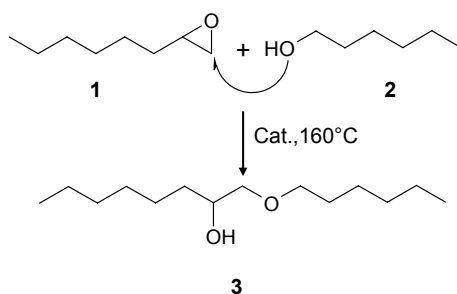


Figure 1-11. Reaction scheme of the nucleophilic ring-opening reaction of 1,2-epoxyoctane with hexanol.

The reaction mechanism adopted from Hama^[19] regarding the synthesis of ethoxylates over metal oxides shown in Figure 1-13 is suggested for the condensation of epoxides with alcohols.

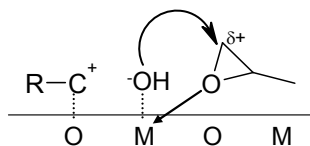


Figure 1-12. Suggested reaction mechanism of ring opening epoxide condensation with alcohol over metal oxide catalysts.

An undesired side reaction is the ring opening reaction of 1,2-epoxy-octane forming 1,2-decan-diol (4) by hydrolysis (4).

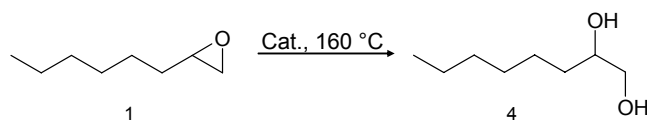


Figure 1-13. Reaction scheme of the ring opening hydrolysis of 1,2-epoxy-octane.

1.5 Scope of the thesis

There is a great demand for developing solid base materials such as hydrotalcites and their derived mixed metal oxides as economical and environmental friendly catalysts. In this study, the influence of Mg/Al ratio on acid base properties of mixed metal oxides, the influence of sodium content of Mg/Al oxides obtained by different synthesis methods on catalytic performance as well as the optimal calcination temperature of Mg/Al hydrotalcites have been investigated to optimize activity and selectivity.

Further, hydrotalcite and Mg/Al mixed oxide derived from layered double hydroxide (LDH) precursors were modified with fluorine and zinc in order to enhance the basic properties. Fluorine was induced into the hydrotalcite framework or the mixed metal oxide via treatment with an aqueous NH_4F solution. Zinc was incorporated during the sol gel process. The structure of the precursors and the modified materials were analyzed by XRD, ^{27}Al - and ^{19}F -MAS NMR. The acid and base site properties of hydrotalcite, the Mg/Al mixed oxide and the modified samples were determined via NH_3 - and CO_2 -TPD. While the concentration of acidic sites was enhanced by the modification with fluorine, the basic site concentration was less influenced. However, the strength of basic sites was increased by the modification with fluorine. Conversion of propan-2-ol was performed to monitor changes in acid-base site properties.

The applications of metal oxide supported Au materials in acid-base type reactions are negligible due to the generally inert nature towards this type of reaction. Thus, it would be of great interest to explore the role of nano-sized gold particles on the support acid-base properties. Au supported on CeO_2 prepared by the method of deposition-precipitation with urea leads to a novel basic catalyst. Two concurrent impacts of this special preparation technique on the surface properties of ceria are observed. First, urea acts as surface modifier within the thermal treatment process by its decomposition. Several nitrogen containing surface intermediates and stable compounds are formed,

adsorbed, and modify thereby the acid-base properties of the support which finally leads to an enhanced base strength. Thermal treatment up to 500 °C does not remove these newly formed compounds completely. Second, Au blocks the least accessible Brønsted acid sites which are present on plain ceria, and thus completely eliminates the activity of ceria to dehydrate propan-2-ol. Moreover, the new basic material catalyzes the dehydrogenation to acetone with high efficiency and without notable deactivation.

1.6 References

- [1] S. A. Arrhenius, *Z. Phys. Chem.* **1887**, *1*, 631.
- [2] J. N. Brønsted, *Recl. TraV. Chim. Pays-Bas* **1923**, *42*, 718.
- [3] N. Lewis, *Valency and Structure of Atoms and Molecules* **1923**, Wiley.
- [4] G. Busca, *Ind. Eng. Chem. Res.* **2009**, *48*, 6486.
- [5] K. Tanabe, W. F. Hölderich, *Appl. Catal., A* **1999**, *181*, 399.
- [6] E. Iglesia, D. G. Barton, J. A. Biscardi, M. J. L. Gines, S. L. Soled, *Catal. Today* **1997**, *38*, 339.
- [7] H. Hattori, *J. Jpn. Pet. Inst.* **2004**, *47*, 67.
- [8] H. Hattori, *Chem. Rev.* **1995**, *95*, 537.
- [9] H. Hattori, *Appl. Catal., A* **2001**, *222*, 247.
- [10] J. Weitkamp, M. Hunger, U. Ryma, *Microporous Mesoporous Mater.* **2001**, *48*, 255.
- [11] A. Gervasini, *Catal. Lett.* **1997**, *43*, 219.
- [12] K. P. C. Vollhardt, *Organische Chemie* **2007**, WILEY-VCH.
- [13] K. C. Waugh, *Appl. Catal.* **1986**, *25*, 121.
- [14] H. Noller, *Z. Phys. Chem. NF* **1985**, *144*, 157.
- [15] S. R. Blaszkowski, R. A. v. Santen, *J. Am. Chem. Soc.* **1996**, *118*, 5152.
- [16] D. Haffad, A. Chambellan, J. C. Lavalley, *J. Mol. Catal. A: Chem.* **2001**, *168*, 153.
- [17] V. Mirkhani, S. Tangestaninejad, B. Yadollahi, L. Alipanah, *Tetrahedron* **2003**, *59*, 8213.
- [18] W. M. Song, Q. G. Deng, D. R. Zhou, D. F. Zhao, *Chem. Res. Chin. Univ.* **2005**, *21*, 601.
- [19] I. Hama, T. Okamoto, H. Nakamura, *J. Am. Chem. Soc.* **1995**, *72*, 781.

Chapter 2

Experimental

2.1 Characterization techniques

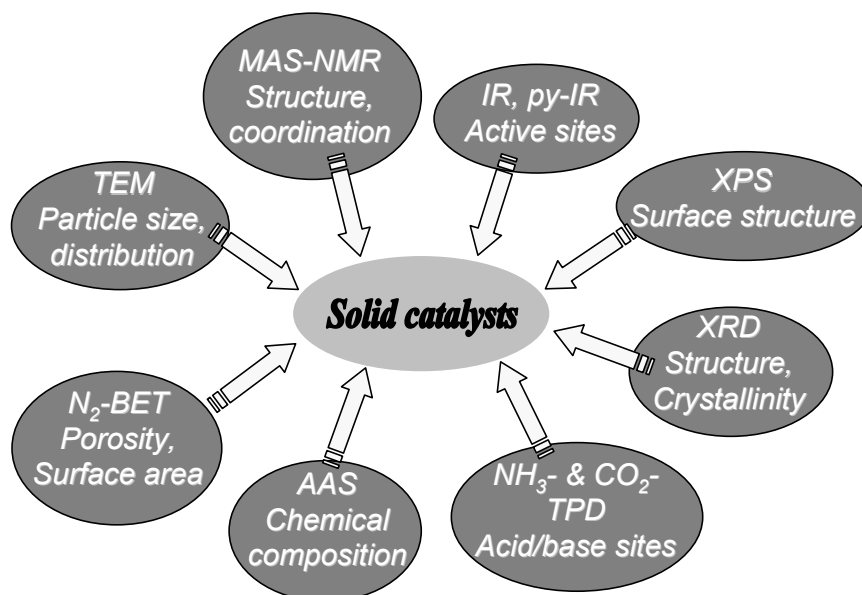


Figure 2-1. Characterization methods of solid materials.

- **AAS**

The metal contents were analyzed by atomic absorption spectroscopy (AAS) carried out with *UNICAM 939 AA-Spectrometer*. The solids (10-50 mg) were dissolved in a boiling mixture of hydrofluoric acid (HF, 0.5 mL) and nitrohydrofluoric acid (0.1 mL) to ensure complete dissolution of the sample.

- **N₂-Adsorption**

The measurement of the specific surface area is based on adsorption of an inert gas as for instance N₂. In theory, at a certain temperature (77 K) one nitrogen molecule occupies a certain space (0.162 nm²). Thus, for the monolayer, the specific surface area can be derived directly. However, in practice multilayer adsorption and capillary condensation hinder a direct calculation of surface area by the amount of adsorbed molecules.^[1] The BET- theory enables to determine the specific surface area corresponding to the pressure.

Specific surface areas and pore volumes were determined by physisorption of N₂ at 77 K. Measurements were carried out in *PMI automatic BET-Sorptometer*. Evaluation was done according to the BET theory.

• XRD

The crystalline structure of all materials was analyzed by XRD using a *Philips X'Pert Pro System* (Cu K_α1-radiation, 0.154056 nm) at 40 kV / 40 mA. Measurements were carried out on a spinner performed with a 1/4'' slit from 0.3° to 0.6° 2θ step size (0.03 ° min⁻¹) and with a 1/6'' slit in the range from 5° to 70° 2θ (0.05 °/min). In-situ experiments were carried out in the *Philips X'Pert Pro System*, as described above, equipped with *HTK 2000 oven*. The samples were heated stepwise (100 °C) from ambient to 700 °C in a flow of 5 mL min⁻¹ synthetic air.

The particle size was determined by the *full-width-at-half-maximum* ($FWHM = H_B$) using the *Scherrer-equation* (Eq. 1). Scherrer was the first one who considered a correlation between the line width of XRD reflexes and the particle size.^[2]

$$H_B = \frac{K \cdot \lambda \cdot 57.3}{D \cdot \cos \theta} \quad (1)$$

Herein K is defined as a constant (*shape factor*), often determined as 1.0, D the average prime particle size vertically to the reflecting lattice plane, θ the diffraction angle and λ the x-ray wavelength.^[3] Generally, an increase of the H_B is caused by a decrease of prime particle size. The particle sizes were determined by in the *X'Pert High Score* software program using the *Scherrer calculation*.

• TGA

Thermo gravimetric analysis (TGA) was used to determine the thermal stability of materials. The experiments were carried out on a *Setaram TG-DSC III (thermo-) gravimetric instrument*. A homebuilt high vacuum system equipped with a *Pfeifer Vacuum Mass Spectrum* (MS) is coupled with the original microbalance system. Conventionally 10 to 20 mg of the solid sample are pressed into wafers and broken into small pieces and filled in a quartz crucible. The sample is placed in the heating block. A non-adsorbing temperature stable reference is simultaneously measured. The

mass loss of the sample is determined relative to the reference. The samples were heated in vacuum from RT to 700 °C with a rate of 10 K·min⁻¹.

- **TPD**

Temperature programmed desorption of ammonia (NH₃-TPD) and carbon dioxide (CO₂-TPD) were used to determine acidic and basic properties. As standard materials for referencing the NH₃-TPD and CO₂-TPD, a H-MFI 90 zeolite and NaHCO₃ were used, respectively. Catalyst samples were activated at elevated temperatures in vacuum for 1 h. Adsorption of ammonia at 0.1 mbar was performed at 100 °C for 1 h. CO₂ (1 mbar) was adsorbed at 40 °C for 1 h. Desorption occurred during heating the samples from corresponding temperature up to 700 °C with a rate of 10 K min⁻¹. Analysis was done with *Pfeifer Vacuum Mass Spectrum* (MS).

- **Solid state MAS-NMR**

Solid state MAS-NMR was used to clarify the structural environment of aluminum and fluorine in the mixed metal oxide lattice. The method complements the XRD when the detection limit of the latter one is reached. In comparison to liquid phase NMR, higher radio frequencies are necessary for solid state NMR. The main difference between liquid and solid state NMR is the limited rotation of molecules in solids, which leads to lower resolutions. The delay between the pulses is longer, as the spin-lattice relaxation time is long, whereas the spin-spin relaxation is fast.

Two reasons for the line broadening in solid state NMR were recognized. One reason is the dipole-dipole interaction. A local magnetic field is created in between two nuclei in the distance of R which is described by the equation 2:

$$B_{local} = -\frac{g_I \mu_N m_I \mu_0}{4\pi R^3} (1 - 3 \cos^2 \Theta) \quad (2)$$

In contrast to liquids this field is not adjusted to zero in solids. The line width in solids is for that reason in general in the order of 10³ Hz.

The second reason for the line broadening is the anisotropism of the chemical shift. The chemical shift depends on the orientation of a molecule, which can be averaged in fluids because of the mobility of molecules. However, in solids the molecules are fixed and create therefore different resonance frequencies. The anisotropism depends by the term $1-3\cos^2\theta$ on the angle between the main axis of the molecule and the orientation of the field.

To reduce the phenomenon of line broadening due to the dipole-dipole coupling and the anisotropism, the magic angle spinning (MAS) method was established (see Figure 2-2). Due to the fact, that the term $1-3\cos^2\theta$, which describes the dipole-dipole coupling and the anisotropism, gets at a angle of $\theta = 54.74^\circ$ zero. The rotation frequency of the sample must be higher than the spectral width of the recorded spectra. This can be achieved by gas-powered rotors.^[4]

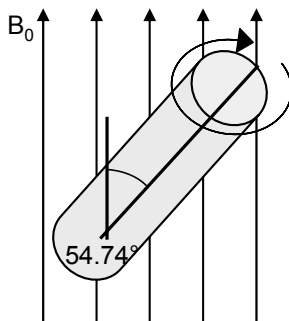


Figure 2-2. Magic angle of the rotor in the external magnetic field B_0 .

- **TPO**

Temperature programmed oxidation (TPO) was carried out on a homebuilt multi reactor set-up equipped with six parallel reactors. The system is operated via HPVvee software wherein temperature and mass flows can be controlled. Mass analysis was done with *Pfeifer Vacuum Mass Spectrum* (MS). The samples were diluted with SiO_2 powder and filled between quartz-wool. The catalysts used in the conversion of propan-2-ol were heated in inert gas flow. Thereby physisorbed pollutions from air and rest of propan-2-ol were eliminated. For oxidation an oxygen/helium flow with 5 % oxygen was steamed over the catalyst sample during heating up from 100 to 900 °C.

- IR

Next to nuclear magnetic resonance (NMR) spectroscopy, ultraviolet (UV) spectroscopy and mass spectroscopy (MS) infrared (IR) spectroscopy is one of the outstanding analytical methods in nowadays. The most important advantages of IR spectroscopy are not only the high variety of applications, but also the high information content resulting from one spectrum. The infrared spectral regions are classified by near ($12\,800 - 4\,000\text{ cm}^{-1}$), mid ($4\,000 - 400\text{ cm}^{-1}$) and far ($400 - 10\text{ cm}^{-1}$) IR. All elementary vibrations are represented in the mid-IR region. The conventional mid-IR spectrometers are based on a Fourier transformed interferometric measurement. A schematic construction is illustrated in Figure 2-3.

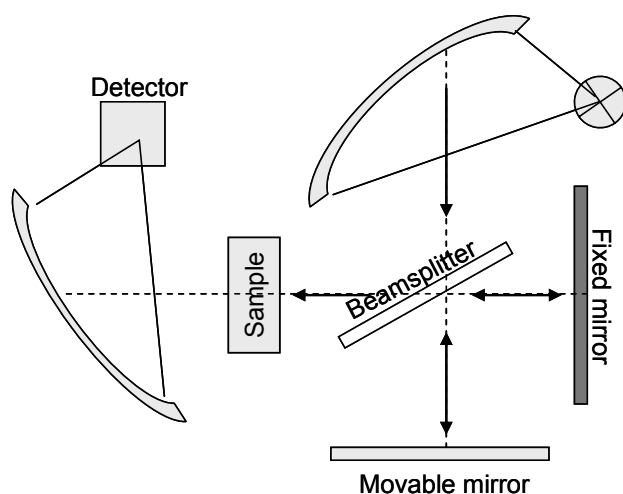


Figure 2-3. Schematic construction of a Fourier transformed spectrometer.

The main vibration modes of a linear tri-atomic active IR molecule, which is changing its dipole moment by excitation, are demonstrated in Figure 2-4.^[5]

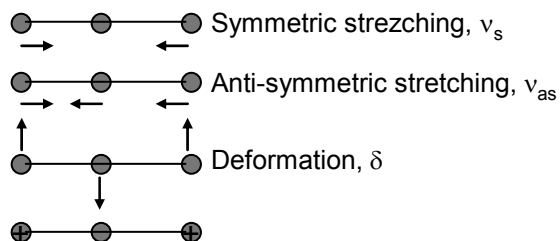


Figure 2-4. Vibrational modes of a linear triatomic molecule.

Infrared spectroscopy was carried out on a *Perkin-Elmer 2000 spectrometer* coupled with a MCT detector, a *Bruker IFS 88 spectrometer* or a *Nicolet spectrometer*. Samples were pressed into self-supporting wafers and activated in vacuum at elevated temperatures for 2 h. The spectra were recorded in transmission mode at a resolution of 4 cm^{-1} in the region from 4000 to 780 cm^{-1} .

Adsorption of probe molecules as for instance pyridine, carbon dioxide, propan-2-ol and methanol was followed by IR. Sample preparation and instruments were used as described above.

- **TEM**

To determine the particle size of metal atoms on the oxide surface transmission electron microscopy was used. The measurements were put out with the *JEOL JEM 100CX* microscope equipped with a wolfram cathode. Inorganic materials, which are often less with water, have to be transformed in a well transparent (gauge 5-500 nm for 100 kV) and vacuum consistent sample. Therefore the metal supported oxides were grinded and dispersed in ethanol. Afterwards the sample were applied on a *Quantifoil Multi A, Cu 200 mesh, double holey film* grid and directly watched.

- **XPS**

Investigations of surface properties for ceria and modified ceria samples were performed by X-ray photoelectron spectroscopy (XPS) at the Institute of Technical Chemistry, University of Leipzig. XPS analysis was carried out using a hemispherical energy analyzer *Phoibos 150* (Specs GmbH, Berlin, Germany) equipped with an X-ray source *XR 50* (Specs GmbH). O 1s, Ce 3d, C 1s and Au 4f lines were monitored using the Mg K_{α} line at 1253.6 eV and excitation energy of 20 kV. Spectrum processing included satellite and Shirley background subtraction. Due to the electrostatic charging, the binding energies (BE) had to be corrected with respect to the C 1s = 284.5 eV taken as the internal standard. All spectra were analyzed using the software package *CasaXPS Version 2.2.24*. Samples have been placed in the transfer chamber for 6 h to remove adsorbed surface components. Measurement time was 30 min. The C 1s carbon signal at 284.5 eV resulted mainly from omnipresent surface layers.

2.2 Catalytic tests

2.2.1 Conversion of propan-2-ol

The catalytic activity of all materials was performed in the conversion of propan-2-ol. The schematic construction of the reaction set-up is illustrated in Figure 2-5. The set-up is equipped with a single down-stream reactor connected to a *Hewlett Packard GC* outfitted with a flame ionization detector. The reactor comprises a quartz-tube with 4 mm diameter and an oven. The catalyst with arbitrary particle size (0.02 g diluted in 0.13 g SiC) was fixed with quartz wool in the quartz-tube. Four different mass flow controllers save the gas-supply with helium, synthetic air or hydrogen. In general the catalyst was heated in a flow of 20 mL·min⁻¹ of helium (MFC4) from ambient to elevated temperature of activation for 2 h. After reaching the reaction temperature MFC4 was switched of and helium was led by MFC2 through the saturator. The saturator was filled with propan-2-ol and cooled permanently to 13 °C (partial pressure = 25 mbar). The helium/propan-2-ol gas mixture was directed over the fixed bed reactor. Unreacted propan-2-ol and dehydrogenation/dehydration products were analyzed by GC. Separation of various components was done by a *Supelco*[®] wax-column.

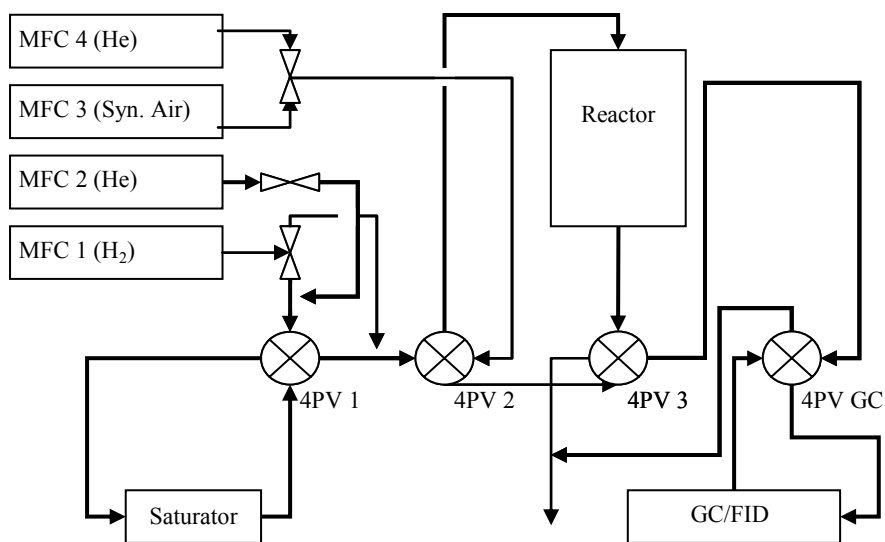


Figure 2-5. Schematic construction of catalytic set-up for propan-2-ol conversion.

The system was automatically controlled by a computer equipped with HP-VEE software. The analysis of gas chromatography was carried out by the CSW program. The automated temperature profile is given in Figure 2-6. After activation the reaction was carried out at four different temperatures and maximal three different carrier gas-flows. After the third temperature step (T_4) the catalyst is cooled down to the first temperature (T_1) discovering deactivation.

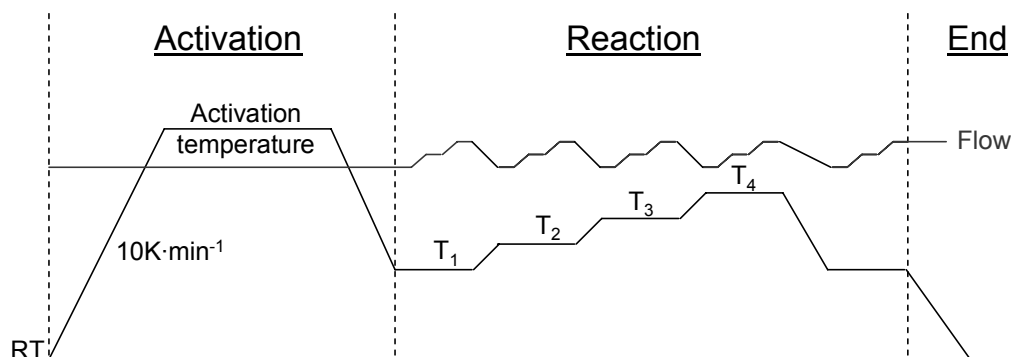


Figure 2-6. Schematic temperature/flow-profile of the automated catalytic set-up.

2.2.2 Hydrogenation of acetone

The hydrogenation of acetone serves as test reaction for the hydrogenation/dehydrogenation ability of metallic catalysts as for instance Au supported on ceria.

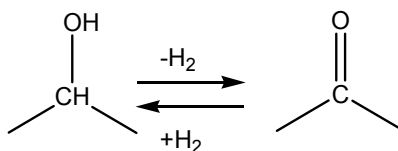


Figure 2-7. Reaction scheme of propan-2-ol dehydrogenation and acetone hydrogenation.

The hydrogenation of acetone was studied in hydrogen atmosphere in the temperature range from 150 to 225 °C with steps of 25 °C. The as-prepared samples (0.2 g diluted in 0.35 g SiC) were fixed with quartz wool in a quartz-tube reactor of 4 mm diameter. The as-prepared samples were first pretreated in a flow of helium of 20 mL·min⁻¹ by heating from ambient to 500 °C (heating ramp 10 °C·min⁻¹) for 2 h in order to activate the sample. Cooling to reaction temperature was reached under He flow

of $20 \text{ mL}\cdot\text{min}^{-1}$, too. During reaction, a flow of hydrogen with $20 \text{ mL}\cdot\text{min}^{-1}$ was saturated with acetone at -12°C (partial pressure 49 mbar) and led over the fixed bed reactor. Un-reacted acetone and hydration products were analyzed by gas chromatography using a *Shimadzu GC-2014* gas chromatograph.

2.2.3 Condensation of 1,2-epoxy-octane with hexanol

The condensation of 1,2-epoxy-octane with hexanol was carried out in a 100 mL flask. Hexanol (2.555 g, 0.025 mol) was added to 1,2-epoxy-octane (4.038 g, 0.026 mol) and heated in N_2 atmosphere to 160°C under stirring. The catalyst (0.066 g, 1 wt.-%) was added and samples were taken every hour. For analysis the catalyst was removed by filtration. The filtrate (100 μL) was mixed with 2,2,4-tri-methylpentane (937 μL), which serves as internal standard for GC-analysis. Un-reacted 1,2-epoxy-octane, hexanol and reaction products were analyzed by gas chromatography using a *Shimadzu GC-2010*.

2.3 References

- [1] I. Chorkendorff, J. W. Niemantsverdriet, *Concepts of modern catalysis and kinetics* **2003**, WILEY-VCH, 183.
- [2] P. Scherrer, *Göttinger Nachrichten* **1918**, 2, 98.
- [3] H. Krischner, B. Koppelhuber-Bitschnau, **1994**.
- [4] P. W. Atkins, **1996**, *Physikalische Chemie, 2. Auflage*, VCH, 614.
- [5] H. Günzler, H.-U. Gremlich, **2002**, *IR spectroscopy An Introduction*, WILEY-VCH, 25f.
- [6] V. Mirkhani, S. Tangestaninejad, B. Yadollahi, L. Alipanah, *Tetrahedron* **2003**, 59, 8213.

Chapter 3

Magnesium/aluminum mixed oxides

Abstract

Mg/Al mixed oxides derived from layered double hydroxide (LDH) precursors with various Mg/Al ratios and sodium contents were synthesized via a sol-gel process. The structure of the resulting materials was analyzed by XRD and ^{27}Al -MAS NMR. The acid and base properties of the Mg/Zn/Al mixed oxides samples were determined via NH_3 - and CO_2 -TPD. The basicity was increased with increasing Mg/Al ratios, whereas the acidity decreased. Infrared spectroscopy with adsorbed CO_2 turned out that the Lewis acidity decreased with decreasing Mg/Al ratio. The remaining sodium contents decreased the dehydration reaction of propan-2-ol dramatically.

3.1 Introduction

There is a great demand for developing solid base materials such as hydrotalcites and their derived mixed metal oxides as economical and environmental friendly catalysts. A large number of organic reactions make use of basic catalysts, e.g. condensation^[1-6] reactions like aldol^[7-14] and Knoevenagel^[15-20] reaction, alkylations^[21, 22], isomerizations^[22] and polymerization^[23-25] reactions. But also the application of acid and base bifunctional catalysts in the synthesis of nitriles was described.^[26]

The use of Mg/Al mixed oxides as effective solid base catalysts and many different synthesis routes have been reported in literature. An intensive experimental research was carried out on exploring the influence of synthesis routes,^[27] each synthesis step and synthesis conditions.^[28] Tunable basicity occurring by ion exchange^[29, 30] as well as targeted re-hydration^[10] of calcined hydrotalcites is one of the demanding features of such materials. Mixed oxides derived from hydrotalcite precursor exhibit a well dispersed structure of (M^IM^{II}O). Due to the intercalation of Al³⁺ into the MgO framework strong basic sites will be created due to the formation of unsaturated O²⁻-sites.^[31] Brønsted basic sites (surface OH-groups or OH⁻ ions in the interlayer), which are involved in the Knoevenagel or Claisen-Schmidt condensation, are originated by calcination at temperatures less than 450 °C or re-hydration.^[32] Among the large variety in tuning acid-base properties, the metal ratio M²⁺/M³⁺ opens a further alternative to modify the acidity/basicity of mixed metal oxides.^[33] Another option will be the insertion of alkali metals exhibits efficiently basic solid catalysts for fine chemical synthesis.^[34, 35]

MgO is a well known solid base with high CO₂ adsorption capacity (5.3 μmol·m⁻²) which is almost 4 times higher compared to Al₂O₃.^[36] However, due to the reaction conditions and the Mg/Al ratio Fischel^[36] found higher selectivities to basic products for the mixed oxide than for bare MgO. The differences in CO₂ adsorption capacity and acetone selectivity in the experiments with temperature programmed desorption of propan-2-ol can be explained by the inhomogeneous distribution of Al in the MgO framework. The active sites of hydrotalcites are defects which expose metal-oxygen pairs. The amount of such defects increased with increasing amount of aluminum.

Calcined hydrotalcites are basic oxides, the surface properties depend on the synthesis method.^[36]

In this study, the influence of Mg/Al ratio on acid base properties of mixed metal oxides, the influence of sodium content of Mg/Al oxides obtained by different synthesis methods on catalytic performance as well as the optimal calcination temperature of Mg/Al hydrotalcites have been investigated to optimize activity and selectivity.

Catalyst synthesis of these type of metal oxides was carried out via sol-gel process, which enables the formation of micro-engineered structures. Thus, it is possible to form oxides with localized microstructures combined with defined pore sizes and surface areas.^[37] Hydrothermal synthesis was established as this method leads to homogeneous mesoporous MgAlO structures with high surface areas.^[38, 39]

3.2 Experimental

3.2.1 Preparation

The commercial hydrotalcite was kindly provided by Cognis and is labeled as HT2. Parts of the sample were calcined for 8 h at 500, 700 and 900 °C (heating rate 5 °C·min⁻¹) in a flow of 100 mL·min⁻¹ of synthetic air. The samples are denoted as HT2-500, HT2-700 and HT2-900.

All chemicals used were obtained from Sigma-Aldrich and if not denoted utilized without further purification.

The mixed metal oxides with Mg/Al ratio of 4:1 were obtained by heating the precursors in air. Hydrotalcites were synthesized by a sol-gel process adopted from the method described by Greenwell.^[40]

An acidic 1 M aqueous solution of metal nitrates was prepared by dissolving Mg(NO₃)₂·6H₂O (123.08 g, 0.48 mol) and Al(NO₃)₃·9H₂O (45.01 g, 0.12 mol) in 0.6 L decarbonized bi-distilled water. A second aqueous alkaline solution (0.6 L) was prepared from a 2 M NaOH and 0.1 M NaHCO₃. Both solutions were heated to 75 °C. For precipitation, the nitrate and alkaline solutions were added drop-wise to 400 mL water giving a pH of 9 at 75 °C. The suspension was aged for 3 h at 85 °C under stirring. After cooling to RT the gel was filtered and added into an autoclave. Hydro-thermal synthesis

was carried out for 16 h at 80 °C. Afterwards the gel was washed with 150-350 mL bi-distilled water until the pH of washing water was 7. The white precipitate was freeze-dried and calcined for 8 h at 600 °C (heating rate 5 °C·min⁻¹) in flow of 100 mL·min⁻¹ of synthetic air. The as-prepared sample is labeled as HT4.

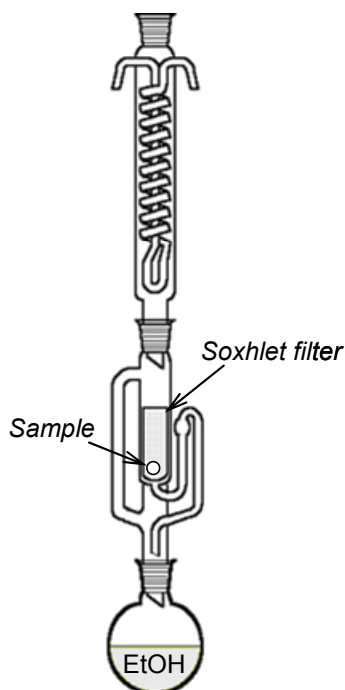


Figure 3-1. Soxhlet extraction apparatus.

To remove the remaining sodium from the calcined sample, a Soxhlet extraction was carried out with ethanol. Therefore, a flask was filled with 500 mL ethanol and 10 g of the sample was added into the Soxhlet filter. The solvent was heated under reflux for 3 days. After cooling to ambient temperature the sample was removed from the filter, freeze-dried and calcined for 8 h at 600 °C (heating rate 5 °C·min⁻¹) in flow of 100 mL·min⁻¹ of synthetic air. The as-prepared sample is labeled as HT4 I sox.

In order to create different sodium contaminated samples, the as-prepared gel was either not washed or alternatively washed with 150 and 350 mL decarbonized bi-distilled water. The samples were denoted as HT4 Na, HT4 Na-150 and HT4 Na-350.

3.2.2 Characterization techniques

3.2.2.1 Textural analysis

The metal content of Mg/Al mixed oxides was analyzed by atomic absorption spectroscopy (AAS) carried out with *UNICAM 939 AA-Spectrometer*.

Specific surface area and pore volume were determined by physisorption of N₂ at 77 K. Measurements were carried out in *PMI automatic BET-Sorptometer*. Evaluation was done according to the BET theory.

The crystalline structure of the precursor and mixed metal oxides was analyzed by XRD using a *Philips X'Pert Pro System* (CuK α 1-radiation, 0.154056 nm) at 40 kV / 40 mA. Measurements were carried out on a spinner performed with a 1/4'' slit from 0.3° to 0.6° 2 θ step size (0.03 ° min⁻¹) and with a 1/6'' slit in the range from 5° or 20 ° to 70° 2 θ (0.05 °/min).

²⁷Al MAS-NMR experiments were performed on a *Bruker AV500 spectrometer* (B₀ = 14.1 T) with a spinning rate of 12 kHz. For temperature adjustment the bearing and drive gas stream were passed through a heat exchanger. The samples were packed in 4 mm ZrO₂ rotors. For ²⁷Al the resonance frequency was 130.3 MHz. The spectra were recorded as sum of 2400 scans with a recycle time of 250 ms. A $\pi/12$ pulse (pulse length = 1.0 μ s) was applied for excitation. The chemical shifts were referenced against an external standard of solid Al(NO₃)₃ (δ = -0.54 ppm).

3.2.2.2 Infrared spectroscopy

Infrared spectroscopy was carried out on a *Perkin-Elmer 2000 spectrometer* coupled with a MCT detector or a *Bruker IFS 88 spectrometer*. Samples were pressed into self-supporting wafers and activated in vacuum at 450 °C for 2 h. The spectra were recorded in transmission mode at a resolution of 4 cm⁻¹ in the region from 4000 to 780 cm⁻¹.

Adsorption of pyridine, CO₂ or propan-2-ol was followed by IR. Sample preparation and instruments were used as described above. Pyridine was adsorbed at 0.1 mbar at 150 °C and out gassed with increasing temperatures from 150 to 250 °C for 2 h. CO₂ was adsorbed at 40 °C and partial pressures from 0.01 to 0.1 mbar. CO₂ was

degassed in by heating to 250 °C in vacuum. Propan-2-ol was adsorbed at 0.1 mbar at 50 °C. After 30 min equilibration the sample was heated under vacuum to 250 °C.

3.2.3 Catalytic tests

The dehydrogenation/dehydration reaction of propan-2-ol was studied in inert atmosphere in the temperature range from 200 to 300 °C. The catalyst with arbitrary particle size (0.02 g diluted in 0.13 g SiC) was fixed in between quartz wool in a quartz-tube reactor of 4 mm diameter. The catalyst was heated in He flow of 20 mL·min⁻¹ from ambient to 450 °C for 2 h, in order to activate the sample. Cooling to reaction temperature was reached under He (20 mL·min⁻¹). For reaction, a helium flow of 40 mL·min⁻¹ was saturated with propan-2-ol at 13 °C (partial pressure 25 mbar) and led over the fixed bed reactor. Un-reacted propan-2-ol and dehydrogenation/dehydration products were analyzed by gas chromatography using a *Hewlett Packard GC* equipped with a flame ionization detector. Separation of various components was done by a *Supelco*[®] wax-column.

3.3 Results

3.3.1 Textural analysis of Mg/Al mixed oxides

The results of textural analysis for Mg/Al mixed oxides are listed in Table 3-1.

The specific surface area of HT2 was 171 m²·g⁻¹. After calcination at 500 °C in synthetic air the specific surface area increased to 219 m²·g⁻¹ indicating the removal of impurities, which stuck in the pores. Further increase of the calcination temperature to 700 and 900 °C resulted in decreasing surface areas through sintering. The metal ratio of Mg/Al of HT2 was 2.1. The sodium content of HT2 was less than 0.002 wt.-%.

HT4 I had a surface area of 58 m²·g⁻¹ the metal ratio of Mg/Al was 4.1, which is slightly more than the nominal one. The sodium content of HT4 I was with 13 wt.-% apparently higher than for HT2. HT4 I was treated via Soxhlet extraction with ethanol to remove sodium. The sodium content of this sample (HT4 I sox.) was 8 wt.-%, and 1.7 times less than for the non-treated sample. In a further experiment the sodium content

was varied by washing the gel obtained during synthesis with different amounts of water. The specific surface area of the sample which was not washed with water during synthesis (HT4 Na) was $29 \text{ m}^2 \cdot \text{g}^{-1}$. The sodium content of HT4 Na was 14 wt.-%. By washing with 150 and 350 mL water, the sodium content was decreased to 3 and 1 wt.-%, respectively. The specific surface areas increased by more than 4 times with decreasing sodium content indicating that sodium sticks in the pores. The reproducibility for the catalyst synthesis was tested. Also the specific surface areas of the different HT4 charges (II-IV) varied in-between 105 and $188 \text{ m}^2 \cdot \text{g}^{-1}$ the metal ratios of Mg/Al were 4.0 for HT4 III and 3.8 for HT4 II and IV. Highest surface area was observed for the sample with the lowest sodium content.

The sodium content of HT2 was not comparable to HT4 which indicates another synthesis method used for HT2 most probably without sodium.

Table 3-1. Textural analysis of Mg/Al mixed oxides.

<i>Sample</i>	<i>Specific</i>	<i>Molar ratio</i>	<i>Metal content (wt.-%)</i>		
	<i>Surface area</i>		<i>Mg</i>	<i>Al</i>	<i>Na</i>
	($\text{m}^2 \cdot \text{g}^{-1}$)	(Mg:Al)			
HT2	171	2.1	33	18	0
HT2-500	219	2.0	20	11	0
HT2-700	213	2.0	19	11	0
HT2-900	149	2.0	26	15	0
HT4 I	58	4.1	21	6	13
HT4 I sox.	33	3.9	34	9	8
HT4 Na	29	3.9	23	6	14
HT4 Na-150	128	3.8	40	12	3
HT4Na-350	182	3.9	41	12	1
HT4 II	188	3.8	42	12	0
HT4 III	120	4.0	21	6	3
HT4 IV	105	3.8	41	12	1
HT4 III-200	91	3.9	25	7	2
HT4 III-300	106	3.8	30	9	3
HT4 III-400	82	3.7	30	9	3

3.3.2 XRD analysis of Mg/Al mixed oxides

The structural analysis of HT2 and HT4 samples was carried out via XRD. The results are illustrated in Figure 3-2. The reflexes of MgO were expected at 35.6, 43.0 and

62.5 °. Both samples were dominated by the cubic MgO structure. Neither for HT2 nor for HT4 separated alumina phases could be identified. Thus, Al is incorporated into the MgO structure resulting in a $\text{Mg}_{(x)}\text{AlO}$ phase^[41] or alumina exists as amorphous species. As the reflex widths of both patterns were very broad, low crystallinity of the materials is expected.

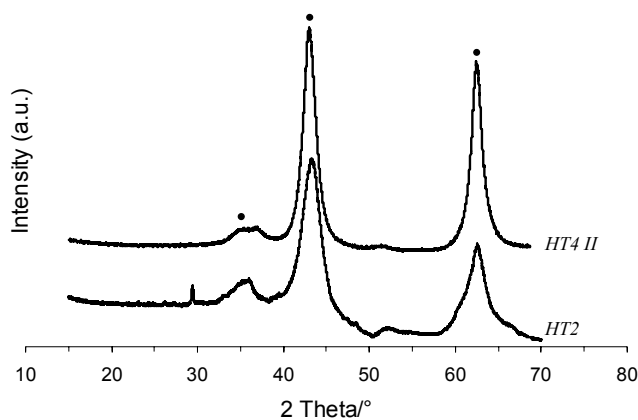


Figure 3-2. XRD patterns of HT2 and HT4 II.

(● MgO cubic)

The XRD patterns of HT4 samples from different batches and the Soxhlet extracted one are shown in Figure 3-3. Reflexes related to MgO and NaNO_3 occurred for all HT4 samples excepted for HT4 II. For HT4 II the peak width was expanded indicating less crystallinity compared to the other HT4s. The XRD analysis confirms the results from AAS analysis wherein for HT4 I, HT4 I sox., and HT4 III the sodium content was ≥ 3 wt.-% and for HT4 II and HT4 IV ≤ 1 wt.-%. However, in no case an alumina phase was observed indicating, that aluminum was incorporated into the MgO structure or exists as amorphous phase.

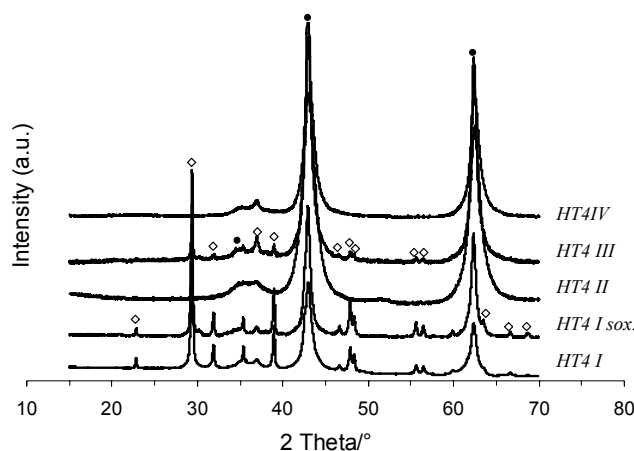


Figure 3-3. XRD patterns of HT4 samples.

(● MgO cubic, ◊ NaNO₃)

The structural transformation of HT4 from the LDH precursor to the mixed oxide was followed in-situ via XRD analysis from RT to 600 °C in a flow of 5 mL·min⁻¹ of synthetic air. The results are illustrated in Figure 3-4. At RT main reflexes were observed at 11.4, 23.0, 34.7, 38.6, 45.6, 60.4, 61.5 and 65.6 related to hydrotalcite structure with the general molecular formula of Mg₆Al₂CO₃(OH)₁₆·H₂O. At 200 °C, the intensity of the reflexes related to the hydrotalcite phase decreased and the reflex widths were broadened indicating structure transformation from hydrotalcite to Mg_(x)AlO. Further temperature increase to 400 °C resulted in a complete transformation to Mg_(x)AlO. Between 400 and 600 °C no further changes could be observed via XRD.

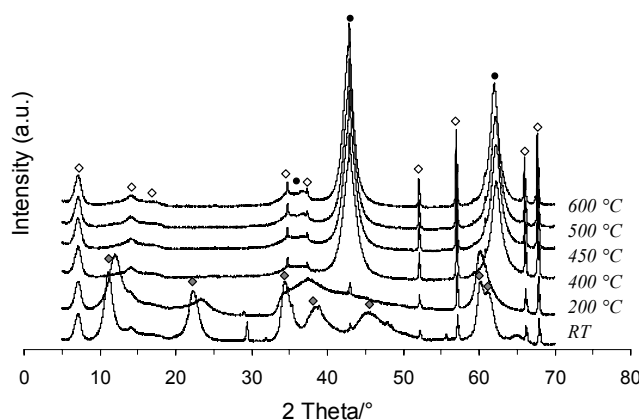


Figure 3-4. XRD patterns of non-calcined and calcined HT4 samples.

(◊ Mg₆Al₂CO₃(OH)₁₆·4H₂O, ● MgO cubic, ◊ Al₂O₃ of sample holder)

3.3.3 ^{27}Al MAS-NMR spectroscopy of Mg/Al mixed oxides

^{27}Al MAS-NMR spectroscopy of the solid materials was used to identify the alumina species in more detail. The results for HT2 and HT4 II are illustrated in Figure 3-5. For both samples signals related to octahedral and tetrahedral Al were observed. The chemical shifts of octahedral Al^{VI} and tetrahedral Al^{IV} are located at 10.88 and 75.35 ppm, respectively, in case of HT2. The ratio of $\text{Al}^{\text{IV}}/\text{Al}^{\text{VI}}$ was 0.62. For HT4 II the signal of Al^{VI} was observed at 9.73 ppm and for Al^{IV} at 77.65 ppm. In comparison to the octahedral Al^{VI} the signal of tetrahedral Al^{IV} was very small. The ratio of $\text{Al}^{\text{IV}}/\text{Al}^{\text{VI}}$ was 0.09. With increasing aluminum content, the amount of tetrahedral Al increased. Thus the incorporation of aluminum in tetrahedral vacancies is preferred.

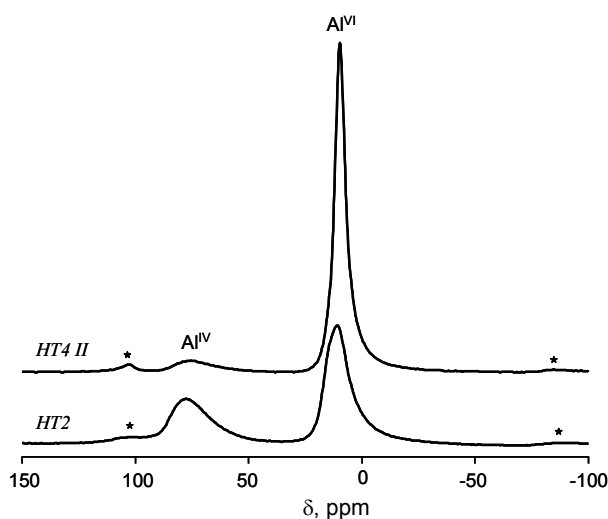


Figure 3-5. ^{27}Al MAS-NMR of Mg/Al mixed oxides.

3.3.4 Infrared spectroscopy of adsorbed pyridine on Mg/Al mixed oxides

The acid site properties of Mg/Al mixed oxides HT2 and HT4 II were determined by infrared spectroscopy of adsorbed pyridine. The samples were heated from ambient to 450 °C with 10 K·min⁻¹ for 2 h in vacuum for activation. Subsequently, the samples were cooled to 150 °C and pyridine was adsorbed at 0.1 mbar for 0.5 h. Afterwards desorption of pyridine was carried out by heating the samples to 250 °C in vacuum.

After adsorption of pyridine on HT2 the difference spectrum exhibits a markedly negative band at 3742 cm^{-1} . At the same time, adsorption bands occurred at 1603, 1576, 1493 and 1445 cm^{-1} assigned to physisorbed pyridine and pyridine interacting with Lewis acidic sites.^[42] The characteristic band at $\sim 1540\text{ cm}^{-1}$ related to pyridine coordination to Brønsted acid sites was not observed. After heating to $250\text{ }^{\circ}\text{C}$, the intensity of the negative band decreased indicating weakly coordinated pyridine via H-bonding to hydroxyl groups on the surface. However, bands related to pyridine coordinated to Lewis acid sites remained after desorption of pyridine at $250\text{ }^{\circ}\text{C}$ in vacuum.

In the difference spectrum of HT4 II adsorption bands similar to pyridine adsorbed on HT2 appeared and disappeared after heating at $250\text{ }^{\circ}\text{C}$. The bands related to pyridine coordinated to Lewis acid sites (1608 and 1447 cm^{-1}) in the spectra of HT4 were slightly shifted to higher wavenumbers in comparison to HT2. Thus the interaction between pyridine and HT4 is expected to be slightly stronger than for HT2. The ratios of L-Pyd/H-Pyd were calculated after adsorption and desorption. For HT4 the ratio was estimated as 5.8 and decreased to 3.6 after desorption. For HT2 the value of L-Pyd/H-Pyd was found to be 6.3 and decreased to 5.2 after desorption. The ratio of Lewis coordinated pyridine to H-bonded pyridine was for HT2 with 6.3 slightly higher than for HT4 indicating that HT2 exhibits higher acid site concentration than HT4. However, for HT2 a stronger acid site strength was observed, as after desorption (L-/H-Pyd = 5.2) the concentration of remaining pyridine was nearly twice the number of HT4.

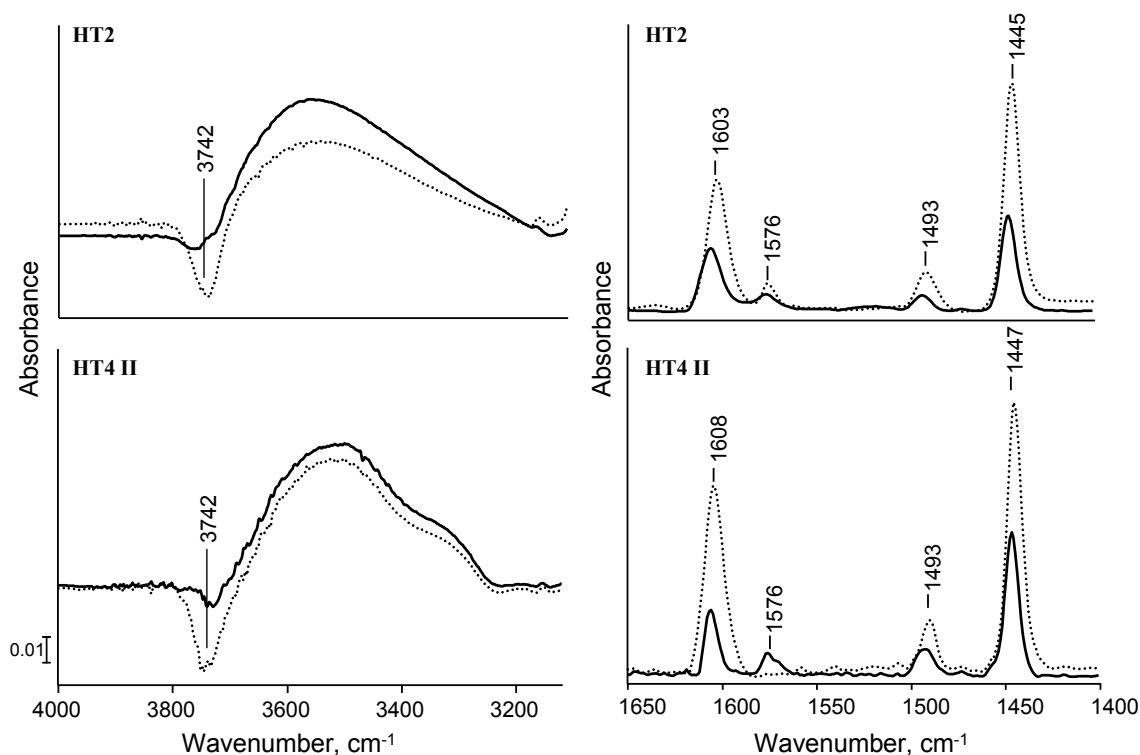


Figure 3-6. Difference spectra after pyridine adsorption on HT2 and HT4 II.

(...Pyridine adsorbed at 0.1 mbar, 0.5 h; –After desorption at 250 °C)

3.3.5 Infrared spectroscopy of adsorbed CO₂ on Mg/Al mixed oxides

The analysis of basic site properties of Mg/Al mixed oxides was investigated via infrared spectroscopy of adsorbed CO₂. The samples were heated with a ramp of 10 K·min⁻¹ for 2 h in vacuum to 450 °C to remove pre-adsorbed CO₂ from air. After activation, the samples were cooled to 40 °C, and CO₂ was adsorbed at different partial pressures. The pressure of CO₂ was increased from 0 to 0.1·10⁻², 5·10⁻² and 10·10⁻² mbar. In Figure 3-7 spectral changes caused by adsorption of CO₂ with different partial pressures on HT2 are shown. Adsorption bands at 1226, 1413, 1529, 1658, 2343 and 2360 cm⁻¹ appeared. The bands at 1413 and 1529 cm⁻¹ have been observed already before adsorption. Former bands were described by Tanabe^[43] as unidentate carbonate formed via adsorption of CO₂ on MgO. The bands at 1226 and 1658 cm⁻¹ can be assigned to CO₂ coordinated to Al sites of the mixed oxides. Hamada^[44] found bands at 1235 and 1645 cm⁻¹ after adsorption of CO₂ on alumina and suggested the interaction of CO₂ with basic surface OH groups and the formation of hydrogen carbonates. The adsorption band

at 2360 cm^{-1} is assigned to Lewis acid sites. Bands occurring at $\sim 2350\text{ cm}^{-1}$ can be assigned to linear adsorbed CO_2 on coordinatively unsaturated cations. The upward shift of free CO_2 (2345 cm^{-1}) depends on the strength of Lewis acid sites.^[44] The intensity of the bands increased with increasing partial pressures.

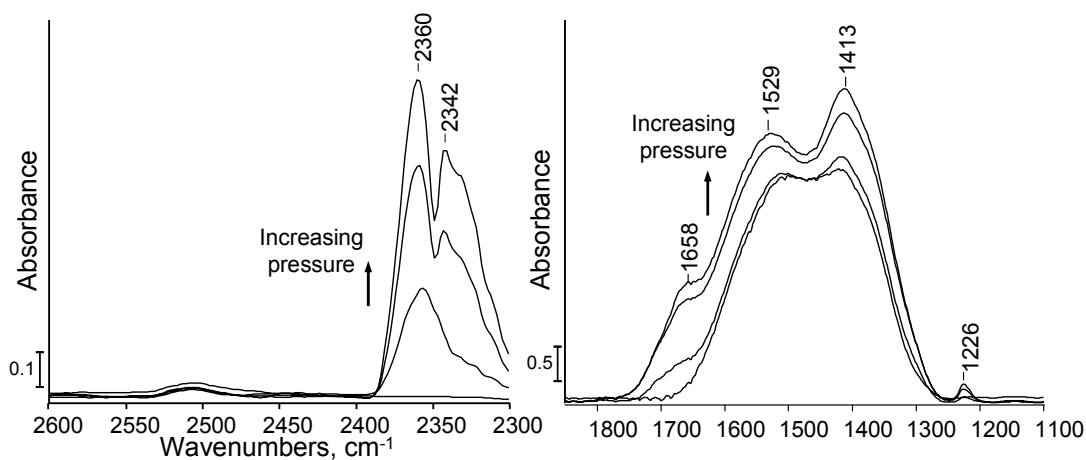


Figure 3-7. IR spectra of adsorbed CO_2 on HT2 (0 , $0.1 \cdot 10^{-2}$, $5 \cdot 10^{-2}$, $10 \cdot 10^{-2}$ mbar).

The infrared spectra upon adsorption of CO_2 for HT4 II are illustrated in Figure 3-8. The spectra show evidence of bands related to unidentate carbonate species at 1559 , 1410 , and 1370 cm^{-1} and bidentate carbonate species correlated to bands at 1787 and 1254 cm^{-1} . As for HT2, linearly adsorbed CO_2 on acidic sites was observed at 2429 and 2350 cm^{-1} . The former band can be assigned to linearly adsorbed CO_2 on Mg^{2+} as for Al^{3+} generally lower frequencies ($2360\text{--}2345\text{ cm}^{-1}$) were observed.^[45] While the spectra of HT2 were dominated by the interaction of CO_2 with alumina species, adsorption bands for HT4 II are more related to magnesium oxide. The upward shift of the band related to $\text{CO}_2\text{--Al}^{3+}$ from 2350 cm^{-1} (HT4) to 2360 cm^{-1} (HT2) indicates a stronger Lewis acidity for HT2.

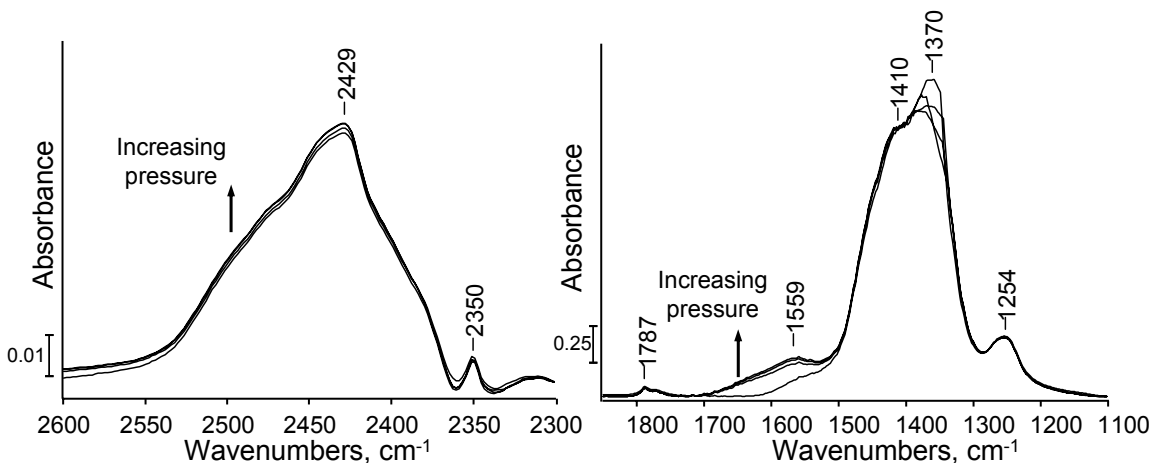


Figure 3-8. IR spectra of adsorbed CO₂ on HT4 (0, 0.1·10⁻², 5·10⁻², 10·10⁻² mbar).

3.3.6 Infrared spectroscopy of adsorbed propan-2-ol on Mg/Al mixed oxides

The adsorption of propan-2-ol on mixed metal oxides was followed by in-situ IR spectroscopy. The samples were heated with a ramp of 10 K·min⁻¹ for 2 h in vacuum to 450 °C. After cooling to 30 °C propan-2-ol was adsorbed at 0.1 mbar for 0.5 h. Afterwards the samples were out-gassed in vacuum and re-heated to 250 °C.

The difference spectra of HT2 and HT4 II after adsorption of propan-2-ol are shown in Figure 3-9 and expose various intense adsorption bands between 3000-2800 cm⁻¹ in the C-H stretching region. Bands related to carboxylate species, symmetric CH₃ and CH₂ deformation bands occurred between 1500-1300. In the low frequency region between 1170-1130 cm⁻¹ characteristic bands for C-H and C-O were observed, too. The bands at 1163 and 1128 cm⁻¹ are correlated to alcoholate species formed during dissociative adsorption of alcohols on oxidic surfaces.^[46, 47] Less intense bands were observed at 2733 and 2628 cm⁻¹ as well as at 1709 cm⁻¹ and ~1630 cm⁻¹. The strong negative band at 3735 cm⁻¹ indicates interaction of propan-2-ol with the surface OH-groups of HT2 and HT4 II. The appearance of the band at 1709 cm⁻¹ (C=O) evidenced the formation of acetone only in case of HT4 II as for HT2 this band was not observed. However, formate species (2732 and 2627 cm⁻¹) created by decomposition of acetone were observed for both samples. Also a small band appeared at 1631/1628 cm⁻¹ which is related to propene. Formation of propene was observed for both Mg/Al mixed oxides.

Due to dehydrogenation of propan-2-ol acetone is formed over dominating basic sites, while the formation of propene occurs over mainly acidic sites. The absence of acetone in case of HT2 indicates the lower basicity of that sample compared to HT4 II where acetone was present.

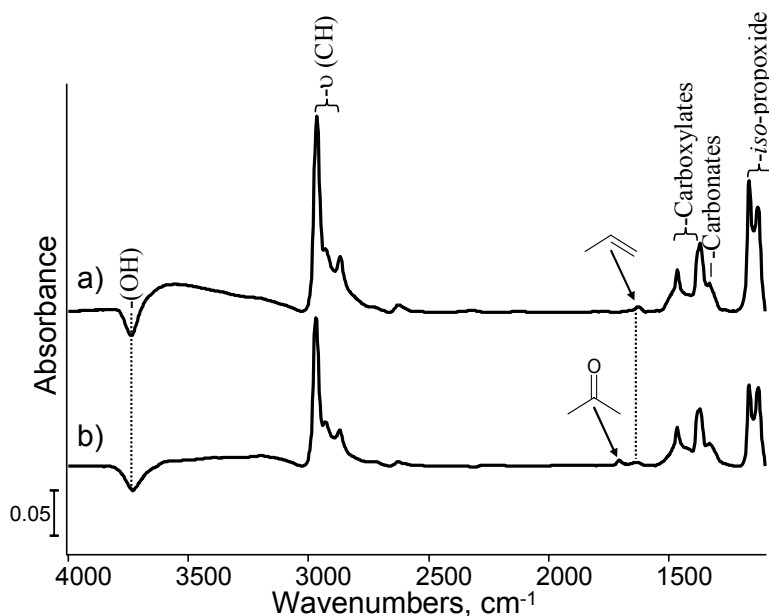


Figure 3-9. Difference spectra of Mg/Al mixed oxides after adsorption of propan-2-ol.

a) HT2 and b) HT4 II

For comparison the difference spectra of HT2 (a) and HT4 II (b) after adsorption of propan-2-ol at 30 °C for 0.5 h at 0.1 mbar and after desorption at 250 °C for 0.5 h in vacuum are illustrated in Figure 3-10. While for HT2 the adsorption bands of the CH stretching vibrations (2965, 2931 and 2869 cm^{-1}) are markedly decreased, the intensity of the broad band between 3700 and 3000 cm^{-1} related to water is clearly increased after out-gassing indicating further conversion of propan-2-ol to propene and water during temperature increase. In case of HT4 II spectral changes due to desorption at 250 °C were marginal. The intensity of CH vibration bands were slightly decreased. Therefore a strong interaction of propan-2-ol with HT4 II is expected.

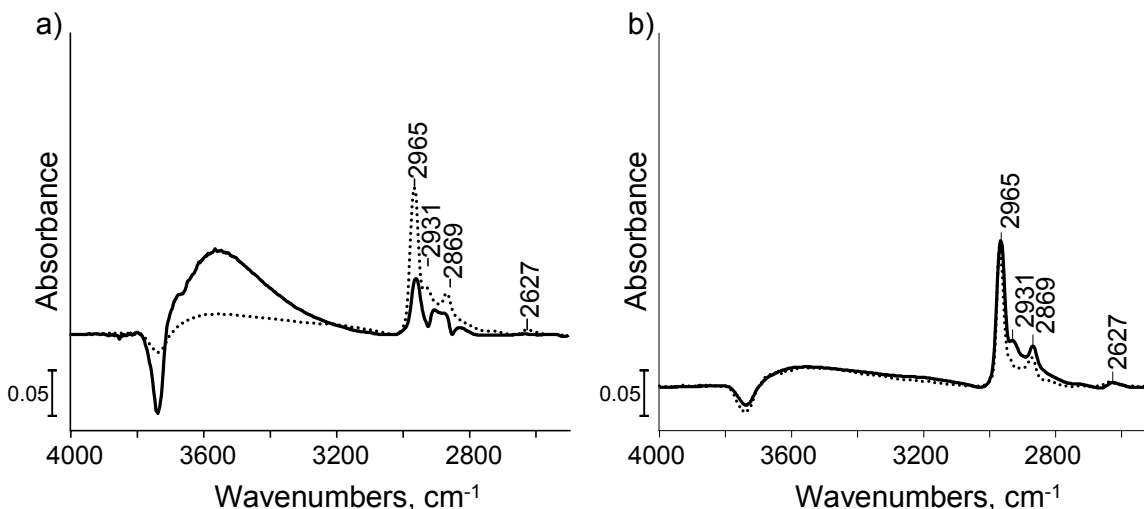


Figure 3-10. Difference spectra of Mg/Al mixed oxides after adsorption at 30 °C and desorption at 250 °C of propan-2-ol. a) HT2 and b) HT4 II
(—propan-2-ol adsorbed at 0.1 mbar, 0.5 h; ...after desorption at 250 °C)

3.3.7 Kinetics of propan-2-ol conversion

The catalytic performance of Mg/Al mixed oxides derived from hydrotalcite precursors was tested in the conversion of propan-2-ol. Generally, propene is formed via dehydration over acid sites, while over dominating basic sites, acetone occurs as main product via dehydrogenation. The selectivity of the reaction can be used as indicator for acid base properties of the mixed oxides in addition to other characterization methods as for instance of pyridine and CO₂ adsorption. The materials were heated from ambient temperature to 450 °C with heating ramp of 10 K·min⁻¹ for 2 h in inert atmosphere to activate the samples. After cooling to reaction temperature, the catalysts were tested at different carrier gas-flows (20-70 mL·min⁻¹) and temperatures (225-300 °C).

3.3.7.1 Influence of Mg/Al ratio

First, the influence of magnesium content was tested. Therefore, two different Mg/Al mixed oxides with a Mg/Al ratio of ~2 (HT2) and ~4 (HT4) were used (see chapter 2.1).

The catalytic activity of HT2 and HT4 in dehydration/dehydrogenation of propan-2-ol at a carrier-gas flow of 50 mL·min⁻¹ is shown in Figure 3-11. The activity of propan-

2-ol conversion increased with increasing temperatures for both catalysts. The rate of acetone formation for HT2 was almost 4 times less than the rate of propene formation at 225 °C. At 250 °C, the rate of dehydrogenation increased from 4 to 12 $\mu\text{mol}\cdot\text{g}^{-1}\cdot\text{s}^{-1}$ and for dehydration the rate was increased from 15 to 47 $\mu\text{mol}\cdot\text{g}^{-1}\cdot\text{s}^{-1}$. At 275 °C, the rate of dehydration was 3 times higher and at 300 °C the rate of propene formation was 2 times higher than the rate of dehydrogenation for HT2. For HT4, the rates of dehydrogenation and dehydration were almost the same at all temperatures. While at temperatures less than 300 °C the rate of acetone formation was slightly higher than for propene formation, at 300 °C the difference was marginal as it turned out to be 351 $\mu\text{mol}\cdot\text{g}^{-1}\cdot\text{s}^{-1}$ for propene and 357 $\mu\text{mol}\cdot\text{g}^{-1}\cdot\text{s}^{-1}$ for acetone. In comparison of HT2 and HT4, the latter catalyst was more active. At 225 °C the rate of dehydrogenation was 22 $\mu\text{mol}\cdot\text{g}^{-1}\cdot\text{s}^{-1}$ for HT4 and therefore more than 5 times higher than for HT2. The rate of dehydration was with 15 and 17 $\mu\text{mol}\cdot\text{g}^{-1}\cdot\text{s}^{-1}$ for HT2 and HT4, respectively, almost the same. Above 275 °C, the activity of dehydration was higher for HT4 than for HT2. Except at 225 °C, the rate of acetone formation was markedly higher for HT4 than for HT2 at all temperatures.

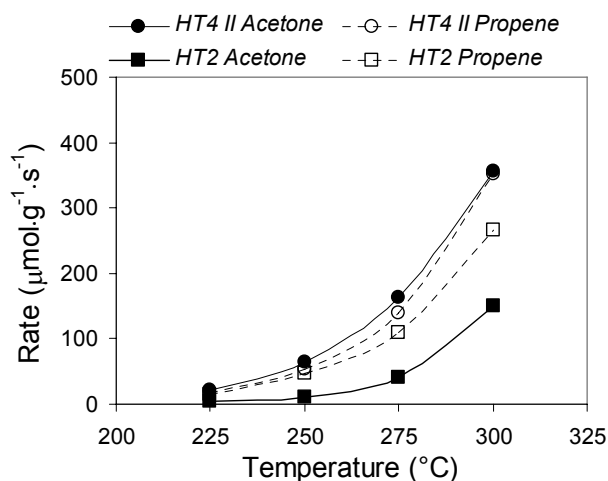


Figure 3-11. Activity of Mg/Al mixed oxides in dehydration/dehydrogenation of propan-2-ol (50 $\text{ml}\cdot\text{min}^{-1}$).

The selectivities of acetone for HT2 and HT4 during conversion of propan-2-ol at different reaction temperatures and for a He-flow of 50 $\text{mL}\cdot\text{min}^{-1}$ are listed in Table 3-2. Whereas for HT2 the selectivity of acetone was increased from 19 to 36 % with

increasing temperature from 225 to 300 °C, for HT4 the inverse performance was observed. The selectivity of acetone for HT4 was slightly decreased from 59 to 50 %.

Table 3-2. Selectivity of HT2 and HT4 II for formation acetone during the conversion of propan-2-ol.

<i>Sample</i>	<i>Selectivity_(acetone) (%)</i>			
	<i>225 °C</i>	<i>250 °C</i>	<i>275 °C</i>	<i>300 °C</i>
HT2	19	20	27	36
HT4 II	59	54	53	50

3.3.7.2 Influence of calcination temperature

The influence of calcination temperature on the catalytic performance of HT2 and HT4 was tested in the conversion of propan-2-ol. Therefore, the catalysts were calcined at elevated temperatures and activated before reaction at 450 °C as described above. HT2 was calcined at 500, 700 and 900 °C and HT4 at 200, 300, 400 and 600 °C.

The activity of acetone formation for HT2 and calcined HT2 samples hardly varied in the temperature range from 250 to 280 °C. The highest activity of dehydrogenation was observed with $277 \mu\text{mol}\cdot\text{g}^{-1}\cdot\text{s}^{-1}$ at 300 °C for HT2 calcined at 500 °C. Less activity was observed at higher calcination temperatures. Further increase of calcination temperature decreased the activity in dehydrogenation. While the calcination of HT2 at 500 and 700 °C was beneficial with respect to the activity of acetone formation compared to the non-calcined sample, the calcination at 900 °C was followed by a decrease of activity. The influence of calcination temperature for HT2 was more pronounced for the dehydration than for the dehydrogenation as can be seen in Figure 3-12. The activity of dehydration for HT2 non-calcined and calcined at 700 °C was almost the same. The highest activity was observed for HT2 calcined at 500 °C, which was $505 \mu\text{mol}\cdot\text{g}^{-1}\cdot\text{s}^{-1}$ at 300 °C. As for dehydrogenation, the lowest activity of dehydration was observed for HT2-900.

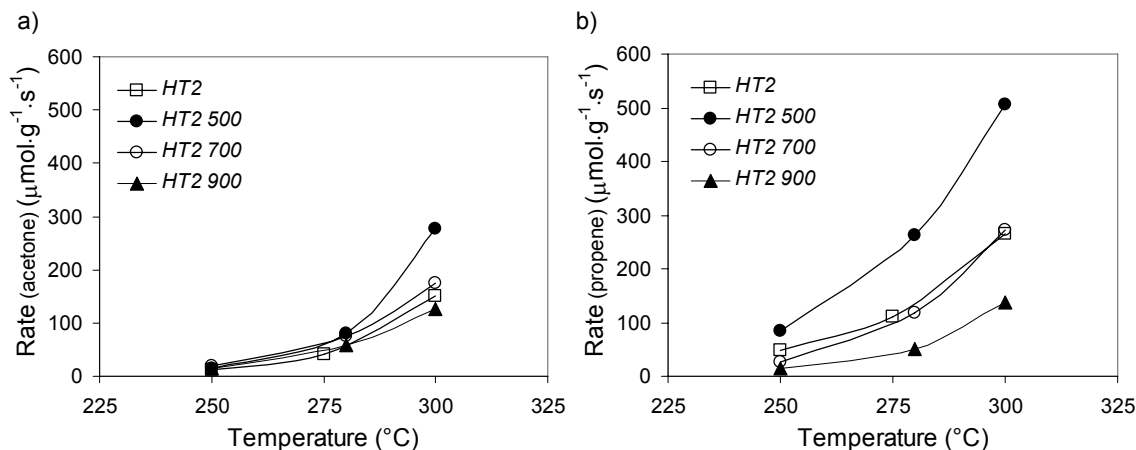


Figure 3-12. Activity of HT2 and calcined HT2 mixed oxides in the conversion of propan-2-ol.

a) Dehydrogenation and b) Dehydration.

The selectivities towards acetone for HT2 depending on all reaction and calcination temperatures is listed in Table 3-3. At 225 $^{\circ}\text{C}$, the selectivity towards acetone for HT2 was decreased by calcination at 500 $^{\circ}\text{C}$ from 20 to 14 %. Calcining at 700 and 900 $^{\circ}\text{C}$ changed the selectivities towards acetone for HT2 to 40 and 50 %, respectively. For HT2 and HT2 500, the selectivities towards acetone were increased with increasing reaction temperatures. However, for the samples calcined at higher temperatures, a decrease of selectivity of acetone was observed with increasing reaction temperatures. The highest selectivity of acetone was found for HT2-900 at 225 $^{\circ}\text{C}$. The selectivity towards acetone decreased at 225 $^{\circ}\text{C}$ in the order HT2-900 > 700 > HT2 > HT2-500. At 300 $^{\circ}\text{C}$ the same order occurred, however, the differences were less significant.

Table 3-3. Selectivities towards acetone for HT2 and calcined HT2 during conversion of propan-2-ol.

Sample	Selectivity _(acetone) (%)			
	250 $^{\circ}\text{C}$	275 $^{\circ}\text{C}$	280 $^{\circ}\text{C}$	300 $^{\circ}\text{C}$
HT2	20	27	n.d.	36
HT2-500	14	n.d.	23	35
HT2-700	40	n.d.	39	39
HT2-900	50	n.d.	50	48

Calcination at different temperatures was also performed for HT4. The resulting materials have been tested in the conversion of propan-2-ol finding an optimum in activity and selectivity.

At 225 °C, the activities in the dehydrogenation of propan-2-ol were low for all samples independent of the calcination temperature. With increasing temperatures the activity of acetone formation increased and the dependence of activity on the calcination temperature was more pronounced. The lowest dehydrogenation activity was observed for HT4 calcined at 300 °C, but the activity was generally increased with increasing calcination temperatures.

The highest dehydration activity was observed for HT4 calcined at 600 °C. With increasing reaction temperature, the dehydration rate increased for all samples. For instance, the rate at 225 °C increased from 3 to 10 $\mu\text{mol}\cdot\text{g}^{-1}\cdot\text{s}^{-1}$ at 300 °C in case of HT4-300 and HT4-400. The activity of HT4-200 in dehydration was slightly higher than for HT4 calcined at 300 and 400 °C. After calcination of HT4 at 600 °C the activity of propene formation markedly increased to 293 $\mu\text{mol}\cdot\text{g}^{-1}\cdot\text{s}^{-1}$ at 300 °C.

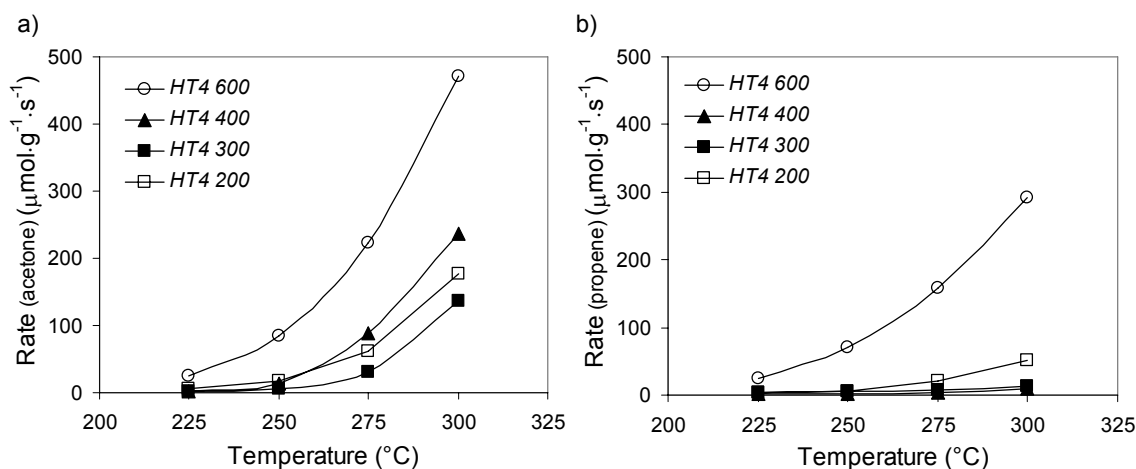


Figure 3-13. Activity of calcined HT4 III in the conversion of propan-2-ol.

a) Dehydrogenation and b) Dehydration.

The selectivities towards acetone depending on the reaction temperature for HT4 calcined at elevated temperatures are listed in Table 3-4. The highest selectivity was observed for HT4 calcined at 400 °C (97 % at 275 °C). With increasing reaction temperature the selectivity of HT4-400 was increased from 82 % at 225 °C to 96 % at 300 °C. For HT4-200 and 300, the selectivity of acetone increased with increasing reaction temperature, too. The lowest selectivity of acetone occurred for HT4-calcined at

600 °C (~50 %), in contrast to the samples calcined at temperatures less than 600 °C, for HT4-600 the selectivity was almost independent from the reaction temperature.

Table 3-4. Selectivities towards acetone for calcined HT4 III during conversion of propan-2-ol.

<i>Sample</i>	<i>Selectivity_(acetone) (%)</i>			
	<i>225 °C</i>	<i>250 °C</i>	<i>275 °C</i>	<i>300 °C</i>
HT4 III-200	73	75	74	78
HT4 III-300	57	56	83	90
HT4 III-400	82	83	97	96
HT4 III-600	50	52	50	48

3.3.7.3 Influence of sodium content

During the synthesis of Mg/Al mixed oxides via the sol-gel method, sodium hydroxide was used to adjust the pH of the reaction mixture. Depending on the washing step, residues of sodium remained in the final catalyst. As the sodium content may have an influence on the catalytic activity three samples of HT4 were synthesized, two of them were washed with either 350 or 150 mL of deionized water, the third one was not washed. After calcination, the samples were labeled as HT4 Na-350, HT4 Na-150 and HT4 Na, respectively.

The activities of HT4 in the conversion of propan-2-ol depending on the sodium content in the temperature range between 225 and 300 °C and for a carrier-gas flow of 50 mL·min⁻¹ are shown in Figure 3-14. The activity of dehydrogenation increased with increasing reaction temperatures. The highest activity of acetone formation was observed for HT4 Na-150 exhibiting an optimum of sodium content as the catalysts with higher (HT4 Na) and lower Na-content (HT4 Na-350) were less active in acetone formation. No dehydration was observed for HT4 Na. The rate of dehydration increased with increasing temperature and decreasing sodium content. Therefore, sodium might inhibit the active sites for dehydration of propan-2-ol.

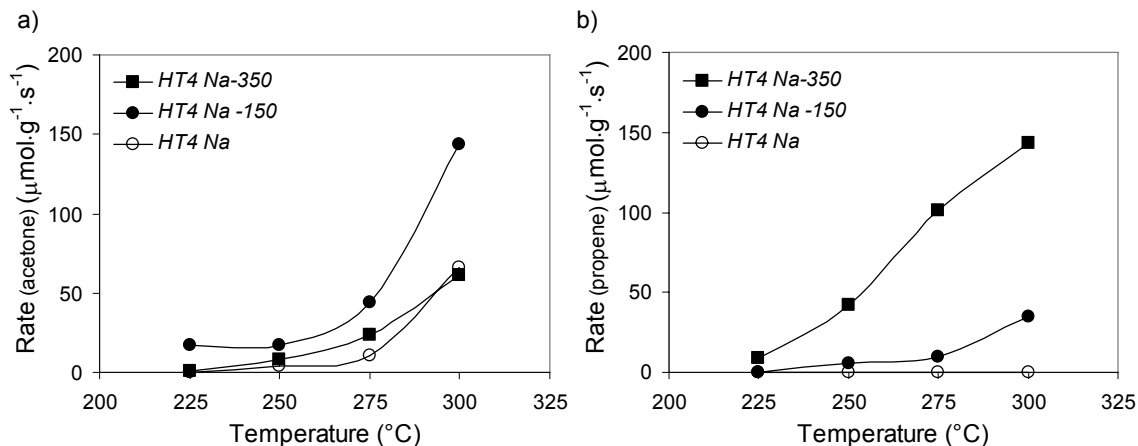


Figure 3-14. Activity of HT4 in the conversion of propan-2-ol depending on the sodium content.

a) Dehydrogenation and b) Dehydration

Sodium was removed from the final material via Soxhlet extraction with ethanol. The catalytic activities are shown in Figure 3-15. The rates of dehydration and dehydrogenation were markedly increased by removal of sodium. The activity of the non-treated sample was almost zero at all temperatures. Due to the removal of sodium the rate of dehydration increased to $49 \mu\text{mol}\cdot\text{g}^{-1}\cdot\text{s}^{-1}$ and for dehydrogenation to $157 \mu\text{mol}\cdot\text{g}^{-1}\cdot\text{s}^{-1}$ at 300°C . The temperature dependence of dehydrogenation on Na content was more pronounced compared to dehydration. At 225°C , dehydration was dominating at temperatures higher than 275°C dehydrogenation was higher and markedly increased at 300°C .

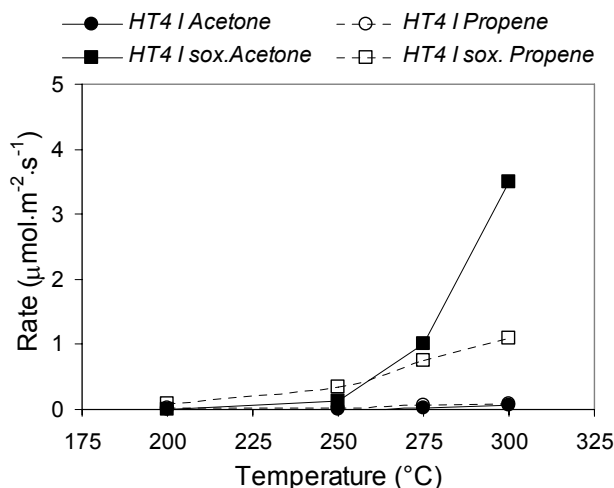


Figure 3-15. Activity of HT4 in dehydration/dehydrogenation of propan-2-ol depending on the sodium content.

The dependency of the selectivity towards acetone formation on the sodium content and temperature is listed in Table 3-5. In the series of HT4 Na, the selectivities towards acetone increased with increasing sodium content as the formation of propene was suppressed. In contrast, an additional extraction of sodium from HT4 I caused a distinct increase of selectivity.

Table 3-5. Selectivities to acetone for HT4 depending on Na-content in the conversion of propan-2-ol.

Sample	Selectivity _(acetone) (%)			
	225 °C	250 °C	275 °C	300 °C
HT4 Na	n.d.	100	100	100
HT4 Na-150	100	74	82	81
HT4 Na-350	12	16	19	30
HT4 I	n.d.	23	27	45
HT4 I sox.	n.d.	25	58	76

3.3.7.4 Reproducibility

Different batches of HT4 were synthesized and tested in the conversion of propan-2-ol to investigate the reproducibility of catalyst synthesis by sol-gel process. The conversion of propan-2-ol for different HT4s is shown in Figure 3-16. The activity varied for each catalyst. The higher the reaction temperature, the higher were the differences in activity for dehydrogenation and dehydration. HT4 I sox. and HT4 IV had almost the

same activity in conversion of propan-2-ol. The activity of HT II and HT4 III were higher than for HT4I sox. and HT4 IV. The highest activity was observed for HT4 III. The difference in activities of HT4 catalysts might be caused by disparate surface areas or sodium contents. Latter ones were described in the previous section.

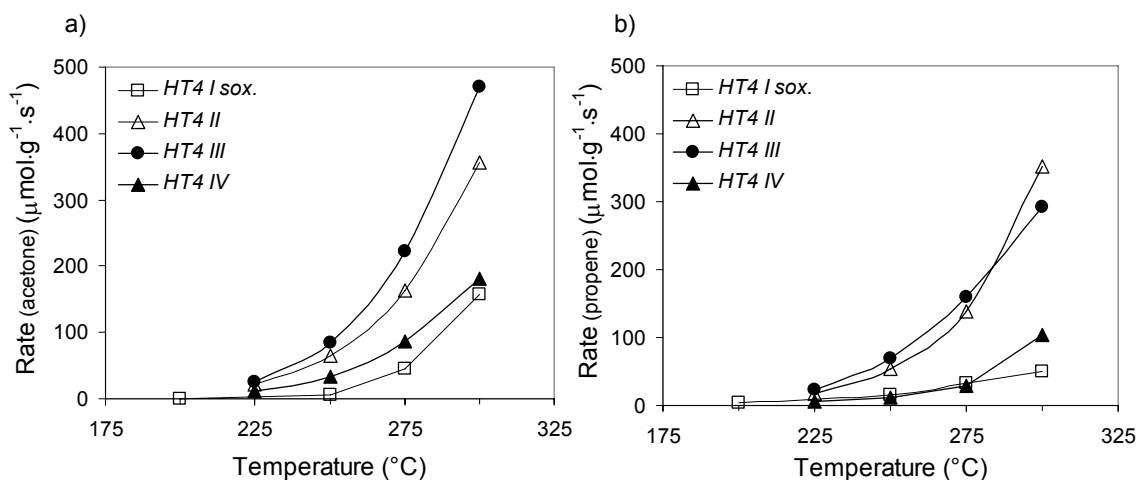


Figure 3-16. Activity of HT4 in the conversion of propan-2-ol.

a) Dehydrogenation and b) Dehydration

The selectivities towards acetone for different HT4 charges and reaction temperatures are listed in Table 3-6. For HT4 I sox., the selectivity increased with increasing reaction temperatures from 34 % at 250 °C to 77 % at 300 °C. The changes in selectivity depending on temperature were less pronounced for HT4 II, HT4 III and HT4 IV compared to HT4 I sox.. The highest selectivity of acetone was observed for HT4 IV at 225 °C with 69 %, whereas, at 300 °C the most selective sample was HT4 I sox. with 77 %.

Table 3-6. Selectivities to acetone for HT4 in the conversion of propan-2-ol.

Sample	Selectivity (acetone) (%)			
	225 °C	250 °C	275 °C	300 °C
HT4 I sox.	0	34	58	77
HT4 II	59	54	53	50
HT4 III	50	52	50	48
HT4 IV	69	73	75	64

3.4 Discussion

Mg/Al mixed oxides with a Mg/Al ratio of 4 were derived from hydrotalcite precursors by sol-gel process and a subsequent calcination in air at different temperatures. A commercial catalyst with Mg/Al ratio of 2 was used to investigate the influence of the Mg/Al ratio on the formation of acid base properties. The chemical composition of the materials was determined by AAS and was close to the nominal ones. The crystalline structure was analyzed by XRD. The structure of all materials was dominated by $\text{Mg}(\text{Al})_x\text{O}$ phase, however, depending on the sodium content, traces of sodium nitrate were identified. The samples exhibited low crystallinity with particle sizes of ~ 5 nm. The structural changes during calcination were followed by in-situ XRD exemplarily for HT4 III. Reflexes related to hydrotalcite phase were broadened and decreased in intensity at 200 °C. Complete transformation to $\text{Mg}_{(x)}\text{AlO}$ was achieved at 400 °C.

^{27}Al MAS-NMR spectroscopy was carried out to clarify the structural constitution of aluminum in the mixed metal oxides. Less octahedral alumina was observed with higher Mg/Al ratio, indicating that alumina was incorporated into the tetrahedral vacancies of MgO .

The acid sites were determined by infrared spectroscopy of adsorbed pyridine. No remarkable differences regarding the kind of acid sites were found between HT2 and HT4. The adsorption bands of both samples are similar to those of pyridine adsorbed on γ -alumina. Characteristic bands were observed at ~ 1445 and $\sim 1605\text{ cm}^{-1}$ which are related to pyd-Al^{3+} [32, 48].

The acid site strength and concentration was higher for HT2 compared to HT4. After desorption, the remaining concentration of pyridine was twice as much for HT2 compared to HT4. Brønsted acidity was neither observed for Mg/Al mixed oxides with Mg/Al ratio of 2 nor for Mg/Al ratio of 4.

The basic site properties were analyzed by infrared spectroscopy with adsorbed CO_2 . However, CO_2 can as well be used as probe molecule for Lewis acid sites like coordinatively unsaturated cations as for instance Al^{3+} or Mg^{2+} [44, 45]. The different types of resulting carbonates are shown in Figure 3-17. On HT2 bicarbonate like species occurred after adsorption of CO_2 on basic OH groups. Also adsorption bands occurred, which were similar to those observed on alumina. For HT2 in contrast to HT4 no

bidentate adsorbed CO_2 was observed. With higher Mg content the adsorbed CO_2 species were more likely related to MgO . Bicarbonate species were not found for HT4. The strength of basic sites decreases in the order $\text{O}^{2-} > \text{M}^{\text{n}+}\text{-O}^{2-} > \text{OH}$. Thus, for HT4 a stronger basicity as for HT2 is expected. Due to adsorption of CO_2 on Al^{3+} a higher acidity for HT2 was observed compared to HT4.

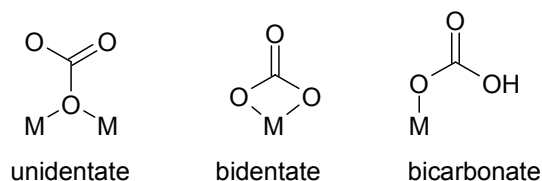


Figure 3-17. Resulting carbonate species on metal oxide surfaces after adsorption of CO_2 .

The acid-base properties of metal oxides and mixed metal oxides can also be determined by the conversion of propan-2-ol.^[48-54] In general, propene is formed by dehydration of propan-2-ol over acid centers. Dehydrogenation to acetone occurs over base or redox sites. The catalytic activity of Mg/Al mixed oxides was performed in the conversion of propan-2-ol. The influence of Mg/Al ratio, the calcination temperature and the sodium content on the selectivity and activity was investigated. The conversion of propan-2-ol at 250 °C and carrier gas-flow of 50 mL·min⁻¹ at a partial pressure of propan-2-ol of 25 mbar was less than 5 % for all catalysts, excepted for HT2 calcined at 500 °C. For this sample a maximum of 11.6 % in conversion was reached.

First, the selectivity towards acetone depending on the Mg/Al ratio will be discussed. Exemplarily, HT2 and HT4 II are compared. The selectivity increased markedly for higher Mg/Al ratio. Less Lewis acid site strength and bidentate carbonate species, determined by CO_2 IR measurements were observed for HT4. Infrared spectroscopy with adsorbed propan-2-ol showed stronger interaction with the alcohol and formation of acetone for HT4 indicating stronger basicity compared to HT2.

Second, the influence of calcination towards activity and selectivity was studied. The rate of acetone formation increased slightly for HT2 after calcination. But the selectivity towards acetone decreased after calcination at 500 °C from 20 to 14 %. As the specific surface area was higher for HT2-500 compared to HT2, impurities for instance water and carbon dioxide which blocks the active sites might be removed after

calcination. Thus, activity was enhanced. Further increase of calcination temperature to 700 °C did markedly increase the selectivity towards acetone to 40 % indicating that further carbonates were removed which had blocked basic sites before. After calcination of HT2 at 900 °C further increase of selectivity was observed confirming the assumption of carbonate removal. The decrease in activity can be explained by sintering effects which is reflected in strong decrease of the specific surface area.

HT4 was calcined at 200, 300, 400 and 600 °C. No linear correlation between calcination temperature and activity was observed. The highest selectivity of acetone with 83 % occurred for HT4 III-400. A further increase of calcination temperature to 600 °C influences the activity of the catalyst positively, as the rate of dehydrogenation was increased from 13 to 84 $\mu\text{mol}\cdot\text{g}^{-1}\cdot\text{s}^{-1}$. But, the selectivity of acetone was negatively influenced with respect to 52 %.

HT4 was synthesized using sodium containing aqueous solution is used. Depending on the amount of washing water, parts of sodium remained in the final materials. The use of sodium seems to be a draw back. Huge amounts of waste water will be produced during the washing step, big filter systems would be necessary to separate the solid products and the washing step is quite time-intensive, too. From the economical point of view, this is a big draw back of the sol-gel process. Therefore it was interesting to which extend the remaining sodium influences the catalytic properties of a mixed metal oxide. The sodium content of HT4 varied from 0 to 14 wt.-%. The results of propan-2-ol conversion revealed that sodium suppressed the dehydration reaction. The selectivity of acetone was 100 % for the highest sodium content. With decreasing amount of sodium, the selectivity dropped down to 16 % for HT4 Na-350. The highest activity of dehydrogenation was observed for the catalyst washed with 150 mL water, resulting in a sodium content of 3.2 wt.-%.

These results have been also observed for samples prepared to test the reproducibility of the synthesis. The highest activity of dehydrogenation for different batches of HT4 II-IV occurred for the sample with a sodium content of 3.2 wt.-%. In contrast when the sodium was removed after calcination by Soxhlet extraction with ethanol, the selectivity decreased. While, after removing sodium via Soxhlet extraction the activity was increased by factor of 5. The reproducibility of catalyst synthesis and the

resulting catalytic properties of Mg/Al mixed oxides derived from hydrotalcite precursor strongly depend on the sodium content. Sodium sticks in the pores and blocks active sites responsible for dehydration. The kinetic results are listed in Table 3-7.

Table 3-7. Kinetic performance of Mg/Al mixed oxides in the conversion of propan-2-ol.

<i>Sample</i>	<i>Conversion (%)</i>	<i>Selectivity (%)</i>	<i>Selectivity (%)</i>	<i>Rate ($\mu\text{mol}\cdot\text{g}^{-1}\cdot\text{s}^{-1}$)</i>	<i>Metal content (wt.-%)</i>
	Propan-2-ol	Acetone	Propene	Acetone	Na
HT2	1.7	20	80	12	0.0
HT2-500	1.6	14	86	14	0.0
HT2-700	1.5	40	60	18	0.1
HT2-900	1.0	50	50	15	0.1
HT4 I	0.2	23	77	1	13.1
HT4 I sox.	0.4	34	66	5	7.8
HT4 Na	0.1	100	0	4	14.0
HT4 Na-150	0.7	74	26	17	3.2
HT4 Na-350	1.5	16	84	8	1.2
HT4 II	3.4	54	46	65	0.0
HT4 III	3.1	52	48	84	3.2
HT4 IV	1.3	72	28	33	1.2
HT4 III-200	0.7	75	25	18	2.4
HT4 III-300	0.3	56	44	6	3.0
HT4 III-400	0.4	83	17	13	3.1

Reaction conditions: $T_r = 250\text{ }^{\circ}\text{C}$, $F_{\text{He}} = 50\text{ mL}\cdot\text{min}^{-1}$ and $p_{\text{iPr-OH}} = 25\text{ mbar}$.

3.5 Conclusions

The influence of the Mg/Al ratio in mixed metal oxides on the acid/base properties was investigated by infrared spectroscopy with adsorbed probe molecules, as pyridine, CO_2 and propan-2-ol. Further, the catalytic performance in the conversion of propan-2-ol which provides an additional test for acid-base properties of oxide catalysts was studied. Moreover, the influence on the catalytic properties by the calcination temperature and the sodium content has been investigated in detail.

High Mg/Al ratio causes high basicities, whereas the acidity decreased. Further on, sodium suppresses the dehydration reaction of propan-2-ol. However, a complete removal of sodium influences the dehydrogenation, thus, an optimal sodium content of HT4 was estimated to 1.2 wt.-%. Removing sodium during the synthesis procedure is

more effective than the post synthesis via Soxhlet extraction. The optimal calcination temperature for HT4 is determined to 400 °C. Calcination at 600 °C increases the activity of the catalyst; however, the selectivity is decreased. Calcination of the commercial catalyst HT2 benefits reactivity and selectivity, an optimal calcination temperature was determined as 700 °C.

The sol-gel process is an effective synthesis method to obtain homogeneous mixed metal oxides. Special attention has to be given to factors as pH, hydrothermal treating, washing and calcination play an important role.

3.6 References

- [1] M. Savonnet, S. Aguado, U. Ravon, D. Bazer-Bachi, V. Lecocq, N. Bats, C. Pinel, D. Farrusseng, *Green Chem.* **2009**, *11*, 1729.
- [2] Y. Y. Wang, X. X. Gong, L. Y. Dai, *Chin. J. Org. Chem.* **2009**, *29*, 1470.
- [3] K. Motokura, M. Tada, Y. Iwasawa, *J. Am. Chem. Soc.* **2009**, *131*, 7944.
- [4] D. P. Debecker, E. M. Gaigneaux, G. Busca, *Chem.-Eur. J.* **2009**, *15*, 3920.
- [5] D. Tichit, M. H. Lhouty, A. Guida, B. H. Chiche, F. Figueras, A. Auroux, D. Bartalini, E. Garrone, *J. Catal.* **1995**, *151*, 50.
- [6] C. Yang, Z. Y. Meng, *Act. Chim. Sinica* **1993**, *51*, 79.
- [7] A. L. Kantam, V. Balasubrahmanyam, K. B. S. Kumar, G. T. Venkanna, F. Figueras, *Advanced Synthesis & Catalysis* **2007**, *349*, 1887.
- [8] S. Abello, F. Medina, D. Tichit, J. Perez-Ramirez, J. E. Sueiras, P. Salagre, Y. Cesteros, *Appl. Catal., B* **2007**, *70*, 577.
- [9] V. K. Diez, C. R. Apesteguia, J. I. Di Cosimo, *J. Catal.* **2006**, *240*, 235.
- [10] S. Abello, F. Medina, D. Tichit, J. Perez-Ramirez, X. Rodriguez, J. E. Sueiras, P. Salagre, Y. Cesteros, *Appl. Catal., A* **2005**, *281*, 191.
- [11] V. K. Diez, C. R. Apesteguia, J. I. Di Cosimo, *Latin American Applied Research* **2003**, *33*, 79.
- [12] R. M. De Graaf, J. Visscher, Y. Xu, G. Arrhenius, A. W. Schwartz, *J. Mol. Evol.* **1998**, *47*, 501.
- [13] J. I. Di Cosimo, V. K. Diez, C. R. Apesteguia, *Appl. Catal., A* **1996**, *137*, 149.
- [14] M. L. Bailly, C. Chizallet, G. Costentin, J. M. Krafft, H. Lauron-Pernot, M. Che, *J. Catal.* **2005**, *235*, 413.
- [15] S. van Dommele, K. P. de Jong, J. H. Bitter, *Top. Catal.* **2009**, *52*, 1575.
- [16] J. Li, H. Sun, X. C. Cai, L. Y. Dai, *Chin. J. Org. Chem.* **2007**, *27*, 1296.
- [17] T. Seki, M. Onaka, *J. Mol. Catal. A: Chem.* **2007**, *263*, 115.
- [18] L. Martins, T. J. Bonagamba, E. R. de Azevedo, P. Bargiela, D. Cardoso, *Appl. Catal., A* **2006**, *312*, 77.
- [19] C. L. Xu, J. K. Bartley, D. I. Enache, D. W. Knight, G. J. Hutchings, *Synthesis-Stuttgart* **2005**, 3468.

- [20] K. P. Volcho, S. Y. Kurbakova, D. V. Korchagina, E. V. Suslov, N. F. Salakhutdinov, A. V. Toktarev, G. V. Echevskii, V. A. Barkhash, *J. Mol. Catal. A: Chem.* **2003**, 195, 263.
- [21] B. C. Ranu, S. Banerjee, R. Jana, *Tetrahedron* **2007**, 63, 776.
- [22] S. V. Bordawekar, R. J. Davis, *J. Catal.* **2000**, 189, 79.
- [23] F. L. Mi, S. S. Shyu, C. K. Peng, *Journal Of Polymer Science Part A-Polymer Chemistry* **2005**, 43, 1985.
- [24] Z. Y. Zhong, P. J. Dijkstra, J. Feijen, *J. Biomater. Sci., Polym. Ed.* **2004**, 15, 929.
- [25] M. J. Climent, A. Corma, S. B. A. Hamid, S. Iborra, M. Mifsud, *Green Chem.* **2006**, 8, 524.
- [26] B. Q. Xu, T. Yamaguchi, K. Tanabe, *Appl. Catal.* **1991**, 75, 75.
- [27] M. J. Climent, A. Corma, S. Iborra, K. Epping, A. Velty, *J. Catal.* **2004**, 225, 316.
- [28] P. Kustrowski, D. Sulkowska, L. Chmielarz, A. Rafalska-Lasocha, B. Dudek, R. Dziembaj, *Microporous Mesoporous Mater.* **2005**, 78, 11.
- [29] J. S. Valente, F. Figueras, M. Gravelle, P. Kumbhar, J. Lopez, J. P. Besse, *J. Catal.* **2000**, 189, 370.
- [30] M. Trombetta, G. Ramis, G. Busca, B. Montanari, A. Vaccari, *Langmuir* **1997**, 13, 4628.
- [31] A. Corma, V. Fornes, F. Rey, *J. Catal.* **1994**, 148, 205.
- [32] H. A. Prescott, Z. J. Li, E. Kemnitz, A. Trunschke, J. Deutsch, H. Lieske, A. Auroux, *J. Catal.* **2005**, 234, 119.
- [33] D. Tichit, B. Coq, *Cattech* **2003**, 7, 206.
- [34] V. Calvino-Casilda, R. Martin-Aranda, I. Sobczak, M. Ziolek, *Appl. Catal., A* **2006**, 303, 121.
- [35] S. I. Fujita, B. M. Bhanage, D. Aoki, Y. Ochiai, N. Iwasa, M. Arai, *Appl. Catal., A* **2006**, 313, 151.
- [36] C. T. Fishel, R. J. Davis, *Langmuir* **1994**, 10, 159.
- [37] L. L. Murrell, *Catal. Today* **1997**, 35, 225.
- [38] X. Zhang, *Mater. Chem. Phys.* **2009**, 116, 415.
- [39] H. Grabowska, M. Zawadzki, L. Syper, W. Mista, *Appl. Catal., A* **2005**, 292, 208.

- [40] H. C. Greenwell, P.J. Holliman, W. Jones, B. V. Velasco, *Catal. Today* **2006**, *114*, 397.
- [41] G. D. Wu, X. L. Wang, B. Chen, J. P. Li, N. Zhao, W. Wei, Y. H. Sun, *Appl. Catal., A* **2007**, *329*, 106.
- [42] M. I. Zaki, M. A. Hasan, L. Pasupulety, *Langmuir* **2001**, *17*, 768.
- [43] Y. Fukuda, K. Tanabe, *Bull. Chem. Soc. Jpn.* **1973**, *46*, 1616.
- [44] M. Haneda, E. Joubert, J. C. Menezes, D. Duprez, J. Barbier, N. Bion, M. Daturi, J. Saussey, J. C. Lavalley, H. Hamada, *P Phys. Chem. Chem. Phys.* **2001**, *3*, 1366.
- [45] F. Prinetto, G. Ghiotti, R. Durand, D. Tichit, *J. Phys. Chem. B* **2000**, *104*, 11117.
- [46] E. Finocchio, G. Busca, V. Lorenzelli, *J. Chem. Soc., Faraday Trans.* **1994**, *90*, 3347.
- [47] C. Hagglund, B. Kasemo, L. Osterlund, *J. Phys. Chem. B* **2005**, *109*, 10886.
- [48] F. M. Bautista, J. M. Campelo, A. Garcia, D. Luna, J. M. Marinas, A. A. Romero, M. R. Urbano, *Catal. Lett.* **1995**, *35*, 143.
- [49] P. Michorczyk, E. Sikora, J. Ogonowski, *React. Kinet. Catal. Lett.* **2008**, *94*, 243.
- [50] A. M. Youssef, A. I. Ahmed, S. E. Samra, N. B. El-Assy, E. A. El-Sharkawy, *Adsorpt. Sci. Technol.* **2000**, *18*, 777.
- [51] C. Lahousse, F. Mauge, J. Bachelier, J. C. Lavalley, *J. Chem. Soc., Faraday Trans.* **1995**, *91*, 2907.
- [52] A. Ouqour, G. Coudurier, J. C. Vedrine, *J. Chem. Soc., Faraday Trans.* **1993**, *89*, 3151.
- [53] A. M. Youssef, L. B. Khalil, B. S. Girgis, *Appl. Catal., A* **1992**, *81*, 1.
- [54] M. Richter, G. Ohlmann, *Appl. Catal.* **1988**, *36*, 81.

Chapter 4

Zinc modified Magnesium/Aluminum Mixed oxides

Abstract

The impact of zinc cations on Mg-Al mixed oxides is explored in the Zn^{2+} concentration range from 20 to 60 mol-%. The Mg/Zn/Al metal oxides are derived by calcination of adequate layered double hydroxide precursors obtained via a sol-gel process. Structural analysis by XRD and ^{27}Al MAS-NMR show that Al^{3+} is incorporated into the MgO/ZnO lattice realizing close vicinity between the different metal cations. The acid site concentration increases with increasing zinc content, while the basic site density remains almost constant. Acetone is the primary reaction product from propan-2-ol elimination with all zinc containing oxides. Already low concentrations of Zn^{2+} lead to highly active, selective and stable catalysts.

4.1 Introduction

Metal oxides derived from hydrotalcites and layered double hydroxides (LDH) are versatile solid base catalysts, which have been thoroughly explored in the past two decades.^[1] The substitution of cations into the LDH precursor materials provides a facile and highly reproducible route to adjust the acid-base properties of the mixed oxides. Such an effect could be associated with generating a higher specific surface area,^[2] but mainly induces an increase of the concentration of partially unsaturated metal cations equivalent to higher Lewis acid site concentrations (see also ref.^[3]). It should be noted that the intrinsic strength of acid and base sites tend to change in a more steady way between the properties of the constituents of the materials.^[4]

An especially interesting case is the incorporation of Zn cations in lattices of aluminum mediated MgO-ZnO mixed oxides. Ghiotti and Boccuzzi^[5], for example, described that new active sites were formed in Zn modified MgO solid solutions. Mg^{2+} acts as a hard acid with low ability to polarize soft bases such as hydride ions (H^-), while Zn^{2+} is a softer acid. Interestingly, it is claimed that in a solid mixture of MgO-ZnO, zinc acts as softer acid compared to the pure ZnO.

The application of zinc oxide or mixed zinc oxide catalysts in the conversion of propan-2-ol has been described.^[6,7,8,9,10,11,12,13,14] ZnO is an excellent alcohol dehydrogenation catalyst achieving selectivities above 90 %. As this reaction is also frequently used as proof for acid-base properties of oxides, it has been our interest to explore the impact of Zn cations on Mg/Al mixed oxides with the goal to customize acid-base properties regarding a higher activity and selectivity with respect to alcohol elimination reactions. TPD experiments by Bowker^[9] suggest that alkoxides are the critical intermediates in this catalytic conversion. The apparent inconsistency of acid-base properties determined by probe molecules such as ammonia (corresponding more to acidic than basic behavior) to the dominating dehydrogenation activity (observed in catalytic reactions with alcohols) of ZnO was discussed by Vinek et al..^[15] The discrepancy of displaying quite acidic properties towards probe molecules and the behavior as solid base in reactions with alcohols has been attributed to the partial reduction of the zinc oxide surface in contact with alcohols. This has been reconfirmed by

hydrogen adsorption experiments of Ghiotti and co-workers⁵ arguing that Zn^{2+} is by far easier reduced than Mg^{2+} . It is interesting to note, however, that the (low) dehydration activity has been clearly associated with the presence of unsaturated zinc ions, i.e., oxygen vacancies and point defects.^[14]

On the other hand the marked basic properties of the oxygen in ZnO are in good agreement with the observed low O1s electron binding energies, i.e., 532-530 eV.¹⁵ Dimitrov^[16] discussed the correlation between optical basicity and the O1s binding energy of simple oxides noting that ZnO had a higher basicity than MgO. The optical basicity is an indicator for the electron donating power of O^{2-} to the M^{n+} cation in MO_x oxides.^[17] This value was also determined by UV/vis spectroscopy of molten Pb^{2+} salts mixed with ZnO or MgO. The position of the $6s \rightarrow 6p$ UV absorption band was used as indicator of the electron (pair) donating power.

Thus, the partly reducible mixed oxide acts via acid-base paired sites and it would be interesting to explore, how the presence of a third (hard) cation influences the overall acid base properties and in particular the catalytic activity towards dehydrogenation. In this chapter, therefore, the influence of zinc on Mg/Al metal oxides is investigated using ^{27}Al MAS-NMR, as well as NH_3 - and CO_2 -TPD to characterize the acid-base properties. Catalytic activity was studied in the gas phase elimination reaction of propan-2-ol, frequently used as test reaction for acid and base properties of surface modified oxides.^[9,18,19,20,21] The application of Mg/Zn/Al oxides as solid base catalyst in liquid phase reactions was explored in the ring-opening reaction of 1,2-epoxy-octane with hexanol.

4.2 Experimental

4.2.1 Zinc modified Mg/Al mixed oxides

Metal oxides containing magnesium, aluminum and zinc were obtained by heating of adequate LDH precursors in air. LDHs were synthesized via a sol-gel process adopted from a method described by Greenwell et al..^[22] The $\text{M}^{2+}/\text{M}^{3+}$ molar ratios were kept constant to 4, while the $\text{Zn}^{2+}/\text{Mg}^{2+}$ ratio was varied from 0.33 to 3 going from low to high content of Zn in the materials.

An acidic aqueous solution (1 M) of metal nitrates was prepared by dissolving $\text{Mg}(\text{NO}_3)_2 \cdot 6\text{H}_2\text{O}$, $\text{Zn}(\text{NO}_3)_2 \cdot 6\text{H}_2\text{O}$ and $\text{Al}(\text{NO}_3)_3 \cdot 9\text{H}_2\text{O}$ in 0.6 L decarbonized bidistilled water. A second alkaline solution was prepared from NaOH (2 M) and NaHCO_3 (0.1 M). Both solutions were heated to 75 °C. For precipitation, the nitrate and alkaline solutions were added drop-wise to 400 mL water giving a pH = 10 at 75 °C. The suspension was aged for 3 h at 85 °C under vigorous stirring. After cooling to RT, the gel was filtered and loaded into an autoclave. Hydrothermal synthesis was carried out for 16 h at 80 °C. The gel was washed with 350 mL bi-distilled water until a pH of 7 of the washing water was reached. The white precipitate was freeze-dried, grounded and heated to 600 °C (heating rate 5 °C·min⁻¹) in a flow of 100 mL·min⁻¹ synthetic air for 8 h.

The used molar contents of metal nitrate precursors and the chemical compositions in the resulting materials are depicted in Table 4-1.

Table 4-1. Molar contents of metals and amounts of nitrate precursors used for metal oxide synthesis.

Mg/Zn/Al Ox Zn-content (mol-%)	Molar ratios			Amount of nitrate precursor (mol·L ⁻¹)		
	Mg	Zn	Al	Mg	Zn	Al
0	4.0	0	1	0.8	-	0.2
20	3.0	1.0	1	0.6	0.2	0.2
26	2.7	1.3	1	0.53	0.27	0.2
40	2.0	2.0	1	0.4	0.4	0.2
54	1.3	2.7	1	0.27	0.53	0.2
60	1.0	3.0	1	0.2	0.6	0.2

4.2.2 Characterization

The metal concentrations of Mg/Zn/Al oxides were analyzed by atomic absorption spectroscopy (AAS) using an *UNICAM 939 AA-Spectrometer*.

Specific surface areas and pore volumes were determined by physisorption of N₂ at 77 K. Measurements were carried out in a *PMI automatic BET-Sorptometer*. Evaluation of the data was done according to the BET theory.

The crystalline structure was analyzed by XRD using a *Philips X'Pert Pro System* (Cu K α , 0.154056 nm) at 40 kV / 40 mA. The measurements were taken by using a spinner and a 1/6'' slit in the range from 20 ° to 70° 2 θ (0.05 °/min).

²⁷Al MAS-NMR measurements were performed on a *Bruker AV500 spectrometer* (B₀ = 14.1 T) at a spinning rate of 12 kHz. The temperature was adjusted by passing the bearing and drive gas stream through a heat exchanger. The samples were packed in 4 mm ZrO₂ rotors. As resonance frequency 130.3 MHz was used. The spectra were recorded as the sum of 2400 scans with a recycle time of 250 ms. A $\pi/12$ pulse (pulse length = 1.0 μ s) was applied for excitation. The chemical shift was referenced against an external standard of solid Al(NO₃)₃ (δ = -0.54 ppm).

Temperature programmed desorption of ammonia (NH₃-TPD) and carbon dioxide (CO₂-TPD) were used to determine the acidic and basic properties. As standard materials for referencing the NH₃-TPD and CO₂-TPD, a H-MFI 90 zeolite and NaHCO₃ were used, respectively. Catalyst samples were activated at 450 °C for 1 h in vacuum. Ammonia was adsorbed at 1 mbar and 100 °C for 1 h and CO₂ (1 mbar) was adsorbed at 40 °C for 1 h. For desorption, the samples were heated to the corresponding temperature (up to 500 °C for CO₂-TPD) with a rate of 10 K·min⁻¹; desorbing gases were monitored with a *Pfeifer mass spectrometer*.

Temperature programmed oxidation (TPO) of used catalysts was carried out on a multi-reactor setup equipped with six parallel reactors and a mass spectrometer as detector for desorbing gases. The samples (0.02 g) were diluted with SiO₂ powder (0.13 g) and filled into the reactor using quartz-wool. The used catalysts were heated at 100 °C for 1 h in a flow of He (50 mL·min⁻¹) to remove physisorbed contaminations from air and of propan-2-ol reaction. For oxidation an oxygen/helium flow (10 mL·min⁻¹) with 5 vol-% oxygen was passed over the catalyst sample during heating from 100 to 900 °C (heating rate of 2°C·min⁻¹).

4.2.3 Catalytic tests

The as-prepared samples (0.02 g diluted in 0.13 g SiC) were fixed with quartz wool in a quartz-tube reactor of 4 mm diameter. The samples were activated by rising the temperature from ambient to 450 °C for 2 h ($10\text{ }^{\circ}\text{C}\cdot\text{min}^{-1}$) in a flow of He ($20\text{ mL}\cdot\text{min}^{-1}$). Then, the catalysts were cooled to reaction temperature and a flow of helium (30, 50 and $70\text{ mL}\cdot\text{min}^{-1}$) saturated with propan-2-ol ($p_{\text{propan-2-ol}} = 25\text{ mbar}$ at $13\text{ }^{\circ}\text{C}$) was passed through the fixed bed reactor. The dehydrogenation/dehydration of propan-2-ol was studied within the temperature range of 225 to 300 °C in temperature intervals of 25 °C. At each temperature the catalyst was treated with propan-2-ol for 80 min. Un-reacted propan-2-ol and dehydrogenation/dehydration products were analyzed by gas chromatography using a *Hewlett Packard 5890 (Series II) GC* equipped with a flame ionization detector. The separation of the various components was done by a Q-column.

The condensation of 1,2-epoxy-octane with hexanol was performed in a 100 mL flask. Hexanol (2.555 g, 0.025 mol) was added to 1,2-epoxy-octane (4.038 g, 0.026 mol) and heated to 160 °C in a nitrogen atmosphere while stirring. The catalyst (0.066 g, 1 wt.-%) was added and samples were taken every hour. The catalyst was removed by filtration. The filtrate (100 μL) was mixed with 2,2,4-tri-methylpentane (937 μL) as internal standard for GC-analysis. The unreacted 1,2-epoxy-octane, hexanol and reaction products were analyzed by gas chromatography using a *Shimadzu GC-2010*.

4.3 Results

4.3.1 Textural analysis

The metal contents, the specific surface areas as well as the concentrations of acid and basic sites determined by CO_2 - and NH_3 -TPD (see also section 4.3.4) of all Mg/Al and Mg/Zn/Al oxides are compiled in Table 4-2. The final molar metal concentrations were close to the nominal ones. The specific surface areas of Mg/Al and zinc containing oxides varied between a maximum value of $188\text{ m}^2\cdot\text{g}^{-1}$ (0 mol-% Zn) and a minimum value of $64\text{ m}^2\cdot\text{g}^{-1}$ (60 mol-% Zn), i.e., it decreased in general with increasing zinc concentration. It should be noted, however, the sample with 40 mol-% Zn had a slightly

higher specific surface area ($111 \text{ m}^2 \cdot \text{g}^{-1}$) than that of the sample with 26 mol-% Zn ($100 \text{ m}^2 \cdot \text{g}^{-1}$).

Table 4-2. Textural analysis and acid-base properties (according to TPD of NH_3 and CO_2) of Mg/Zn/Al oxides.

Sample	$(\text{Mg/Zn})_{(\text{Mg}+\text{Zn})/\text{Al}}$ $(\text{mol}:\text{mol}:\text{mol})$	S_{BET} $(\text{m}^2 \cdot \text{g}^{-1})$	Acid sites $(\mu\text{mol} \cdot \text{m}^{-2})$	Basic sites $(\mu\text{mol} \cdot \text{m}^{-2})$
Mg/Zn/Al Ox-0	(1:0) _{3,8} :1	188	0.15	0.098
Mg/Zn/Al Ox-20	(2.5:1) _{3,8} :1	123	0.13	0.019
Mg/Zn/Al Ox -26	(1.7:1) _{3,8} :1	100	0.18	0.022
Mg/Zn/Al Ox -40	(1:1.2) _{3,9} :1	111	0.21	0.019
Mg/Zn/Al Ox -54	(1:2.4) _{3,8} :1	75	0.24	0.031
Mg/Zn/Al Ox -60	(1:4) _{3,7} :1	64	0.70	0.040

4.3.2 XRD analysis

The X-ray diffractograms of the Mg/Zn/Al oxides and the mean particle size are compiled in Figure 4-1. The particle sizes were determined using the half width of the MgO reflection at $2\theta = 42.8^\circ$ (0 mol-% Zn) or of the ZnO reflection located at $2\theta = 34.5^\circ$ (≥ 20 mol-% Zn). The particle size increased with increasing zinc content from 6 nm (0 mol-% Zn) to 25 nm (54 mol-% Zn).

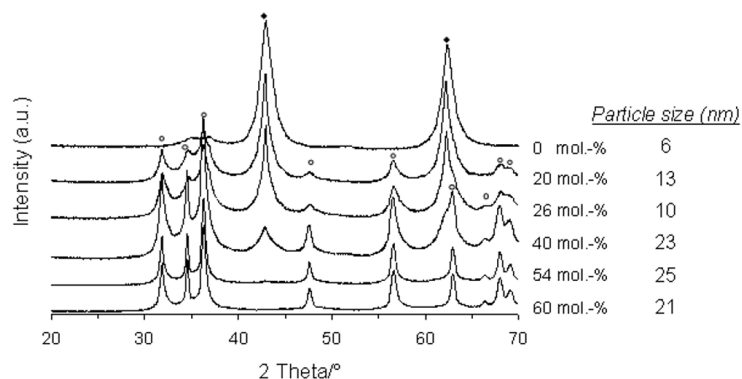


Figure 4-1. XRD analysis of MgAl and Mg//Zn/Al metal oxides. (°ZnO, ♦MgO).

For all zinc containing samples the ZnO reflex at $2\theta \sim 34^\circ$ was observed, however, with decreasing zinc content the shape of the reflex was more diffuse. The reflex at $2\theta = 42.8^\circ$ (MgO) decreased with lower magnesium contents. The main reflexes of Al_2O_3 are generally observed at $2\theta = 37.0^\circ$, 45.6° and 67.1° . However, a separated alumina phase was not identified. It is speculated that for Mg/Zn/Al oxides with 54 and 60 mol-% zinc one phase including all three metals was formed as no separated phases for MgO and Al_2O_3 were observed.

4.3.3 ^{27}Al MAS-NMR spectroscopy

^{27}Al MAS-NMR spectroscopy of the solid materials was used to identify changes in the aluminum coordination by variation of the Mg/Zn ratio (see Fig. 4-2). All ^{27}Al MAS-NMR spectra exhibit two main signals at around 75 and 9 ppm characteristic for tetrahedral Al^{IV} and octahedral Al^{VI} , respectively.^[23,24] With zinc contents higher than 26 mol-% a broadening of the signal at 75 ppm was observed indicating distortion of the tetrahedral environment. A further increase of the zinc content (> 40 mol-%) led to the formation of an additional signal at 65 ppm. The signal is attributed to a second type of tetrahedral aluminum species, most probably in the vicinity of zinc.^[25,26] The ratio of tetrahedral Al^{IV} to octahedral aluminum Al^{VI} varied from 0.09 (0 mol-% Zn) to 0.89 (54 mol-% Zn).

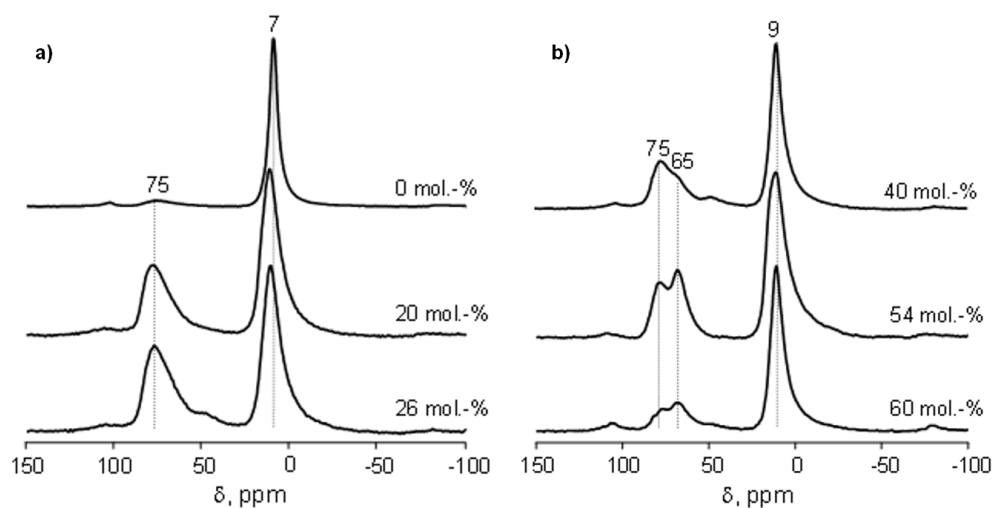


Figure 4-2. ^{27}Al -MAS NMR spectra of Mg/Al and Mg/Zn/Al oxides.

4.3.4 Acid and base properties determined by NH_3 - and CO_2 -TPD

The ammonia desorption profiles for Mg/Al and Mg/Zn/Al oxides (see Figure 4-3a) displayed a maximum at approximately 215 °C for all samples. The intensity of the desorption maximum of the material with a zinc content of 60 mol-% was two times higher than for all other samples. The profiles of the materials with a zinc content below 60 mol-% hardly varied showing only a slight increase in intensity with higher Zn contents.

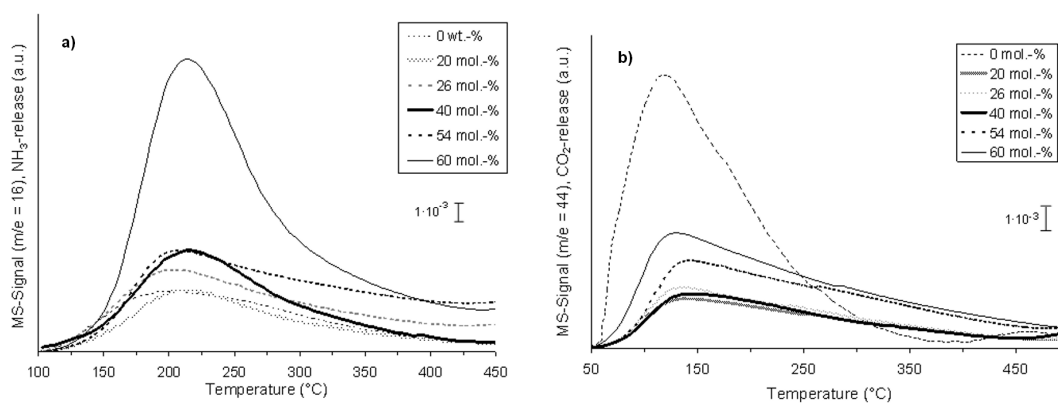


Figure 4-3. TPD-desorption profiles for Mg/Al and Mg/Al/Zn oxides. a) NH_3 -TPD and b) CO_2 -TPD.

The desorption profiles of carbon dioxide for Mg/Zn/Al oxides hardly varied (see Figure 4-3b). Broad peaks with maxima between 100 and 150 °C were observed for all samples. In comparison to the sample without zinc, the intensity of the desorption peak markedly decreased, while the position of the maximum was slightly shifted to higher temperatures by modification with zinc indicating a slightly stronger interaction.

4.3.5 Kinetics of elimination reactions of propan-2-ol

The catalytic activities between 225 and 300 °C in dehydrogenation (a) and dehydration (b) of propan-2-ol for the Mg/Al and Mg/Zn/Al catalysts are shown in Figure 4-4 and summarized in Table 4-3.

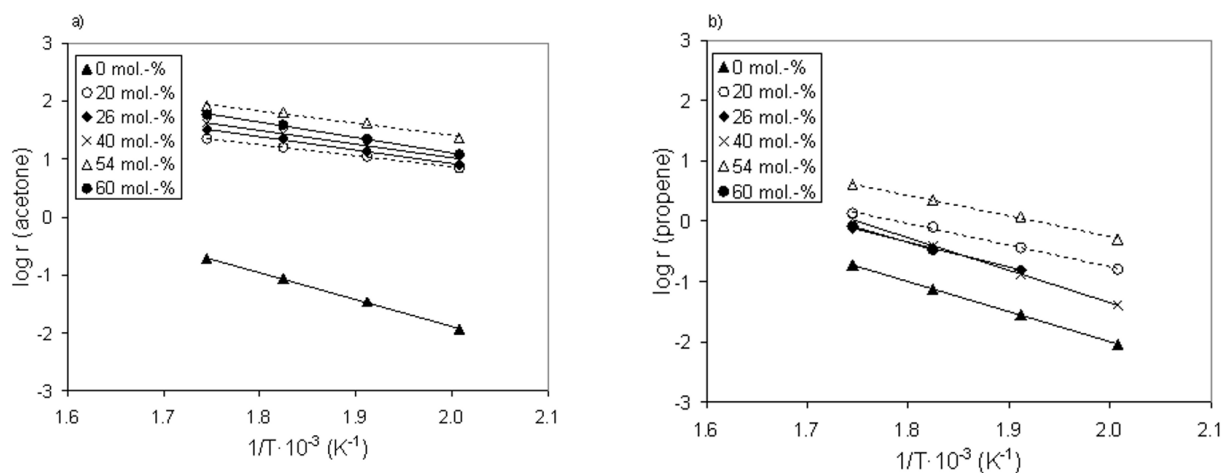


Figure 4-4. log rate of product formation of propan-2-ol conversion vs. $1/T$ for Mg/Al and Mg/Zn/Al oxides (carrier gas flow = 50 mL·min⁻¹). a) Acetone and b) Propene.

The elimination of hydrogen and water from propan-2-ol leading to acetone and propene, respectively, was markedly increased by adding zinc to Mg/Al oxides, i.e., by a factor of almost 200 in case of dehydrogenation and a factor of 11 for dehydration. In general, the activity of propan-2-ol dehydrogenation was increased with increasing zinc contents. Independent of the reaction temperature, the highest rate of acetone formation was found for the catalyst with 54 mol-% zinc. Even though the rate of dehydrogenation (see Fig. 4-4a) was increasing, a nearly constant apparent energy of activation $40 \pm 11 \text{ kJ} \cdot \text{mol}^{-1}$ was observed.

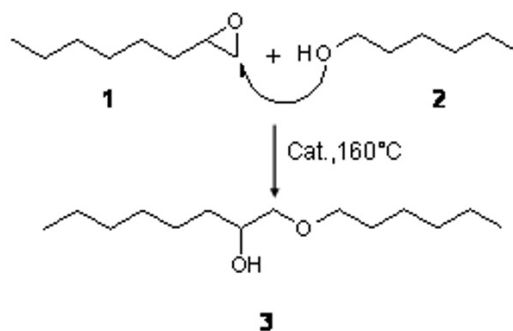
Table 4-3. Selectivities towards acetone of Mg/Al and Mg/Zn/Al oxides between 225-300 °C for propan-2-ol conversion.

Temperature (°C)	Selectivity _(acetone) (%)					
	Mg/Zn/Al O _x -0	Mg/Zn/Al O _x -20	Mg/Zn/Al O _x -26	Mg/Zn/Al O _x -40	Mg/Zn/Al O _x -54	Mg/Zn/Al O _x -60
225	56	98	100	100	98	100
250	55	97	99	99	97	100
275	54	95	98	99	97	99
300	50	94	98	98	95	99

The rate of dehydration was significantly lower than that of dehydrogenation for all zinc containing catalysts. With zinc contents higher than 20 mol-%, the rate of propene formation hardly varied with the exception of the catalyst with 54 mol-% zinc, which proved to be the most active one. The apparent energy of activation for dehydration was $79 \pm 14 \text{ kJ} \cdot \text{mol}^{-1}$ for all catalysts except for Mg/Zn/Al O_x-40 ($103 \text{ kJ} \cdot \text{mol}^{-1}$).

4.3.6 Application in the condensation of 1,2-epoxy-octane with hexanol

Ring opening reactions of epoxides are useful routes in organic synthesis of allylic and aliphatic compounds catalyzed by acids and bases.^[27,28,29] The reaction of 1,2-epoxy-octane (1) with hexanol (2) is a nucleophilic substitution in which the alcohol acts as the nucleophile and 1-(hexyloxy)octane-2-ol (3) is formed as the main product. The reaction scheme of the nucleophilic ring-opening reaction of the epoxide is depicted in Figure 4-5.

**Figure 4-5.** Reaction scheme of the nucleophilic ring-opening reaction of 1,2-epoxy-octane with hexanol.

The catalytic performance of zinc modified Mg/Al oxides in the ring-opening reaction of 1,2-epoxy-octane with hexanol at 160 °C is shown in Figure 4-6. The highest yield of 1-(hexyloxy)octane-2-ol was observed for the catalyst with the lowest zinc content, i.e., 20 mol-%. Increasing zinc contents led to a significant drop in the activities. The yield decreased in the order Mg/Zn/Al O_x 20 > 26 > 40 > 54 > 60 mol-% zinc.

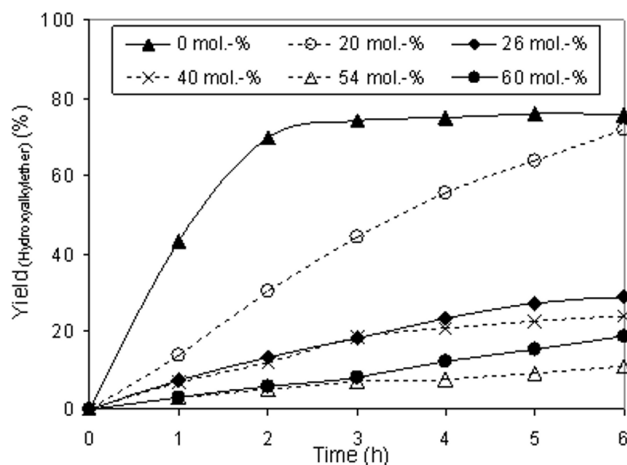


Figure 4-6. Yield of 1-(hexyloxy)octane-2-ol with zinc modified Mg/Al oxides at 160 °C.

4.4 Discussion

Mg/Zn/Al oxides with different Mg/Zn ratios were synthesized via a sol-gel process adopted from the method described by Greenwell et al.^[22] While the Mg/Zn ratio was varied, the aluminum concentration was kept constant giving a total molar M^{2+}/M^{3+} ratio of 4. The crystal structure of the sample without zinc was dominated by MgO. The addition of zinc led to an additional phase attributed to ZnO indicating the coexistence of two oxide phases. Apparently aluminum was incorporated into both lattices. For higher zinc contents, i.e., 54 and 60 mol-%, the diffraction peaks related to MgO disappeared. Thus, one can conclude that a mixed phase, containing all three metal cations, was formed.

The results from ²⁷Al MAS-NMR indicate the incorporation of aluminum into the MgO or ZnO lattice at least partially in a tetrahedral coordination. This is in accordance with conclusions by O'Dell.^[30] Note that for the parent material only a signal attributed to octahedral coordinated aluminum was observed indicating that Al³⁺ is either

exclusively incorporated into ZnO domains or that the presence of ZnO is needed to form tetrahedrally coordinated Al in vicinity to MgO. These findings are in perfect agreement with the fact that ZnO crystallizes in a wurzit structure and thus, forms tetrahedral vacancies, whereas MgO as the classical cubic structure forms octahedral vacancies.

It is also important to notice that with variation of the zinc content different tetrahedral aluminum species were observed. While with 20 mol-% zinc only one tetrahedral species occurred at 75 ppm, an additional tetrahedral aluminum species appeared at around 65 ppm for materials with higher zinc contents. The signal at 75 ppm can be attributed to Al in the vicinity of MgO/ZnO whereas the signal at 65 ppm is attributed to Al^{3+} in ZnO vacancies. The upfield shift to 65 ppm can be explained by the higher optical basicity (i.e., the higher electron donating power) of ZnO compared to MgO. Thus, Al^{3+} is more shielded when it is adjacent to ZnO and the NMR signal is shifted to lower values. In line with their relative concentrations, the signal at 65 ppm increased with higher Zn^{2+} concentration, while the signal at 75 ppm decreased indicating a higher concentration of Al^{3+} in the vicinity of ZnO. It is unclear at present, why the highest concentration of tetrahedrally coordinated aluminum was found for the sample with 54 mol-% Zn^{2+} . This indicates that the higher crystallinity of ZnO (deduced from the X-ray diffractograms of Mg/Zn/ AlO_x -60) caused the lower incorporation degree of Al in the ZnO lattice.^[31]

The acid site density of Mg/Zn/Al oxides increased concurrently with increasing zinc contents. This is in line with the larger cation radius and the higher reducibility (the propensity to generate oxygen vacancies) of ZnO compared to magnesia or alumina. In contrast, the concentration of base sites decreased markedly upon addition of CO_2 . Given the alleged higher base strength of ZnO, the stabilization of CO_2 is drastically lower. Note, however, that this is in line with the lower thermal stability of ZnCO_3 compared to MgCO_3 . Thus, judged from the characterization with probe molecules one can conclude that the addition of Zn^{2+} to the magnesia-alumina mixed oxides leads to an increase of the concentration of acid sites and a decrease of the concentration of base sites without markedly changing the qualitative aspects of the interactions.

The rate for the elimination of hydrogen from propan-2-ol (see Table 4-4) was 1.2 times higher than for the elimination of water in case of Mg/Al mixed oxide without zinc.

The selectivity towards acetone (base catalyzed product) increased markedly from approximately 50 % for the catalyst without zinc to > 90 % for zinc containing catalysts. In comparison to the Mg/Zn/AlOx-0, the rate of dehydrogenation was increased by a factor of almost 200 after addition of zinc. This increase is paralleled by a drastic decrease of the apparent energy of activation indicating that the higher rate is associated with a lower barrier in the rate determining step. While being beyond the scope of the present chapter, one can speculate that this is associated either with easier hydride abstraction by Zn^{2+} or easier recombination of the proton and the hydride in the Zn^{2+} rich phase. The Mg/Zn/AlOx-54 is the most active material.

Table 4-4. Conversions of propan-2-ol, selectivities to acetone/propene and rates of formation, basic/acid ratios of Mg/Al and Mg/Zn/Al metal oxides at 275 °C.

<i>Sample</i>	<i>Conversion</i>	<i>Selectivity</i>	<i>Rate</i>	<i>Rate</i>	<i>Ratio</i>	<i>Ea</i>	<i>Ea</i>
	(%)	(%)	($\mu\text{mol}\cdot\text{s}^{-1}\cdot\text{m}^{-2}$)	($\mu\text{mol}\cdot\text{s}^{-1}\cdot\text{m}^{-2}$)	Acid/basic sites	($\text{kJ}\cdot\text{mol}^{-1}$)	($\text{kJ}\cdot\text{mol}^{-1}$)
Mg/Zn/Al Ox	Propan-2-ol	Acetone	Acetone	Propene		Acetone	Propene
0	9	54	0.09	0.07	2	89	95
20	67	95	16	0.8	7	37	68
26	50	98	22	0.4	8	44	79
40	51	99	28	0.4	11	45	103
54	19	97	64	2.2	8	40	65
60	27	99	39	0.3	18	51	93

^{b)} Carrier gas flow (He) = 50 mL·min⁻¹

It is interesting to note that also the rate of dehydration increased through the addition of Zn^{2+} . As this kind of reaction needs acid and base sites, the higher concentration of Lewis acid sites is beneficial for the rate of reaction. The fact that the strength and concentration of base sites did not increase in the series of mixed oxides shows that the much more pronounced increase of the rate of dehydrogenation must be related to the specific properties of the Zn^{2+} cations.^[32]

Let us then analyze the impact of the Zn^{2+} cations on the ring opening reaction of epoxides with alcohols described in the literature as an acid or base catalyzed reaction.^{27,28,29} In the Lewis acid catalyzed route, the epoxide C-O bond is polarized by

the cation inducing a positive charge at the α C-atom that in turn is attacked by the oxygen of the reacting alcohol. In the base catalyzed mechanism, the alcohol is activated by the abstraction of a proton from the OH group and an alkoxide anion is formed. The latter acts as nucleophile and preferentially attacks the epoxide at the α C-atom. Of course, also in this case polarization of the epoxide bonds would facilitate the reaction. The present results show that the yield of 1-(hexyloxy)octane-2-ol decreased with increasing deprotonation ability (determined by the dehydrogenation of propan-2-ol) of the Mg/Zn/Al oxides. This indicates that the polarization of the C-O bond in the epoxide by Zn^{2+} cations is weak and as the base strength also did not increase in this series of mixed oxides the overall activity drops with increasing concentration of Zn^{2+} .

4.5 Conclusions

Mg/Zn/Al oxides with different Mg/Zn ratios were derived from LDH precursors in order to study the impact of Zn^{2+} on their basic properties. While the preparation led to mixed oxides with MgO and ZnO phases, a mixed oxide phase including all three metals was formed for Zn^{2+} concentrations above 40 mol-%. The presence of Zn^{2+} leads to a higher concentration of Lewis acid sites, the strength of the base sites was not enhanced. The high activity for dehydrogenation of alcohols has been identified to be related with the specific ability of the Zn^{2+} cations to facilitate hydrogen abstraction and/or the recombination of H^+ and H^- and/or the desorption of hydrogen. In contrast to the pronounced facilitation of these elementary steps, the polarization of the epoxide C-O bond was found to be very weak, and the presence of Zn^{2+} cations was not beneficial for the epoxide ring opening reaction. As with other cases the present results indicate that the use of alcohol elimination reactions to evaluate acid-base properties of mixed oxides is at best problematic, because the specific chemistry in elementary steps dominates over general acid-base properties.

4.6 References

- [1] H.A Prescott, ZJ Li, E Kemnitz, A Trunschke, J Deutsch, H Lieske, Auroux A, *J. Catal.* **2005**, 234, 119.
- [2] P.F. Rossi, G. Busca, V. Lorenzelli, M. Waqif, O. Saur, J.C. Lavalley, *Langmuir* **1991**, 7, 2677.
- [3] K. Shibata, T. Kiyoura, J. Kitagawa, T. Sumiyosh, K. Tanabe, *Bull. Chem. Soc. Jpn.* **1973**, 46, 2985.
- [4] J.A. Lercher, H. Noller, *J. Catal* **1982**, 77, 152.
- [5] G. Ghiotti, F. Boccuzzi, *J. Chem. Soc., Faraday Trans.* **1983**, 79, 1843.
- [6] S.P. Naik, J.B. Fernandes, in: Recent Advances In Basic And Applied Aspects Of Industrial Catalysis, Vol. 113, eds. T. S. R. Prasada Rao, G. Murali Dhar (Elsevier, Amsterdam, **1998**.
- [7] R.M. Gabr, M.M. Girgis, A.M. Elawad, B.M. Abouzeid, *Mater. Chem. Phys.* **1994**, 39, 53.
- [8] J.M. Vohs, M.A. Barteau, *J. Phys. Chem.* **1991**, 95, 297.
- [9] M. Bowker, *J. Catal.* **1986**, 99, 53.
- [10] B. Jóvér, J. Juhász, G. Szabó, *Z. Phys. Chem.(NF)* **1978**, 111, 239.
- [11] S. Kolboe, *J. Catal.* **1969**, 13, 208.
- [12] G. Djéga-Mariadassou, L. Davignon, *J. Chem. Soc., Faraday Trans.* **1982**, 78, 2447.
- [13] F. Pepe, Angeletti C. , S. Rossi, *J. Catal.* **1989**, 118, 1.
- [14] O. Perez-Lopez, A.C. Farias, N.R. Marcilio, J.M.C. Bueno, *Mater. Res. Bull.* **2005**, 40, 2089.
- [15] H. Vinek, J.A. Lercher, H. Noller, *React. Kinet. Catal. Lett* **1980**, 15, 21.
- [16] V. Dimitrov, T. Komatsu, R. Sato, *J. Ceram. Soc. Jpn.* **1999**, 107, 21.
- [17] J.A. Duffy, *J. Chem. Educ.* **1996**, 73, 1138.
- [18] A. Gervasini, *Catal. Lett.* **1997**, 43, 219.
- [19] K.C. Waugh, *Appl. Catal.* **1986**, 25, 121.
- [20] H. Noller, *Z. Phys. Chem. (NF)* **1985**, 144, 157.

- [21] A. Ouqour, G. Coudurier, J.C. Vedrine, *J. Chem.Soc., Faraday Trans.* **1993**, 89, 3151.
- [22] H.C. Greenwell, P.J. Holliman, W. Jones, B.V. Velasco, *Catal. Today* **2006**, 114, 397.
- [23] Y. Wang, X.W. Han, A. Ji, L.Y. Shi, S. Hayashi, *Microporous and Mesoporous Mater* **2005**, 77, 139.
- [24] P.J. Schilling, L.G. Butler, A. Roy, H.C. Eaton, *J. Am. Ceram. Soc.* **1994**, 77, 2363.
- [25] M. Reinholdt, J. Mieke-Brendle, L. Delmotte, M.H. Tuilier, R. le Dred, R. Cortes, A.M. Flank, *Eur. J. Inorg. Chem.* **2001**, 2831.
- [26] I. Hannus, Z. Konya, J. B. Nagy, P. Lentz, I. Kiricsi, *Appl. Catal. B* **1998**, 17, 157.
- [27] H.C. Chidwood, B.T. Freure, *J. Am. Chem. Soc.* **1946**, 68, 680.
- [28] R.E. Parker, N.S. Isaacs, *Chem. Rev.* **1959**, 59, 737.
- [29] V. Mirkhani, S. Tangestaninejad, B. Yadollahi, L. Alipanah, *Tetrahedron* **2003**, 59, 8213.
- [30] L.A. O'Dell, S.L.P. Savin, A.V.M. Chadwick, E. Smith, *Solid State Nucl. Magn. Reson.* **2007**, 31, 169.
- [31] A.A. Da Silva, de Souza, A. Gonçalves, M.R. Davolos, *J. Sol-Gel Sci. Technol.* **2009**, 49, 101.
- [32] H. Noller, J.A. Lercher, H. Vinek, *Mater. Chem. Phys.* **1988**, 18, 577.

Chapter 5

Fluorine modified Magnesium/Aluminum Mixed oxides

Abstract

Mg/Al mixed oxides derived from layered double hydroxide precursors were modified with fluoride anions in order to probe their impact on acid-base properties as well as their catalytic activity. Fluorine was incorporated via treatment with an aqueous NH_4F solution. The structure of the precursors and the modified materials were analyzed by XRD, ^{27}Al - NMR and ^{19}F - MAS NMR. The modification of Mg/Al mixed oxides with fluorine led to an incorporation of fluoride anions in various configurations. Overall, the concentration of acid sites was enhanced by this modification, while it rather decreased the concentration of the basic sites. The rate of dehydrogenation of propan-2-ol drastically increased on presence of F^- anions, while the rate of dehydration was hardly influenced. This indicates that the fluoride anions improve the ability of the mixed oxides to abstract protons from polar molecules without increasing the overall base strength of the mixed oxide.

5.1 Introduction

The use of hydrotalcites, layered double hydroxides (LDH) and their derived mixed metal oxides as precursors for solid base catalysts is well established.^[1] Examples for catalyzed reactions include aldol condensation, olefin isomerization, alkylation of diketones, epoxidation of activated olefins with H₂O₂, Claisen-Schmidt condensation or the H-transfer from alcohols to ketones and aldehydes. These experiments have spurred the interest in solid base catalysis in the last 20 years. Recently, new motivation to develop base catalysts has emerged from the interest in converting biomass and in particular to catalyze the transesterification of (glyceride) esters, but also other catalytic transformations of oxofunctionalized feedstocks.^[2] Note achieving an adequate CO₂ capture it will also require tailored solid bases.^[3] Subtle tailoring of the base properties is, therefore, important for the development of solid base catalysts and sorbents.

The basic properties of hydrotalcites are related to the substitution of lattice anions by OH⁻ forming Brønsted base sites. Calcination of the hydrotalcites transforms them reversibly to a solid Lewis base.^[4] One of the exceptional advantages of hydrotalcites and their related mixed metal oxides is the subtly tunable basicity, which depends foremost on the chemical composition.^[5]

The fact that hydrotalcites are anion exchangers enables a wide range of variations in their chemical compositions. Chloride exchange for example has been shown to drastically decrease the basic properties of hydrotalcites.^[6] On the other hand Wei and Sun^[7] reported recently that the modification of Mg/Al mixed oxides with fluorine is a surprisingly effective method to increase their efficiency in reactions claimed to be catalyzed by solid bases. This is on the first sight surprising given the high electronegativity of fluorine, but the modification of layered double hydroxides (LDH) with fluorine led to highly active solid base catalysts for C-C bond formation. However, also supported fluoride salts such as KF (KF/alumina) possess high basicity, which was explained by the highly polarized F⁻ anion in the LDH.

Choudary et al.^[8] observed poor performance in the catalytic Knoevenagel reaction and Michael addition for LDH derived materials calcined at temperatures even as low as 250 °C. Since many reactions are operated at higher temperatures (e.g.,

purification of H₂ from CO (200-300 °C) wherein CO is converted to methane over a calcined Ni-hydrotalcites catalyst or synthesis of γ -butyrolactone (275 °C)), it is necessary to develop catalysts, which are active and stable at reaction temperatures higher than 250 °C.^[9]

In this chapter, the influence of fluorine on different Mg/Al mixed metal precursors of the solid base catalyst has been investigated using ²⁷Al-, ¹⁹F- MAS NMR, NH₃- and CO₂-TPD. The catalytic performance with respect to the dehydration and dehydrogenation of propan-2-ol were also used to test the acid and base properties of the solid base catalysts.^[10,11,12,13,14] The viability of the Mg/Al mixed oxides and their fluorine modified derivatives as solid base catalysts was also tested in the condensation of 1,2-epoxy-octane and hexanol.

5.2 Experimental

5.2.1 Materials

5.2.1.1 Mg/Al mixed oxide precursors

The Mg-Al mixed oxide precursor with an Mg/Al ratio of 2 was provided by Cognis and is denoted as HT2. It was calcined at 600 °C. The magnesium-aluminum mixed oxide with a Mg/Al ratio of 4 (HT4) was prepared using a hydrotalcite precursor obtained by a sol-gel process^[15] and subsequent calcination in synthetic air. An acidic aqueous solution of metal nitrates was prepared by dissolving Mg(NO₃)₂·6H₂O (123.08 g, 0.48 mol) and Al(NO₃)₃·9H₂O (45.01 g, 0.12 mol) in 0.6 L decarbonized bidistilled water. A second, alkaline solution was prepared from NaOH (48.00 g, 1.2 mol) and NaHCO₃ (5.04 g, 0.06 mol) in 0.6 L decarbonized bidistilled water. Both solutions were heated to 75 °C. For precipitation, the nitrate and alkaline solutions were added drop-wise to 400 mL water at 75 °C giving a pH = 10. The suspension was aged for 3 h at 85 °C under vigorous stirring. After cooling to RT the gel was filtered and loaded into an autoclave. Hydrothermal synthesis was carried out for 16 h at 80 °C. The gel was washed with 350 mL bi-distilled water until a pH of 7 of the washing water was reached. The white precipitate was freeze-dried, ground and heated to 600 °C (heating rate 10 °C·min⁻¹) in a flow of 100 mL·min⁻¹ synthetic air for 8 h.

5.2.1.2 Fluorinated Mg/Al mixed oxides

An aqueous ammonium-fluoride solution was prepared with deionized water. The water was heated to 90 °C for 2 h in order to remove dissolved carbonates. The NH_4F -solution was added to 8 g of the calcined Mg/Al precursor in a 2 L Schlenk flask. The pH was adjusted to 8 using an ammonia solution (25 %) as the buffer. The mixture was stirred in inert atmosphere for 48 h at ambient temperature. The resulting solid was filtered and washed with deionized water until the pH was 7. The solvent was removed by freeze-drying under reduced pressure. The solid was ground and heated to 500 °C (heating rate $10\text{ }^\circ\text{C}\cdot\text{min}^{-1}$) in a flow of $100\text{ mL}\cdot\text{min}^{-1}$ synthetic air for 8 h.

The used precursor solids and their chemical compositions are compiled in Table 5-1. The nomenclature of the fluorinated Mg/Al mixed oxides indicates the concentration of the $\text{NH}_4\text{F}_{\text{aq}}$ -solution used for the material synthesis.

Table 5-1. Amounts of Mg/Al mixed oxide precursors (calcined at 600 °C) and concentrations of NH_4F solution used for the synthesis of fluorinated Mg/Al mixed oxides.

<i>Sample</i>	<i>Precursor</i>	$\overset{m}{(precursor)}$	$m(\text{NH}_4\text{F})$	$V(\text{NH}_4\text{F})_{\text{aq}}$	$c(\text{NH}_4\text{F})_{\text{aq}}$	$n(\text{NH}_4\text{F})_{\text{aq}}$
		(g)	(g)	(mL)	($\text{mol}\cdot\text{L}^{-1}$)	(mmol)
HT2-F 0.1	HT2	8	2.96	800	0.1	80
HT2-F 0.2	HT2	8	5.93	800	0.2	160
HT4-F 0.1	HT4	8	2.96	800	0.1	80
HT4-F 0.2	HT4	8	5.93	800	0.2	160

5.2.2 Characterization

The metal contents of Mg/Al mixed oxides and fluorinated Mg/Al mixed metal oxides as well as the fluoride contents were analyzed by atomic absorption spectroscopy (AAS) using an *UNICAM 939 AA-Spectrometer*.

Specific surface areas and pore volumes were determined by physisorption of N_2 at 77 K. The Measurements were carried out in a *PMI automatic BET-Sorptometer* and the evaluation was done according to the BET theory.

The crystalline structure of the precursors and the fluorinated mixed metal oxides were analyzed by XRD using a *Philips X'Pert Pro System* (Cu $\text{K}\alpha$ 1-radiation, 0.154 nm)

at 40 kV / 40 mA. The measurements were taken by using a spinner and a 1/6'' slit in the range from 5° or 20 ° to 70° 2 θ (0.05 °/min).

^{27}Al - and ^{19}F - MAS NMR measurements were performed on a *Bruker AV500 spectrometer* ($B_0 = 14.1\text{ T}$) at a spinning rate of 12 kHz. The temperature was adjusted by passing the bearing and drive gas stream through a heat exchanger. The samples were packed in 4 mm ZrO_2 rotors. The resonance frequency of 130.3 MHz was used for the measurements of ^{27}Al - MAS NMR. The spectra were recorded as the sum of 2400 scans with a recycle time of 250 ms. A $\pi/12$ pulse (pulse length = 1.0 μs) was applied for excitation. The chemical shift was referenced against an external standard of solid $\text{Al}(\text{NO}_3)_3$ ($\delta = -0.54\text{ ppm}$). For ^{19}F - MAS NMR the resonance frequency of 470.3 MHz was used. The spectra were recorded as the sum of 100 scans with a recycle time of 5.2 ms. A $\pi/12$ pulse (pulse length = 2.3 μs) was applied for excitation. The chemical shift was referenced against an external standard of solid CFCl_3 ($\delta = 0\text{ ppm}$).

Temperature programmed desorption of ammonia (NH_3 -TPD) and carbon dioxide (CO_2 -TPD) was used to determine the acidic and basic properties of the solid base catalysts. As standard materials for referencing the NH_3 -TPD and CO_2 -TPD, a H-MFI 90 zeolite and NaHCO_3 were used, respectively. Catalyst samples were activated at 450 °C for 1 h in vacuum. Ammonia was adsorbed at 1 mbar and 100 °C for 1 h and CO_2 (1 mbar) was adsorbed at 40 °C for 1 h. For desorption, the samples were heated to the corresponding temperature (up to 700 °C for CO_2 -TPD) with a rate of 10 $\text{K}\cdot\text{min}^{-1}$; desorbing gases were monitored with a Pfeifer mass spectrometer. Note that the concentration of sites is calibrated to a standard material.

5.2.3 Catalytic experiments

The as-prepared samples (0.02 g diluted in 0.13 g SiC) were fixed with quartz wool in a quartz-tube reactor with a diameter of 4 mm. The samples were activated by rising the temperature from ambient to 450 °C for 2 h (10 °C $\cdot\text{min}^{-1}$) in a flow of He (20 $\text{mL}\cdot\text{min}^{-1}$). The samples were cooled down to reaction temperature and a flow of helium (30, 50 and 70 $\text{mL}\cdot\text{min}^{-1}$) saturated with propan-2-ol ($p_{\text{propan-2-ol}} = 25\text{ mbar}$ at 13 °C) was passed over the fixed bed reactor. The dehydrogenation/dehydration of

propan-2-ol was studied within the temperature range of 225 to 300 °C using steps of 25 °C. At each reaction temperature the catalytic reaction was performed for 80 min. Unreacted propan-2-ol and dehydrogenation/dehydration products were analyzed by gas chromatography using a *Hewlett Packard 5890 (Series II) GC* equipped with a flame ionization detector. The separation of the various components was done by a Q-column.

The condensation of 1,2-epoxy-octane with hexanol was performed in a 100 mL flask. Hexanol (2.555 g, 0.025 mol) was added to 1,2-epoxy-octane (4.038 g, 0.026 mol) and heated to 160 °C in a N₂ atmosphere while stirring. The catalyst (0.066 g, 1 wt.-%) was added and samples were taken every hour. The catalyst was removed by filtration. The filtrate (100 µL) was mixed with 2,2,4-tri-methylpentane (937 µL) as internal standard for GC-analysis. The un-reacted 1,2-epoxy-octane, hexanol and reaction products were analyzed by gas chromatography using a *Shimadzu GC-2010*.

5.3 Results

5.3.1 Textural analysis

The metal content, the specific surface areas of the precursors and the fluorinated Mg/Al mixed oxides are compiled in Table 5-2. It also includes the concentrations of acid and basic sites determined by CO₂- and NH₃-TPD (Figure 5-1 and Figure 5-2, see also section 5.3.5). The specific surface area of the solid base catalyst was hardly influenced when HT2 (Mg/Al = 2.0) was fluorinated with a 0.1 molar ammonium-fluoride solution (HT2 = 171 m²·g⁻¹/ HT2-F 0.1 = 167 m²·g⁻¹). When the sample was treated with a higher concentration of ammonium-fluoride, the specific surface area of HT2 increased to 186 m²·g⁻¹. The Mg/Al ratio of HT2 (approximately 2) increased slightly after fluorination. For HT4 (Mg/Al = 4.0), the specific surface area decreased from 188 to 162 m²·g⁻¹ and to 145 m²·g⁻¹ for HT4-F 0.1 and HT4-F 0.2, respectively. For both oxides the fluorine content was also doubled by treatment with the 0.2 M NH₄F_{aq}-solution compared to the 0.1 M solution. Overall, the fluorine content of fluorinated HT4 was, however, higher compared to fluorinated HT2.

Table 5-2. Textural analysis and acid-base properties of precursors (calcined at 600 °C) and fluorinated Mg/Al mixed oxides (calcined at 500 °C). The concentration of acid and basic sites has been calibrated to a standard material.

<i>Sample</i>	<i>Mg/Al</i> (mol:mol)	<i>F content</i> (wt.-%)	<i>S_{BET}</i> (m ² ·g ⁻¹)	<i>Acid sites</i> (μmol·m ⁻²)	<i>Basic sites</i> (μmol·m ⁻²)		
					W ^a	S ^b	Total
HT2	2.1	-	171	0.51	0.060	0.040	0.10
HT2-F 0.1	2.3	9	167	0.46	0.006	0.384	0.39
HT2-F 0.2	2.2	18	186	0.68	0.013	0.377	0.39
HT4	3.8	-	188	0.15	0.098	0.002	0.10
HT4-F 0.1	3.7	14	162	0.58	0.047	0.003	0.05
HT4-F 0.2	4.0	26	145	0.90	0.009	0.001	0.01

^aW = weak

^bS = strong sites

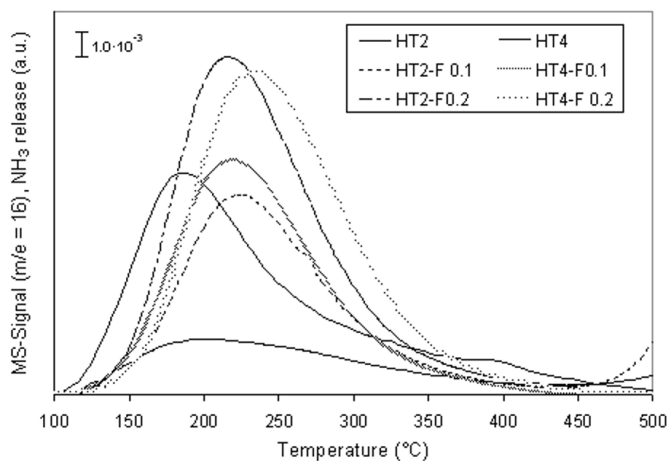


Figure 5-1. NH₃-TPD of plain and anion exchanged Mg/Al mixed oxides.

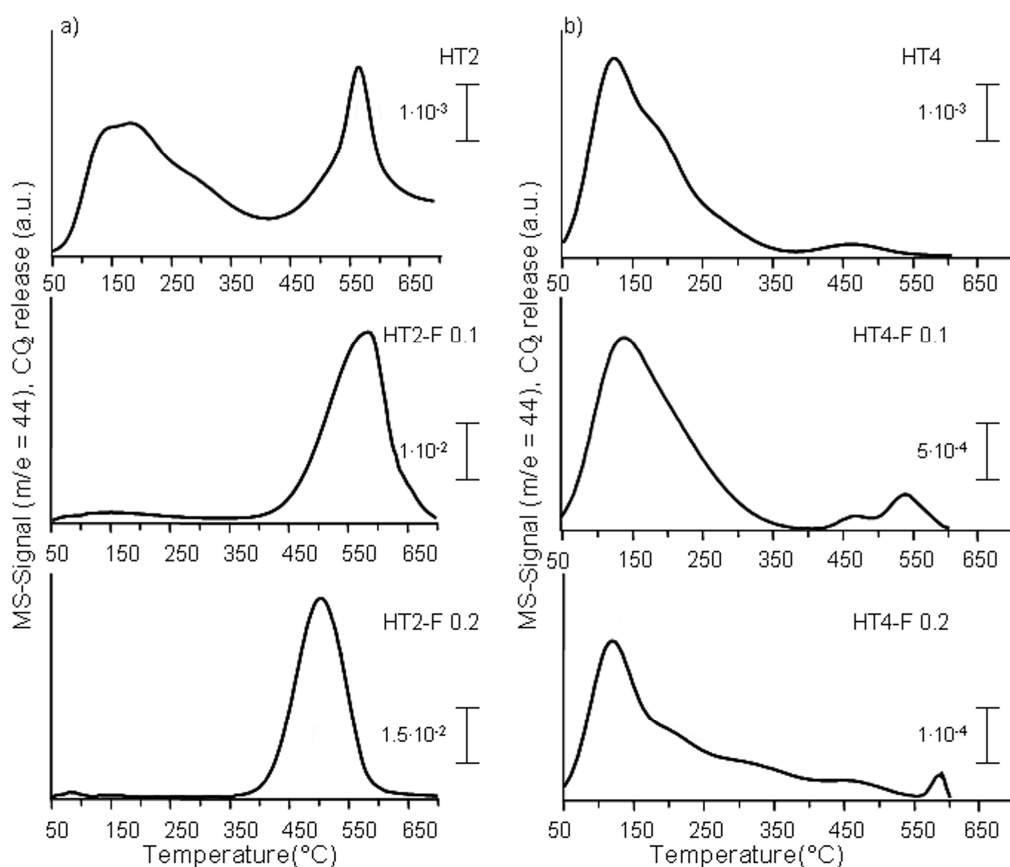


Figure 5-2. CO₂-TPD of plain and anion exchanged Mg/Al mixed oxides.

5.3.2 XRD analysis

The XRD patterns of the Mg/Al mixed oxides (HT2 and HT4) and the F⁻ exchanged samples are depicted in Figure 5-3. The diffraction peaks of MgO were observed at $2\theta = 35.6, 43.0$ and 62.5° , those of hydrotalcite occurred at $2\theta = 11.7, 23.4, 35.0, 39.7, 47.0, 53.9$ and 61.5° .

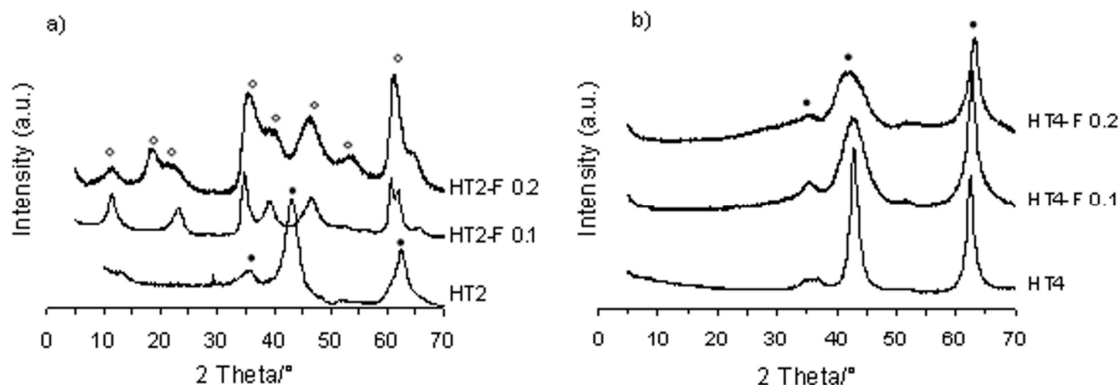


Figure 5-3. XRD patterns of plain and anion exchanged Mg/Al mixed oxide samples. [a) HT2 series. b) HT4 series] (with ● MgO (cubic), ◇ $\text{Mg}_6\text{Al}_2\text{CO}_3(\text{OH})_{16}\cdot 4\text{H}_2\text{O}$).

The pattern of HT2 was dominated by cubic MgO, while after fluorination the initial hydrotalcite structure was stabilized. The reconstruction of the LDH structure (hydrotalcite in our case) due to the so called memory effect of the calcined precursor was described by Tichit et al.⁶, who obtained a meixnerite (LDH structure) from calcined $\text{Mg}(\text{Al})\text{O}$ spinel. The reconstruction ability provides a lower calcination temperature than used for the formation of the oxides. As the widths of the peaks in all diffractograms were very broad, the samples possess a low crystallinity. The primary particle size was estimated from the Scherrer equation to be 6 to 7 nm.

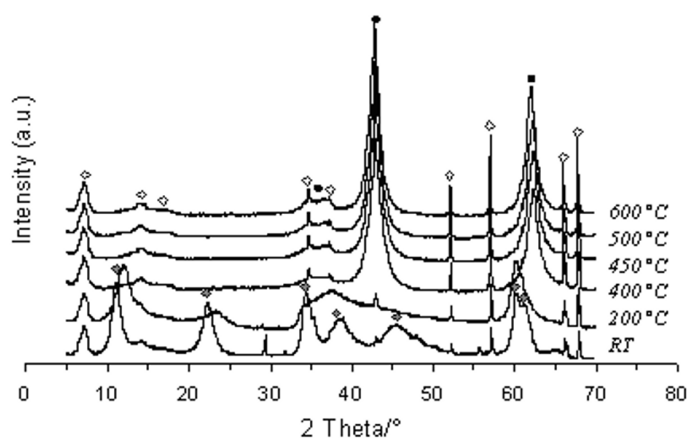


Figure 5-4. Structural transformation of HT4 from the LDH precursor to the mixed oxide was followed by in situ XRD

The reflexes of HT4 and fluorinated HT4 samples corresponded to cubic type MgO. In the fluoride exchanged samples, a broadening of the reflex at 43.0° was observed indicating a distortion of the MgO-phase.

The structural transformation of HT4 from the LDH precursor to the mixed oxide was followed by in situ XRD analysis from RT to 600°C in a flow of $5\text{ mL}\cdot\text{min}^{-1}$ of synthetic air. The results are illustrated in Figure 5-4. At RT main diffraction peaks were observed at $2\theta = 11.4, 23.0, 34.7, 38.6, 45.6, 60.4, 61.5$ and 65.6° related to the hydrotalcite structure with the general molecular formula of $\text{Mg}_6\text{Al}_2\text{CO}_3(\text{OH})_{16}\cdot\text{H}_2\text{O}$. At 200°C , the intensity of the diffraction peaks decreased and their widths increased. This indicates a structural transformation of the compound from hydrotalcite to Mg_xAlO_y . Further temperature increase to 400°C resulted in a complete transformation to Mg_xAlO_y . Between 400 and 600°C further changes of the structure were not observed by XRD.

5.3.3 ^{27}Al - MAS NMR spectroscopy

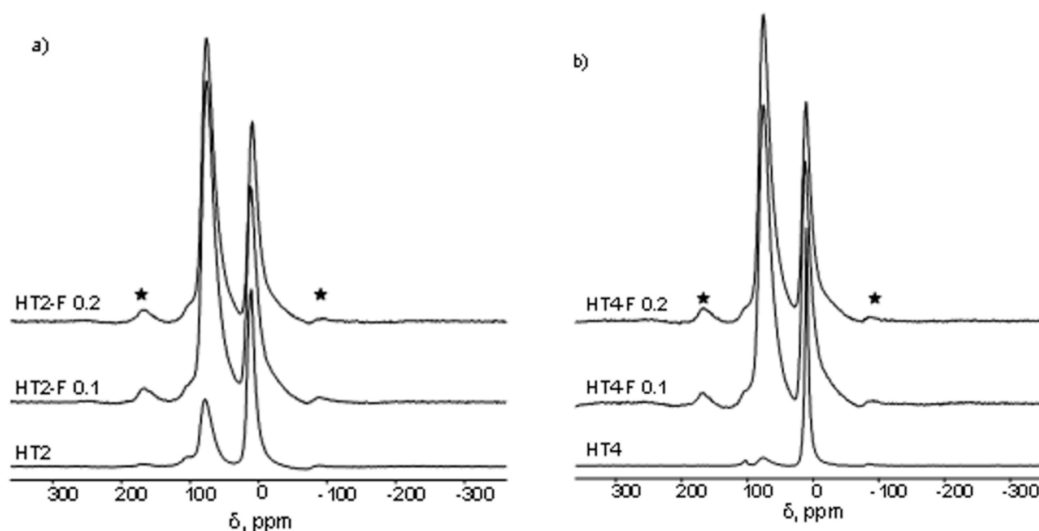


Figure 5-5. ^{27}Al - MAS NMR of plain and anion exchanged Mg/Al mixed oxide samples. [a) HT2 series b) HT4 series] (★satellites).

MAS NMR spectroscopy of the solid materials was used to identify changes in the crystal structure after fluorination of the Mg/Al mixed oxides. The ^{27}Al - MAS NMR spectra of HT2, fluorinated HT2 (a), HT4 and fluorinated HT4 (b) are compiled in Figure 5-5. The chemical shifts of octahedral and tetrahedral coordinated Al are located at approximately 11 and 75 ppm, respectively.^[16,17] In the case of HT2, tetrahedral and octahedral coordinated aluminum species were found, while the fluorinated HT2 samples showed a clear increase of the signal related to tetrahedral aluminum.

In comparison to the signal of HT2, the HT4 signal of tetrahedral aluminum was very small compared to the octahedral aluminum species. But similar to the results of fluorinated HT2, an increase of the signal at 75 ppm after fluorination was observed for HT4. Thus, the ratio between tetrahedral and octahedral alumina species was increased from 0.62 (HT2) to 1.85 for HT2-F 0.2. The conversion of octahedral to tetrahedral alumina was even more pronounced for HT4 indicated by the distinctive increase of the ratio from 0.09 to 1.82 for HT4-F 0.2. It is interestingly to note that the tetrahedral/octahedral ratios for HT2-F and HT4-F were almost identical (1.82 and 1.85, respectively).

5.3.4 ^{19}F - MAS NMR spectroscopy of fluorine modified Mg/Al mixed oxides

All ^{19}F - MAS NMR spectra of fluorinated Mg/Al mixed oxides are dominated by one main signal at approximately -184 ppm (see Figure 5-6). The signal is related to a MgF_2 -type species adjacent to oxygen atoms.^[18] Furthermore, in case of HT2-F0.1 a broad shoulder at -147 ppm was observed. With increasing degree of fluorination of HT2-F this shoulder shifted to -151.3 ppm. It is attributed to F^- coordinating to aluminum cations. This high field shift was also observed by Zhang et al.^[19] for higher fluorine contents. They described this type of fluoride as a bridging type between two Al atoms (S2). Fluoride species coordinating to one Al (S1) at -161 ppm or to three Al (S3) at -132 ppm (see Figure 5-7) were not observed.

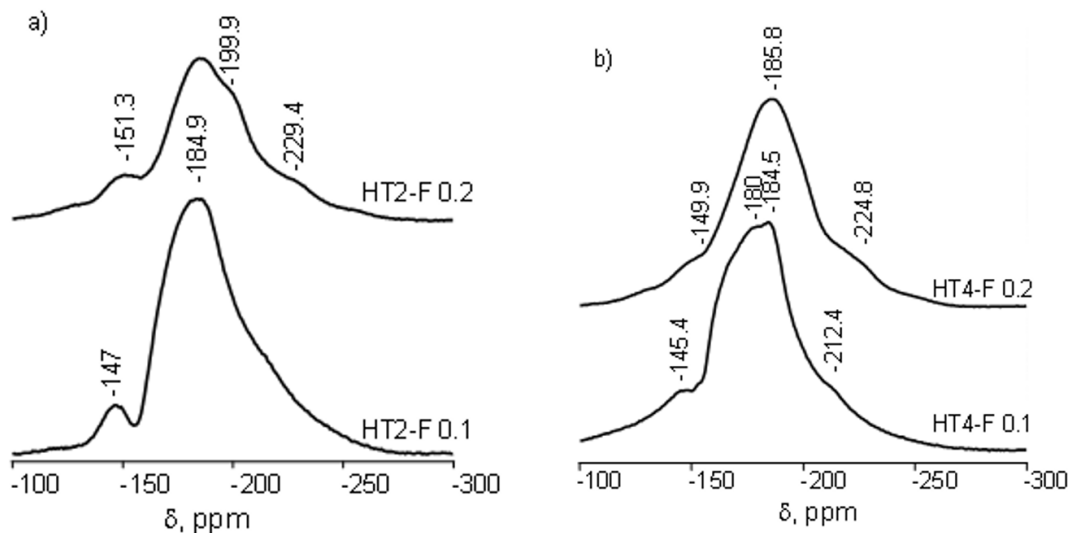


Figure 5-6. ^{19}F - MAS NMR of plain and anion exchanged Mg/Al mixed oxide samples. [a) HT2 series b) HT4 series].

Two further small shoulders at -199.9 and -229.4 ppm were distinguished for HT2-F0.2. According to Prescott¹⁸ terminal F^- coordinated to Mg is expected at -200 ppm and bridging fluoride with a Mg-F distance of 1.7 Å should be observed at -218 ppm.

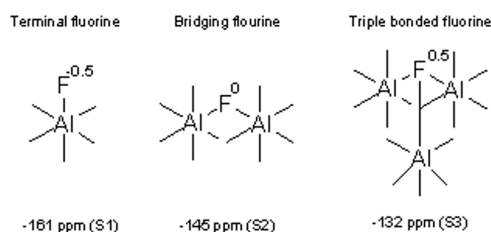


Figure 5-7. Possible surface structures of fluorinated γ -alumina.^[19]

For Mg/Al mixed oxides with higher magnesium concentrations (HT4) the signals attributed to bridging Al-F structures were observed at -145.4 (HT4-F0.1) and 149.9 ppm (HT4-F0.2). Note, compared to HT2 the Al-F signals were shifted to lower field. The Mg-F signals were observed at -184.5 (HT4-F0.1) and -185.8 ppm (HT4-F0.2). In case of lower fluoride content an additional signal was observed at -180 ppm. This resonance is

attributed to a second, highly diluted Mg-F species as described by Reinholdt.^[20] The high field signal at < -200 ppm occurred at -212.4 ppm for HT4-F0.1 and was shifted to -224.8 ppm with increasing fluorine content. In both cases a fluoride anion is suggested to assume a bridging position between two Mg^{2+} cations.

5.3.5 Base properties determined by TPD of CO_2

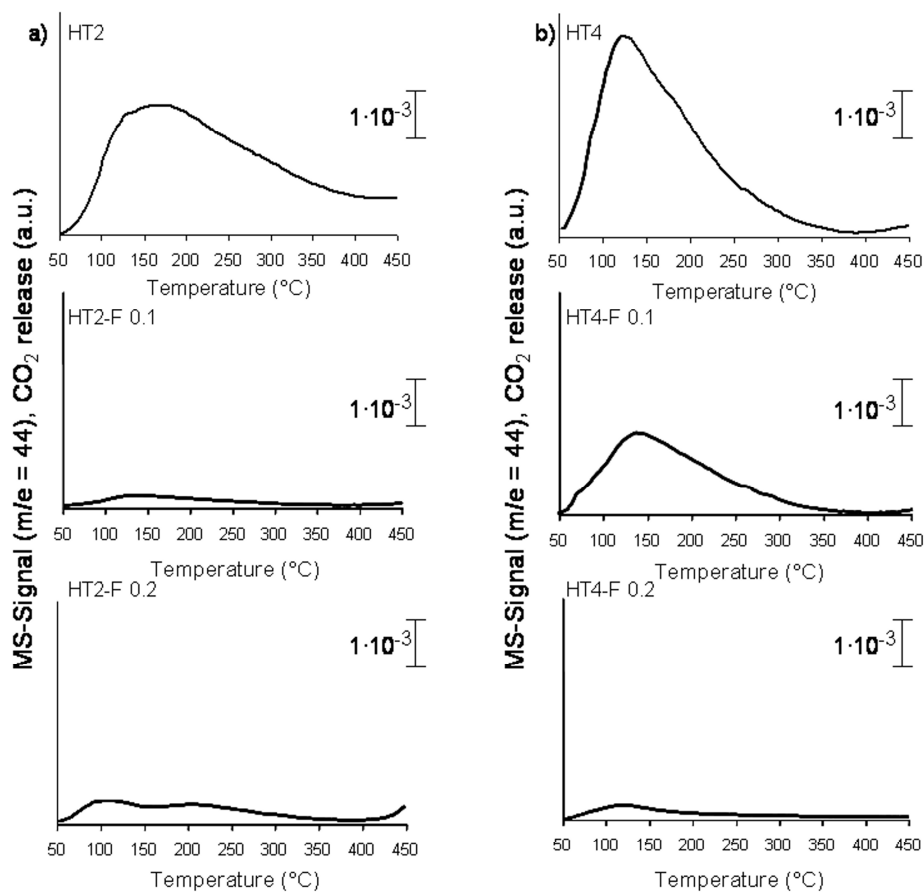


Figure 5-8. CO_2 -TPD of plain and anion exchanged Mg/Al mixed oxides.

The desorption profile of HT2 (Figure 5-8) shows a broad structured peak with a maximum at temperatures below 350°C as well as a more narrow desorption peak at 550°C . According to the two desorption maxima in the CO_2 -TPD, the basic sites are

classified as weak (W) and strong sites (S) (see Table 5-2). After modification with fluoride anions, the more intense low temperature maximum disappeared and the high temperature desorption peak broadened and markedly grew in intensity for HT2-F0.1 and HT2-F0.2. Note that the desorption maximum of the high temperatures peak was at higher temperatures for HT2-F 0.1 compared to HT2-F0.2.

With HT4, fluorination hardly changed the overall appearance of the desorption profile. While fluoride modification, overall, led to the appearance of a further desorption maximum at around 550 °C, the concentration of CO₂ desorbing from such sites did not show a correlation with the fluoride concentration in the sample.

5.3.6 Kinetics of elimination reactions of propan-2-ol

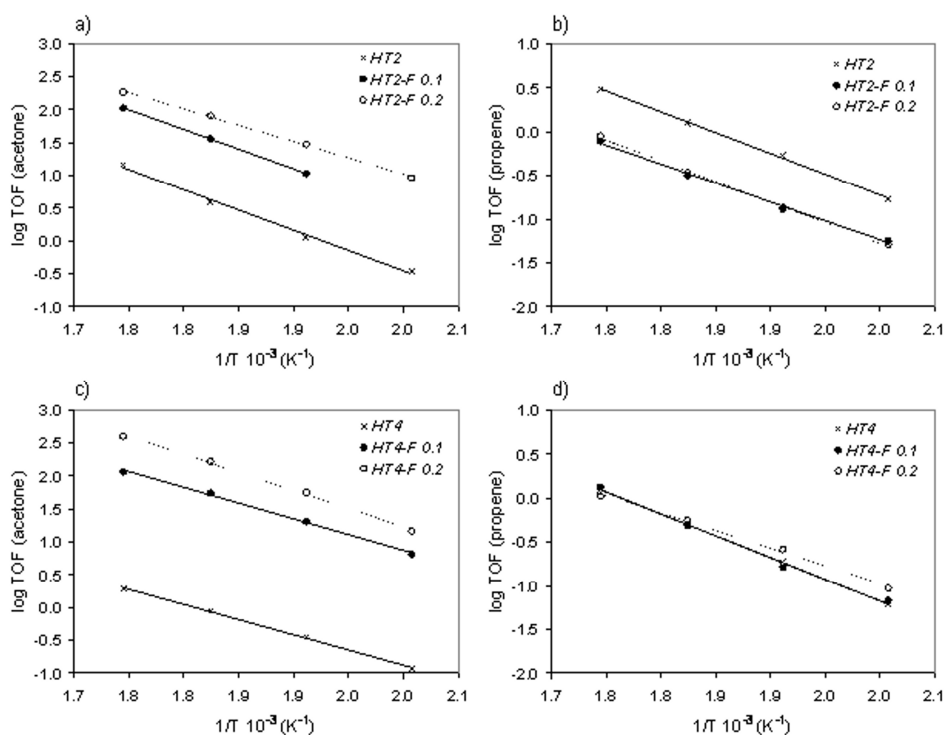


Figure 5-9. Turnover frequency of product formation from propan-2-ol conversion as function of the inverse temperature for various Mg/Al and F-modified Mg/Al mixed oxide samples. [HT2 and fluorinated HT2: a) formation of acetone and b) formation of propene; HT4 and fluorinated HT4: c) formation of acetone and d) formation of propene].

The catalytic properties of the Mg/Al mixed oxides and their fluoride modified derivatives were explored with respect to the elimination reactions of propan-2-ol. Generally, propene is formed via dehydration on catalysts with dominating acid sites, while acetone is formed as the main dehydrogenation product when basic sites are dominating. The selectivity to propene and acetone has been, therefore, used as an indicator of the acidic or basic properties of mixed oxides in addition to TPD of NH_3 and CO_2 .

The TOF of acetone formation (see Figure 5-9.) increased for both series of materials with increasing fluoride content. In contrast, the TOF for the dehydration decreased slightly (HT2 series) or hardly changed (HT4 series). The increase in the TOF for dehydrogenation was accompanied by a nearly constant apparent energy of activation of 107 ± 12 kJ/mol. The apparent energies of activation for dehydration hardly changed (83 kJ/mol). With HT4 the apparent energy of activation for propan-2-ol dehydrogenation was slightly lower (97 ± 8 kJ/mol), while the apparent energy of activation for dehydration again was 85 ± 8 kJ/mol.

Table 5-3. Conversions of propan-2-ol, selectivities to acetone/propene and TOFs^a of acetone formation, basic/acid ratios of Mg/Al and anion exchanged mixed metal oxides.

Sample	Conversion	Selectivity	TOF	TOF	Ea	Ea
	(%)	(%)	(s ⁻¹)	(s ⁻¹)	(kJ·mol ⁻¹)	(kJ·mol ⁻¹)
	Propan-2-ol	Acetone	Acetone	Propene	Acetone	Propene
HT2	4	27	3.9	1.3	118	91
HT2-F 0.1	1	60	36.7	0.3	115	83
HT2-F 0.2	5	82	81.3	0.3	95	91
HT4	9	54	0.9	0.5	89	95
HT4-F 0.1	9	90	55.5	0.5	91	95
HT4-F 0.2	6	75	167.2	0.7	105	77

^a TOF was determined by using the weak basic site density for acetone and the acid site density for propene.

The yield-conversion plots for Mg/Al mixed oxides and fluorinated samples at 275 °C are shown in Figure 5-10. The selectivity towards dehydrogenation for HT2 was

27 % and increased with increasing content of fluorine to 60 % (HT2-F 0.1) and 82 % (HT2-F 0.2). For HT4 the selectivity to acetone increased with fluorination from 54 to 90 % (HT4-F 0.1). The straight lines show that none of the products undergoes secondary reactions to a significant extent.

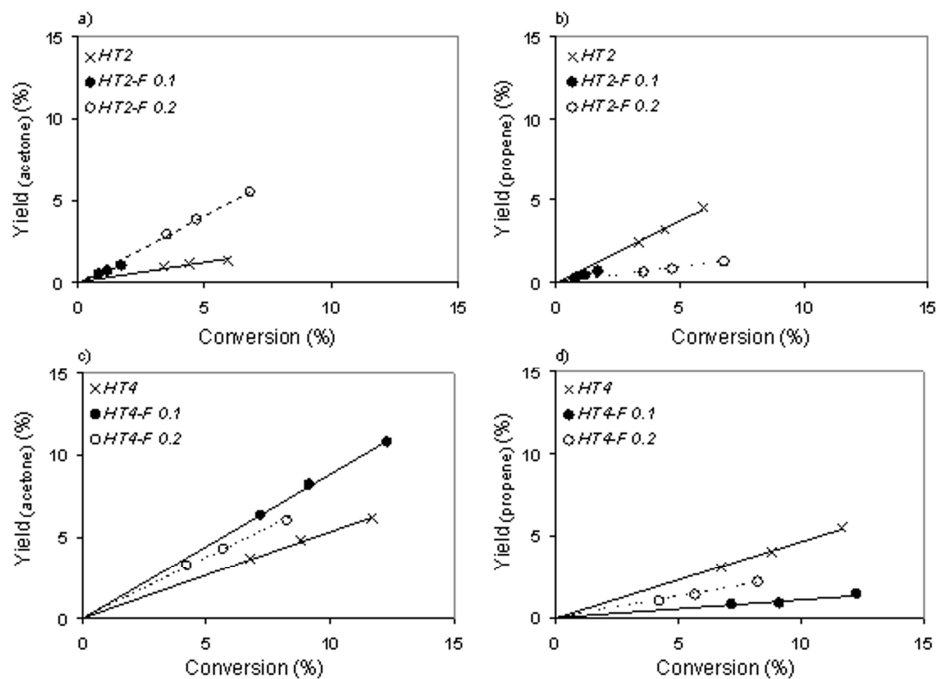


Figure 5-10. Yield conversion plots of propan-2-ol dehydrogenation and dehydration under variation of the He/propan-2-ol-flow (30, 50 and 70 mL/min) for precursors (calcined at 600 °C) and fluorinated Mg/Al mixed oxides (calcined at 500 °C) at 275 °C. [HT2 and fluorinated HT2: yield of a) acetone and b) propene; HT4 and fluorinated HT4: yield of c) acetone and d) propene].

5.3.7 Catalytic condensation of 1,2-epoxy-octane with hexanol

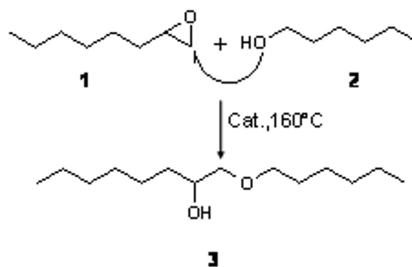


Figure 5-11. Reaction scheme of the nucleophilic ring-opening reaction of 1,2-epoxy-octane with hexanol.

Ring opening reactions of epoxides are useful routes in organic synthesis of allylic and aliphatic compounds catalyzed by acids and bases.^[21,22,23] The reaction of 1,2-epoxy-octane (1) with hexanol (2) is a nucleophilic substitution in which the alcohol acts as the nucleophile and 1-(hexyloxy)octane-2-ol (3) is formed as the main product. The reaction scheme of the nucleophilic ring-opening reaction of the epoxide is depicted in Figure 5-11.

The catalytic performance of Mg/Al mixed oxides and fluorine modified Mg/Al oxides during the ring-opening reaction of 1,2-epoxy-octane with hexanol at 160 °C is shown in Figure 5-12. In the series of fluoride modified catalysts, the yield of 1-(hexyloxy)octane-2-ol decreased with increasing concentration of fluorine. The decrease in activity due to fluorination was significantly higher in case of HT2 compared to HT4. While the yield of 1-(hexyloxy)octane-2-ol was 63 % for HT2, it dropped to less than 10 % for fluorinated HT2. In comparison, for HT4 only a slight decrease in activity from 76 to 67 % was observed for HT4-F0.1. A further decrease to 51% was observed for HT4-F0.2. The high selectivity (> 75 %) to the target reaction was maintained in both cases.

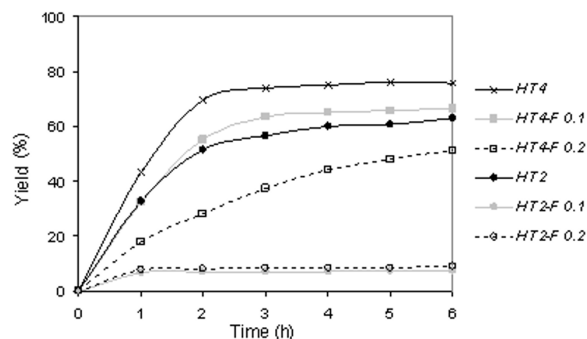


Figure 5-12. Yield of 1-(hexyloxy)octane-2-ol with F-modified and Mg/Al mixed oxides ($T = 160^{\circ}\text{C}$).

5.4 Discussion

Fluorinated Mg/Al mixed oxides were prepared in order to adjust the basicity of the Mg/Al mixed oxides. While both, the parent and the fluorinated samples, show the expected mutual impact of the acidic (alumina) and the basic (MgO) component [24,25], the subtle effects were seen to depend on the local structures induced by the different precursor structure and chemical composition (HT2 had Mg/Al ratio of 2.1 and HT4 of 3.8). With the differing concentration of the two main chemical constituents in the corresponding precursors one notes that with the higher Mg content, MgO became the dominating phase. This indicates that the higher MgO content led either to the formation of very small X-ray amorphous domains of hydrotalcite or it suppressed its formation entirely. With fluorine modified mixed oxides, the fluorination of the HT2 stabilized the hydrotalcite structure, which is speculated to related to the memory effect^[6] (reconstruction of LDHs by treatment in aqueous solutions and calcination at lower temperatures), while HT4 and fluorinated HT4 samples crystallized only in the MgO or a MgO dominated Mg_xAlO_y mixed phase similar to the material reported also by Wu et al..^[7]

There was no trend observable for changes of the specific surface areas of HT2 with increasing degree of fluorination, while the specific surface area of HT4 decreased with increasing amount of fluorine. Using ^{27}Al - MAS NMR, octahedral and tetrahedral alumina species were identified in both materials (HT2 and HT4). A significant increase of tetrahedral alumina is observed after fluorination. For HT4, the conversion of Al

species was more pronounced than for HT2, because HT4 had a lower percentage of tetrahedral Al in its starting material than HT2.

The fluoride species were identified via ^{19}F - MAS NMR using the five differently coordinated fluorine types potentially be present in the solid catalyst.^[18,19,20,26] The main signal in the NMR spectrum of HT2-F0.1 is attributed to a MgF_2 species and the sharp shoulder at -147 ppm to a bridging Al-F structure. For HT2-F0.2, two further signals of fluorine coordinated to magnesium, characteristic for terminal and bridging Mg-F structures, are present. In comparison to HT2-F0.1, the intensity of the Al-F related signal is smaller, but shifted to higher field (-151 ppm). The shift of the signal of HT2-F0.2 related to Al-F indicates a higher polarization of the Al-F bond towards the fluorine atom. Thus, the electron density is redistributed towards fluorine atom in HT2-F0.2, which should lead to a higher positive charge at the metal cations.

Similarly to the spectrum of fluorinated HT2, the NMR spectrum of fluorinated HT4 was dominated by MgF_2 . However, in the spectrum of HT4-F0.1 an additional Mg-F species related to a fluoride ion bridging among three MgO octahedra was observed. This additional Mg-F species resembles more a terminal than a bridging Mg-F structure. The Mg-F species observed in HT4-F0.2 resembles in contrast more a bridging Mg-F. The same trend with respect to the polarization of the Al-F bond as for fluorinated HT2 was observed. With increasing fluorine content, the signal of Al bound F was shifted from -145 to -150 ppm indicating high polarity for HT4-F0.2.

Two different kinds of basic sites with different strength (weak and strong) were observed for the Mg/Al mixed oxides and the fluorine modified samples by CO_2 -TPD. The concentration of weak basic sites was markedly decreased by the modification of HT2 with fluorine, while the concentration of strong basic sites was distinctly increased. However, one should note, that the 10-fold increase of desorbing CO_2 in case of fluorinated HT2 samples, at temperatures higher than the activation temperature, has (at least partially) to be attributed to carbonate anions, which are apparently stabilized in the partly anion exchanged hydrotalcite structure.

In comparison to the calcined precursor, the density of basic sites decreased for HT4 with the fluoride modification. While this decrease is moderate for HT4-F0.1, i.e., a factor of two, it was very pronounced for HT4-F0.2. The decreased basicity due to

fluorination has been explained by the distortion of the minor phase (MgF_2) in the main lattice (MgO).^[18] While this is a reasonable explanation, it is more likely that this strong decrease is related to the selective exchange of the most undercoordinated oxygen cations and hydroxyl groups for fluorine.

This is in line with the increase in the concentration of moderately strong acid sites (i.e., accessible Mg^{2+} cations), as discussed below. Their higher electronegativity and smaller ionic radius compared to O^{2-} of the cations allow for a better accessibility and a higher acid strength of the cations. Note that in contrast to MgO , aluminum cations are preferentially tetrahedrally coordinated after fluorine modification in both materials and in that way better shielded than in the starting material. The concentration of acid sites, as determined by desorption of ammonia, shows an almost identical surface averaged density of sites for materials with the concentration of fluoride anions. This suggests not only very similar surface structures (considering the overall difference in chemical composition between Mg and Al cations) it also shows that the modification was dominating the surface structure. In both cases the increase in acid site concentration is attributed to the increase in coordinatively unsaturated Mg^{2+} .

Thus, judging from the sorption/desorption of probe molecules the modification of the $\text{MgO-Al}_2\text{O}_3$ mixed oxide with fluorine leads to heterogeneous samples in which the concentration of strong basic sites (attributed to a stabilization of carbonate ions via thermal stabilization of the hydrotalcite structure) is increased, while the concentration of weak base sites (attributed to coordinatively unsaturated surface oxygen and hydroxyl groups) is decreased. In parallel, the concentration of weak acid sites increases, which is concluded to be caused by a better accessibility of the Mg^{2+} cations, caused by the partial substitution of the oxygen and hydroxide anions.

Given that overall picture of the modification of the acid-base properties let us analyze the conversion of propan-2-ol is an indicator for the acid and base properties of the mixed oxide/fluoride catalysts. The TOF for the formation of acetone increased with F-content (see Figure 5-13a), while the formation of propene was unaffected (see Figure 5-13b). Thus, fluorinating the samples had the apparent effect that the entire Mg/Al mixed oxide catalyst became more basic (accelerated TOF for dehydrogenation).

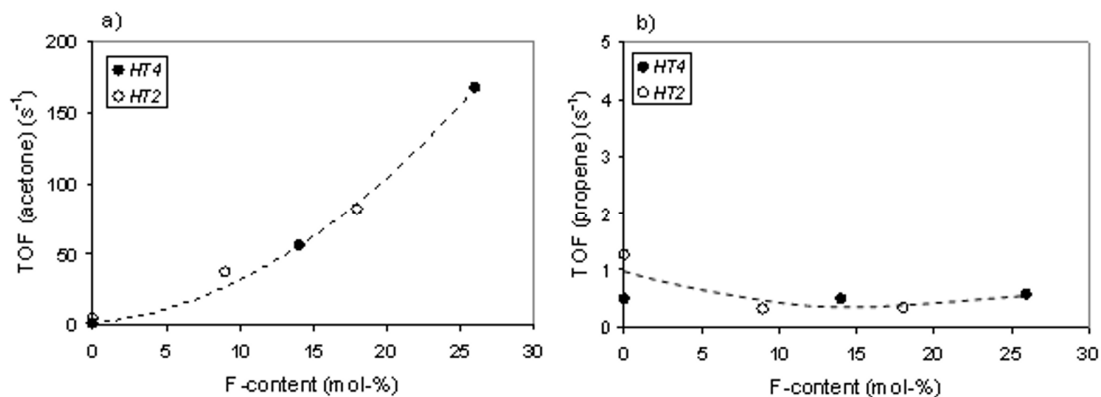


Figure 5-13. TOFs of product formation of propan-2-ol conversion depending on the fluorine content at 275°C for various Mg/A mixed oxide samples [a) Formation of acetone and b) Formation of propene].

This apparent discrepancy between the variation of the measured acid-base properties and the catalytic performance can be understood and explained by the three elementary steps of dehydrogenation (and dehydration) of propan-2-ol. In the first step, the alcohol adsorbs dissociatively on an acid base pair, i.e., the alcohol O-H bond cleaves forming an OH group with a basic oxygen, while the alkoxide is stabilized by the cation. In the second step, a hydride is abstracted from the intermediate by another accessible acid site. The third step includes the recombination of two H atoms to form hydrogen and the desorption of products into the gas phase. It should be noted that this sequence can occur simultaneous (concerted mechanism) or in steps (ionic mechanism). In this sequence the fluorine anion plays the critical role in enhancing the concentration of the alkoxy groups at the surface through the more facile abstraction of the hydrogen of the alcohol hydroxy group by the fluoride anion. The transiently formed HF is speculated to be rapidly hydrolyzed by OH groups (forming water and F⁻) or helps in forming H₂ at a coordinatively unsaturated Mg²⁺ site that has adsorbed H⁻. While the stable catalyst behavior points to the fact that the former reaction is limited in extent, the current data do not allow speculations with respect to the rates at which such reactions occur. The quite constant apparent energies of activation point to the fact that the increase of the rate rather enhances one of the reaction steps in quasi equilibrium (by stabilizing a higher equilibrium concentration of an intermediate) and not the rate determining step.

In contrast to dehydrogenation, the fluorine coordination surprisingly does not accelerate the dehydration of propan-2-ol. The higher concentration of acid sites (accessible Mg^{2+} cations) did not lead to an enhanced rate of cleavage of the C-O bond. Because the overall concentration of the acid sites is increased in the modified samples, the higher concentration of fluoride anions must negatively influence the stabilization of the propyl carbenium ion. As the formation of fluoro alkanes has not been observed, the interaction between the propyl carbenium ion and the fluoride anion must be very weak. The interaction of the carbenium ion with the more compact F^- anion is much weaker than with the more polarizable O^{2-} anion.

Similarly, the ring opening reaction of an epoxide with an alcohol, in specific the reaction of 1,2-epoxy-octane with hexanol to 1-(hexyloxy)octane-2-ol, is catalyzed by moderately strong bases. Also in this case, the modification with fluoride anions had a negative impact on the catalytic activity. While the higher concentration of Mg^{2+} in the mixed oxide was positive for the rate (HT4 was more active than HT2), the substitution of F^- in the surface reduced the rate. Thus, the reaction requires specifically the presence of basic oxygen and also in this case the enhanced concentration of weak Lewis acid sites did not positively affect the rate of formation or the concentration of reactive intermediates.

5.5 Conclusions

Mg/Al mixed oxides derived from LDH precursors were modified with fluorine in order to study the much-claimed positive impact on their basic properties. The fluoride modification led to a substitution of surface oxygen atoms and hydroxyl groups as well as to an increase of the concentration of unsaturated Mg cations (Lewis acid sites). With some of the materials the presence of fluorine in the materials led to a surprising stabilization of the hydrotalcite structure, without changing, however, the impact of the fluorine substitution. It led, overall, to a somewhat higher polarity of the surface, but not to a better stabilization of the reversibly adsorbed CO_2 indicating a lower density of accessible basic sites. The higher concentration of unsaturated cations is concluded to be related to the substitution of O^{2-} (and OH^-) by the smaller and more compact F^- .

The differences in the catalytic performance reflect the influence of the particular properties of the fluoride anions. While they seem to enhance the proton accepting properties, probably by generating a transiently stable HF species and lead so to the stabilization of secondary propoxy groups by accessible Mg^{2+} cations, the stabilization of the more polarizable sec. propyl carbenium ions is not improved. This leads to an increase in the dehydrogenation, which is, in this case, not an indication of a higher base strength. Similarly, the formation of the ring opening of an epoxide by reacting it with an alcohol is not favored.

Thus, overall, the introduction of F⁻ anions into alumina - magnesia mixed oxides improves their ability to abstract protons from polar molecules in catalyzed reactions, while the base properties are not enhanced and the concentration of moderately strong Brønsted acid sites is enhanced.

5.6 References

- [1] J. S. Valente, F. Figueras, M. Gravelle, P. Kumbhar, J. Lopez, J. P. Besse, *J. Catal.* **2000**, 189, 370.
- [2] A. Sivasamy, K. Y. Cheah, P. Fornasiero, F. Kemausuor, S. Zinoviev, S. Miertus, *Chem. Sus. Chem.* **2009**, 2, 278.
- [3] W. L. Dai, S. L. Luo, S. F. Yin, C. T. Au, *Appl. Catal. A* **2009**, 366, 2.
- [4] F. Figueras, *Top. Catal.* **2004**, 29, 189.
- [5] H. A. Prescott, Z. J. Li, E. Kemnitz, A. Trunschke, J. Deutsch, H. Lieske, A. Auroux, *J. Catal.* **2005**, 234, 119.
- [6] D. Tichit, B. Coq, *Cattech.* **2003**, 7, 206.
- [7] G. D. Wu, X. L. Wang, B. Chen, J. P. Li, N. Zhao, W. Wei, Y. H. Sun, *Appl. Catal., A* **2007**, 329, 106.
- [8] B. M. Choudary, M. L. Kantam, V. Neeraja, K. K. Rao, F. Figueras, L. Delmotte, *Green Chem.* **2001**, 3, 257.
- [9] B. F. Sels, D. E. De Vos, P. A. Jacobs, *Catal. Rev.Sci. Eng.* **2001**, 43, 443.
- [10] A. Gervasini, *Catal. Lett.* **1997**, 43, 219.
- [11] K. C. Waugh, *Appl.Catal.* **1986**, 25, 121.
- [12] M. Bowker, *J. Catal.* **1986**, 99, 53.
- [13] H. Noller, *Z. Phys. Chem. NF* **1985**, 144, 157.
- [14] A. Ouqour, G. Coudurier, J. C. Vedrine, *J. Chem. Soc., Faraday Trans.* **1993**, 89, 3151
- [15] H. C. Greenwell, P.J. Holliman, W. Jones, B. V. Velasco, *Catal. Today* **2006**, 114, 397.
- [16] Y. Wang, X. W. Han, A. Ji, L. Y. Shi, S. Hayashi, *Microporous Mesoporous Mater.* **2005**, 77, 139.
- [17] P. J. Schilling, L. G. Butler, A. Roy, H. C. Eaton, *J. Am. Ceram. Soc.* **1994**, 77, 2363.
- [18] H. A. Prescott, Z. J. Li, E. Kemnitz, J. Deutsch, H. Lieske, *J. Mater. Chem.* **2005**, 15, 4616.
- [19] W. P. Zhang, M. Y. Sun, R. Prins, *J. Phys. Chem. B* **2002**, 106, 11805.

- [20] M. Reinholdt, J. Miehe-Brendle, L. Delmotte, M. H. Tuilier, R. le Dred, R. Cortes, A. M. Flank, *Eur. J. Inorg. Chem.* **2001**, 2831.
- [21] H.C. Chidwood and B.T. Freure, *J.Am.Chem.Soc.* **1946**, 68, 680.
- [22] R.E. Parker and N.S. Isaacs, *Chem.Rev.* **1959**, 59, 737.
- [23] V. Mirkhani, S. Tangestaninejad, B. Yadollahi, L. Alipanah, *Tetrahedron* **2003**, 59, 8213.
- [24] H. Noller, J.A. Lercher and H. Vinek, *Mater. Chem. Phys.* **1988**, 18, 577.
- [25] J.A. Lercher and H. Noller, *J. Catal.*, **1982**, 77, 152.
- [26] H. M. Kao, Y. C. Chen, *J. Phys. Chem. B* **2003**, 107, 3367.

Chapter 6

Au supported on Ceria

Abstract

Au supported on CeO₂ prepared by the method of deposition-precipitation with urea leads to a basic catalyst. Au acts in two ways as surface modifier. First, Au selectively interacts with Ce⁴⁺ cations by either blocking the access or reducing Ce⁴⁺ to Ce³⁺. Secondly, the resulting Au⁺ cations act as soft weak Lewis acid sites stabilizing carbanion intermediates and enhancing the hydride abstraction in the dehydrogenation of alcohols. In consequence, the so synthesized basic catalyst catalyzes the dehydrogenation to acetone with high efficiency and without notable deactivation. As Au also quantitatively blocks the access to strongly acidic Ce⁴⁺ cations or reduces them to Ce³⁺, the dehydration of propanol pathway is eliminated.

6.1 Introduction

Ceria was first time published in 1882 by Hartley^[1] when he analyzed rare earth minerals in British minerals. In 1930, more than 40 years later, ceria was first mentioned as catalyst material. Kodama^[2] reported the influence of titania, zirconia and ceria on the catalytic reduction of CO₂ under normal pressure. Since that time, ceria was recognized as interesting and challenging catalyst material as can be seen by the increasing number of publications related to that field. From 1981 to 2000 about 1566 citations were found related to the subject catalysis. Nowadays, roughly 3000 publications are correlated to the topic ceria in catalysis. Hereunder the most common application of ceria as catalyst or catalyst additive is the three-way-catalyst for automotive exhaust purification.^[3] High oxygen mobility accompanied by good redox properties, due to the highly active $\text{Ce}^{4+} \leftrightarrow \text{Ce}^{3+}$ redox-couple, promotes ceria in comparison to other oxide supports. Oxygen vacancies are assumed to be the most active sites on the surface. The activity of ceria depends among others on nature, number, distribution and diffusion of the oxygen vacancies across the surface.^[4] They can be formed, for example, by low and high temperature reduction, respectively, on the surface or in the bulk of ceria.

Ceria crystallizes in the fluorite type structure wherein each O²⁻ ion is surrounded by a tetrahedron of Ce⁴⁺ cations.^[5] The fluorite lattice exhibits a quite open structure and facilitates oxygen diffusion from the bulk to the surface. This is accompanied by reduction of the bulk, which is called chemical pump effect.^[6] The reducibility of ceria can be related to its textural and morphological properties. The more perfect the crystallinity of the oxide, the more difficult it is to reduce.

Reduction of ceria takes place under CO or hydrogen atmosphere. While during treatment in hydrogen surface OH-groups are formed which depends on the reduction temperature, reduction with CO leads to formation of CO₂ and oxygen vacancies on the surface. Therefore, CO is regarded as a more appropriate reducing agent than hydrogen.^[3]

The ability as oxygen storage and releasing material as well as the promoter effect for noble metal catalysts are obviously two key characteristics of ceria and determines its use.^[7]

Ceria is widely used as support in transition metal or noble metal catalysis because of its outstanding properties.^[8] Ceria facilitates the increase of the metal dispersion and thermal stability, stabilizes small metal particles and shows special features regarding metal-support interactions.^[9]

Metal oxide catalysts have attracted wide interest because of their outstanding performance for reactions including the removal of CO in the presence of H₂ via PROX (= preferential oxidation of CO)^[10], oxidation of unsaturated ketones^[11], hydrogenation of nitro compounds^[12] and WGS.^[13]

Among the variety of metals, metal oxide-supported Au has been recognized as interesting catalytic material. The potential of Au/ceria materials is reflected in the expanding number of publications. 1967, the opportunity of gold on ceria thin films as efficient energy solar absorber was described as one of the first applications.^[14] The unique properties of ceria-supported Au catalysts depend on a variety of features, i.e., the dispersion of the nano-scaled particles,^[15-17] the oxidation state of the Au particles,^[18, 19] and the type of ceria used.^[20-23] There is an ongoing discussion about the nature of the active gold species. In combination with the catalytic activity being related to several above mentioned factors like the nature of the support, the influence of the calcination temperature, the oxidation state of the metal and of the cerium support atoms some ambiguity remains about the governing factors for the activity of those catalysts.

Not only the catalytic oxidation over oxide supported gold metal nanoparticles has been widely explored,^[9, 24-26] but also the benefits as hydrogenation catalyst were analyzed.^[27] Furthermore, the use of ceria supported gold catalysts in the low temperature water-gas shift reaction was investigated.^[28, 29] One example for the importance of oxygen vacancies of ceria in the activation of Au was investigated by synchrotron-based high-resolution photoemission in the reaction of SO₂ with Au/ceria (111) surfaces.^[30]

Up to now applications of metal oxide supported Au materials in acid-base type reactions are negligible due to the generally inert nature towards this type of reaction. Thus, it would be of great interest to explore the role of nano-sized gold particles on the support acid-base properties.

Conceptually, solid bases act either as bifunctional (acid-base) catalysts via polarization of bonds or as proton abstracting agents inducing the catalytic cycle.^[31] The

characterization of basic materials by probe molecules is not straightforward, since their application is limited to a certain range of base strength.^[32] Use of characteristic probe reactions may thus be one way out. Therefore, the well-established probe reaction of conversion of propan-2-ol was used as test reaction. Depending on the nature and strength of active sites, propan-2-ol is either dehydrated to propene as well as condensed to di-iso-propylether on acidic sites, or dehydrogenated to acetone on predominantly basic sites.^[33-36] According to the literature, propan-2-ol is converted to acetone and propene over ceria.^[37, 38] Ceria does not only exhibit acid and base sites occurring on metal oxides, but also shows redox properties due to its high oxygen mobility. These redox sites give an additional reaction pathway depending on the reaction atmosphere (oxidizing or reducing) either to propene or acetone.^[39] So, it would be of special interest to explore the influence of metal particles on the selectivity of the dehydration/dehydrogenation of propan-2-ol over modified ceria catalysts.

Generally, supported Au particles might on the one hand block sites, but may also lead to the generation of new sites at the interface between the particle and the support. Potential hydrogenating/dehydrogenating as well as further hydride transfer properties might open additional reaction pathways. As the role of positively charged gold may play a role in the conversion also the oxidation state of the gold species will be investigated, due to the ability of additional Lewis acid sites in case of unreduced Au^I and Au^{III}.

The preparation of Au/ceria materials can be achieved by different approaches.^[40-43] Deposition-precipitation (DP) with urea is one of the most frequently used methods.^[44] The DP method has the advantage of (i) yielding narrower particle size distributions and (ii) localizing Au exclusively on the surface.^[43] Urea as deposition agent facilitates the deposition of Au from the solution onto the support.^[45] However, the as-prepared samples are treated subsequently in different atmospheres to activate the materials. Besides the influence of the conditioning atmospheres on the ceria support it has to be considered that upon urea decomposition^[46] during the activation an in situ formation of carbon dioxide and ammonia lead to the appearance of several intermediates which may change the surface properties. The extent of the catalyst modification by using a co-precipitant may not be easily predictable and will (i) influence the final material and vice versa will (ii) also be influenced by the interaction between Au and the support. It is known, that

removal of carbon dioxide from a ceria surface needs temperatures above 500 °C.^[47] Thus, if an as-prepared sample based on urea deposition is treated below 500 °C, surface species (mainly carbonates but also intermediates of urea decomposition) may remain.^[48] Thus the influence of urea on the evolution of surface properties of gold supported ceria with respect to its acid-base properties was studied, too.

6.2 Experimental

6.2.1 Preparation

All chemicals were obtained from Sigma-Aldrich and if not denoted utilized with no further purification.

6.2.1.1 Ceria

- a) Commercial ceria was obtained from Merck and pre-treated in synthetic air at 100 mL·min⁻¹ by increasing the temperature from ambient to 600 °C with 10 K·min⁻¹ for 8 h. Ceria prepared by this method is labeled as *CeO₂*.
- b) The self made ceria was synthesized by different preparation methods. First, Ce(CO₃)₂·xH₂O (99.9 % purity) was calcined in a flow of synthetic air at 100 mL·min⁻¹ by increasing the temperature from ambient to 600 °C at 10 K·min⁻¹ for 6 h. Ceria prepared by this method is labeled as *CeO₂ (C600)*.
- c) Second, cerium nitrate was precipitated as described previously elsewhere.^[49] 1.15 L of a 2 M Ce(NO₃)₃·6H₂O aqueous precursor solution was mixed with 575 mL of a 3 M ammonia solution and stirred at RT for 24 h. The precipitate was centrifuged and washed with 1.1 L of a water/ethanol (1:1) mixture until the pH was 7. The resulting precipitate was purple. The precipitate was dried at 60 °C for 8 h and calcined in a flow of synthetic air at 100 mL·min⁻¹ by increasing the temperature from ambient to 600 °C at 10 K·min⁻¹ for 8 h. Ceria prepared by this method is labeled as *CeO₂ (N600)*.
- d) A further synthesis was used as leaned on a method described by Corma et al. elsewhere.^[50] An aqueous solution of 0.8 M Ce(NO₃)₃·6H₂O (25.18 g, 0.058 mol) was mixed with 218 mL of a 0.8 M ammonia solution under vigorous stirring at ambient

temperature. Afterwards the dispersion was heated under reflux at 100 °C for 24 h. After cooling to RT, the as prepared precipitate was filtered and dried in vacuum. Ceria prepared by this method is labeled as *CeO₂ (N100)*.

6.2.1.2 Ceria-urea

A series of urea modified ceria catalysts with different amounts of urea was prepared. For that purpose, the pre-treated ceria (3 g) was suspended in 300 mL deionized water, heated to 80 °C and mixed with urea (0.9 g, 0.015 mol). The suspensions were stirred at 80 °C for 16 h. Afterwards the materials were dried in vacuum at ambient temperature for 16 h. The catalyst modified with urea is labeled as *CeO₂-urea*.

A further urea modified ceria sample was prepared by adding HCl as precipitation agent. The materials were washed with 150 mL deionized water and centrifugated. Further reconditioning was done as described above.

6.2.1.3 Au/Ceria

Au/ceria catalysts were prepared from commercial ceria as well as from self made ceria. For preparation of gold supported ceria catalysts, the deposition-precipitation method with urea (DP urea) as described previously by Delannoy et al.^[23] was used. The Au precursor was prepared by dissolving HAuCl₄·3H₂O (1 g, 2.54 mmol) in 100 mL of deionized water (0.0254 mol·L⁻¹). The pre-treated ceria (3 g) was suspended in 300 mL deionized water and heated at 80 °C. Various Au loadings were generated by adding an appropriate amount of the precursor solution followed by adding urea immediately (see Table 6-1). Several materials with different nominal wt.-% Au loadings were prepared. The suspensions were stirred at 80 °C for 16 h. Afterwards the materials were washed with deionized water. Washing was repeated with 350 mL (with centrifugation after each washing step) until the pH of the solution was 7 and neither Au⁺ nor Cl⁻ were verified by testing with NaBH₄ (in case of gold) and AgNO₃ (in case of chloride). The samples were dried in vacuum at ambient temperature for 16 h.

Table 6-1. Amount of Au-precursor solution and urea used for synthesis of modified ceria samples.

<i>Sample</i>	<i>H₂AuCl₄</i> (<i>solution</i>)	<i>Urea</i>
[Au-loading wt.-%]	[mL]	[g]
CeO ₂ -urea	-	0.90
Au/CeO ₂ (0.1)	0.60	0.09
Au/CeO ₂ (0.4)	2.40	0.36
Au/CeO ₂ (0.8)	4.80	0.72
Au/CeO ₂ (1.0)	6.00	0.90

Deposition precipitation of Au with NaOH was carried out as described elsewhere.^[50] An 0.2 M aqueous solution of NaOH was added to 6 mL of an aqueous solution of H₂AuCl₄ (1 g, 2.54 mmol) so that the pH was 10. The Au solution was then added to 3 g of the filtered ceria dispersion obtained as described under 6.2.1.1 d). Again, the pH was adjusted to 10 by adding 0.2 M NaOH_{aq}. The mixture was stirred at ambient temperature for 18 h. Afterwards the precipitate was filtered and washed with 1.2 L deionized water until the pH of the solution was 7 and no Cl⁻ was verified by testing with AgNO₃. The precipitate was dried in vacuum at RT for 48 h. Afterwards the solid was suspended in 20 g 1-phenylethanol and heated to 160 °C. The suspension was stirred under reflux at 160 °C for 20 min. The suspension was cooled to ambient temperature and filtered. The solid was washed with 200 mL acetone and 400 mL deionized water, and dried in vacuum. The as prepared catalyst is labeled as *Au/CeO₂-NaOH (1.0, N100)*.

6.2.2 Characterization Techniques

6.2.2.1 Bulk techniques

Analysis of elemental composition was performed by inductive coupled plasma emission spectroscopy at the LRS Laboratories de Réactivité et Surface (Université Pierre et Marie Curie, France).

Specific surface areas and pore volumes were determined by physisorption of N₂ at 77 K. Measurements were carried out in *PMI automatic BET-Sorptometer*. Evaluation was done according to the BET theory.

The crystalline structure of the synthesized and modified materials was analyzed by XRD using a *Philips X'Pert Pro System* (CuK_α1-radiation, 0.154056 nm) at

40 kV / 40 mA. Measurements were carried out on a spinner performed with a $1/4''$ slit 2θ step size ($0.03^\circ \text{ min}^{-1}$) and with a $1/6''$ slit in the range from $2\theta = 20^\circ$ - 70° ($0.05^\circ \text{ min}^{-1}$). In-situ experiments were carried out in the *Philips X'Pert Pro System*, as described above, equipped with a *HTK 2000 oven*. The samples were heated stepwise (100°C) from ambient to 700°C in a flow of $5 \text{ mL}\cdot\text{min}^{-1}$ synthetic air.

Temperature programmed desorption of ammonia (NH_3 -TPD) and carbon dioxide (CO_2 -TPD) were used to determine acidic and basic properties. As standard materials for referencing the NH_3 -TPD and CO_2 -TPD, a H-MFI 90 zeolite and NaHCO_3 were used, respectively. Catalyst samples were activated at 500°C in vacuum for 1 h. Adsorption of ammonia at (1 mbar) was performed at 100°C for 1 h. CO_2 (1 mbar) was adsorbed at 40°C for 1 h. Desorption occurred during sample heating from corresponding temperature up to 700°C with a rate of $10 \text{ K}\cdot\text{min}^{-1}$. Analysis was done with *Pfeifer Vacuum Mass Spectrum* (MS).

6.2.2.2 Surface techniques

For transmission electron microscopy (TEM) images the samples were grinded, suspended in ethanol and ultrasonically dispersed. An appropriate amount of the as-prepared dispersion was dropped on a copper-grid supported carbon film. Micrographs were recorded on a *JEM-2010 Jeol* transmission microscope operating at 120 kV.

Investigations of surface properties for ceria and modified ceria samples were performed by X-ray photoelectron spectroscopy (XPS) at the Institute of Technical Chemistry, University of Leipzig. XPS analysis was carried out using a hemispherical energy analyzer *Phoibos 150* (Specs GmbH, Berlin, Germany) equipped with an X-ray source *XR 50* (Specs GmbH). O 1s, Ce 3d, C 1s and Au 4f lines were monitored using the Mg K_α line at 1253.6 eV and excitation energy of 20 kV.

6.2.2.3 Infrared spectroscopy

Infrared spectroscopy was carried out on a *Perkin-Elmer 2000 spectrometer* coupled with a MCT detector or a *Bruker IFS 88 spectrometer*. Samples were pressed into self-supporting wafers and activated in vacuum at 500°C for 2 h. The spectra were

recorded in transmission mode at a resolution of 4 cm^{-1} in the region from 4000 to 780 cm^{-1} .

Adsorption of pyridine, methanol or propan-2-ol was followed by IR. Sample preparation and instruments were used as described above. Pyridine was adsorbed at 0.1 mbar at $50\text{ }^{\circ}\text{C}$ and out gassed with increasing temperatures from 150 to $250\text{ }^{\circ}\text{C}$ for 2 h.

Methanol or propan-2-ol was adsorbed at $50\text{ }^{\circ}\text{C}$ and a partial pressure of 0.1 mbar. The sample was equilibrated at this temperature for 0.5 h, afterwards, the adsorbate was removed by heating to $300\text{ }^{\circ}\text{C}$ in vacuum.

6.2.3 Catalytic tests

6.2.3.1 Conversion of propan-2-ol

The dehydrogenation/dehydration reaction of propan-2-ol was studied in inert atmosphere in the temperature range from 150 to $225\text{ }^{\circ}\text{C}$ with steps of $25\text{ }^{\circ}\text{C}$. The catalyst with arbitrary particle size (0.02 g diluted in 0.13 g SiC) was fixed with quartz wool in a quartz-tube reactor of 4 mm diameter. The catalyst was heated in H_2 or He flow of $20\text{ cm}^3\cdot\text{min}^{-1}$ from ambient to 300 or $500\text{ }^{\circ}\text{C}$ for 2 h, in order to activate the sample. Cooling to reaction temperature was reached under He ($20\text{ mL}\cdot\text{min}^{-1}$). For reaction, a helium flow of $40\text{ mL}\cdot\text{min}^{-1}$ was saturated with propan-2-ol at $13\text{ }^{\circ}\text{C}$ (partial pressure 25 mbar) and led over the fixed bed reactor. Un-reacted propan-2-ol and dehydrogenation/dehydration products were analyzed by gas chromatography using a *Hewlett Packard GC* equipped with a flame ionization detector. Separation of various components was done by a *Supelco*[®] wax-column.

6.2.3.2 Hydrogenation of acetone

The hydrogenation of acetone was studied in hydrogen atmosphere in the temperature range from 150 to $225\text{ }^{\circ}\text{C}$ with steps of $25\text{ }^{\circ}\text{C}$. The as-prepared samples (0.2 g diluted in 0.35 g SiC) were fixed with quartz wool in a quartz-tube reactor of 4 mm diameter. The as-prepared samples were first pretreated in a flow of helium of $20\text{ mL}\cdot\text{min}^{-1}$ by heating from ambient to $500\text{ }^{\circ}\text{C}$ (heating ramp $10\text{ }^{\circ}\text{C}\cdot\text{min}^{-1}$) for 2 h in

order to activate the sample. Cooling to reaction temperature was reached under He flow of $20 \text{ mL} \cdot \text{min}^{-1}$, too. During reaction, a flow of hydrogen with $20 \text{ mL} \cdot \text{min}^{-1}$ was saturated with acetone at -12°C (partial pressure 49 mbar) and led over the fixed bed reactor. Unreacted acetone and hydration products were analyzed by gas chromatography using a *Shimadzu GC-2014* gas chromatograph.

6.3 Results

6.3.1 Characterization

The results of textural analysis of ceria, ceria-urea and Au loaded ceria samples are summarized in Table 3-1. The specific surface areas of commercial ceria supported samples were found to be less than $7 \text{ m}^2 \cdot \text{g}^{-1}$. The modification of ceria did not influence the specific surface area of the final material. The final gold loadings were 8 (0.16 wt.-% Au), 18 (0.37 wt.-%), 36 (0.7 wt.-%), 43 (0.84 wt.-%) and 98 (1.94 wt.-%) $\mu\text{mol} \cdot \text{g}^{-1}$. The Au particle size was increased with higher Au loadings.

Table 6-2. Textural analysis of ceria, modified urea and Au/ceria samples.

Sample	Specific surface area	Au-content	Au-Particle Size	Acid sites ¹⁾	Basic sites ²⁾
	$[\text{m}^2 \cdot \text{g}^{-1}]$				
CeO ₂	6	-	-	16	0.5
CeO ₂ - urea	5	-	-	9	1.4
Au/CeO ₂ (0.1)	5	0.16	-	-	-
Au/CeO ₂ (0.4)	5	0.37	-	11	1.1
Au/CeO ₂ (0.8)	6	0.71	-	13	1.6
Au/CeO ₂ (1.0)	5	0.84	1.35	13	0.9
Au/CeO ₂ (2.0)	6	1.94	2.05	-	-

¹⁾ Determined by NH₃-TPD (100-500 °C)

²⁾ Determined by CO₂-TPD (40-500 °C)

The results of the textural analysis for self-prepared ceria derived from the nitrate and carbonate precursor as-well as for the Au/urea modified samples are listed in Table 6-3. The specific surface areas were in the range between 44 and $49 \text{ m}^2 \cdot \text{g}^{-1}$. Due to the deposition of Au the specific surface areas of CeO₂ (N600) and (C600) were slightly

decreased. The Au-loadings were close to the nominal ones. However, the particle sizes differ markedly. The mean Au particle size of Au/CeO₂ (N600) was more than 4 times less compared to Au/CeO₂ (C600). The acid and base site density of CeO₂ (N600) and (C600) hardly varied.

Table 6-3. Textural analysis of ceria (N600, C600) and loaded (N600, C600) samples.

<i>Sample</i>	<i>Specific surface area</i>	<i>Au-content</i>	<i>Au-Particle Size</i>	<i>Acid sites</i> ¹⁾	<i>Basic sites</i> ²⁾
	[m ² ·g ⁻¹]	[wt.-%]	[nm]	[μmol·g ⁻¹]	[μmol·g ⁻¹]
CeO ₂ N600	45	-	-	30	3.0
Au/CeO ₂ N600 (1.0)	44	0.95	1.57	19	3.2
CeO ₂ C600	49	-	-	22	2.2
Au/CeO ₂ C600 (1.0)	44	1.00	6.85	19	3.3

The specific surface areas and final Au loadings of self prepared ceria (N100), by precipitation with ammonia, and Au loaded ceria samples, prepared via DPu and NaOH method are given in Table 6-4. The specific surface area was found to be ~ 40 m²·g⁻¹. There was no linear correlation between the specific surface area and precipitation with Au. The final Au-loading was less in case of Au/CeO₂-NaOH (N100, 1.0) than for Au precipitated on ceria with urea as precipitation agent. The acid site concentration was decreased by adding Au to ceria. A more detailed study on Au particles is given in the next part, by TEM analysis.

Table 6-4. Textural analysis of ceria (N100) and Au loaded ceria (N100) samples.

<i>Sample</i>	<i>Specific surface area</i>	<i>Au-content</i>	<i>Au-Particle Size</i>	<i>Acid sites</i> ¹⁾	<i>Basic sites</i> ²⁾
	[m ² ·g ⁻¹]	[wt.-%]	[nm]	[μmol·g ⁻¹]	[μmol·g ⁻¹]
CeO ₂ N100	41	-	-	24	0.1
Au/CeO ₂ N100-urea	44	0.89	1.73	16	0.8
Au/CeO ₂ N100-NaOH	37	0.40	-	13	2.0

¹⁾ Determined by NH₃-TPD (100-500 °C)

²⁾ Determined by CO₂-TPD (40-500 °C)

The size and dispersion of the gold particles were analyzed by TEM. Four samples were investigated in detail as Au particles could be identified only for higher Au

loadings above 1 wt.-% (see Figure 6-1 and Figure 6-2). The nano-sized particles are well dispersed on the ceria surface. The particle size distributions were determined based on 150 particles (Figure 6-1). The mean particle size in case of Au/CeO₂ (1.0) was 1.35 nm, while with increasing amount of gold (2 wt.-%) the mean particle size was increased to 2.05 nm.

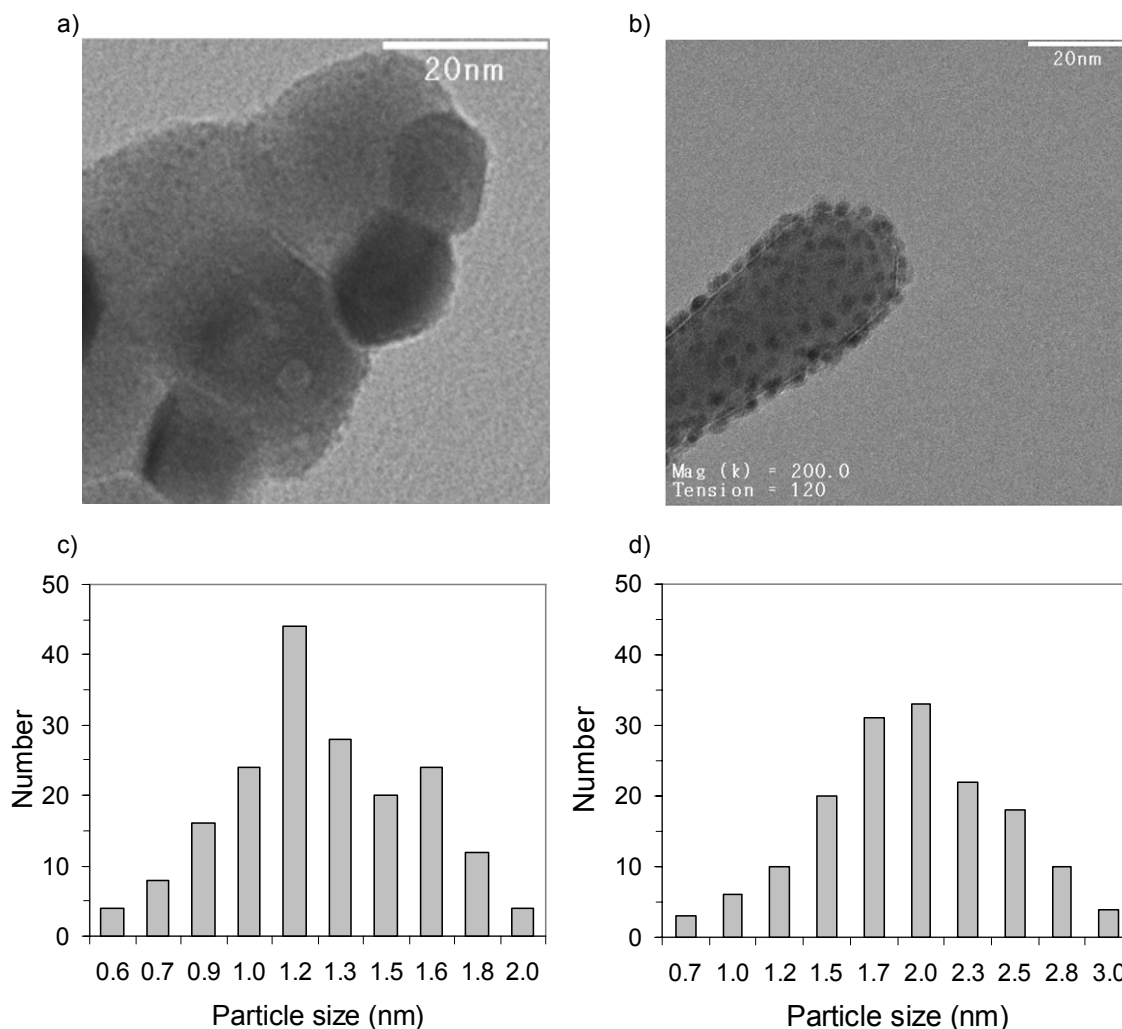


Figure 6-1. TEM pictures and particle size distribution of Au/ceria samples with higher Au-loadings. TEM pictures of Au/ceria: a) 1 wt.-% and b) 2 wt.-%
Particle size distribution of Au/ceria: c) 1 wt.-% and d) 2 wt.-%.

The Au particles on self prepared ceria (N600) were well dispersed. In contrast for Au loaded on ceria (N100) by the DPu method the particles were less well dispersed, as in the other cases. Au loaded on ceria (N100) via deposition precipitation with NaOH, not

shown here, was also followed by inhomogeneous dispersion of the metal particles. The particle size distributions of 1 wt.-% Au supported on ceria N600 and N100, determined as described above, by 150 particles are shown in Figure 6-2 c) and d), respectively. The mean particle size of Au was determined as 1.57 nm in case of Au/CeO₂ (N600, 1.0) and 1.73 nm for Au/CeO₂ (N100, 1.0).

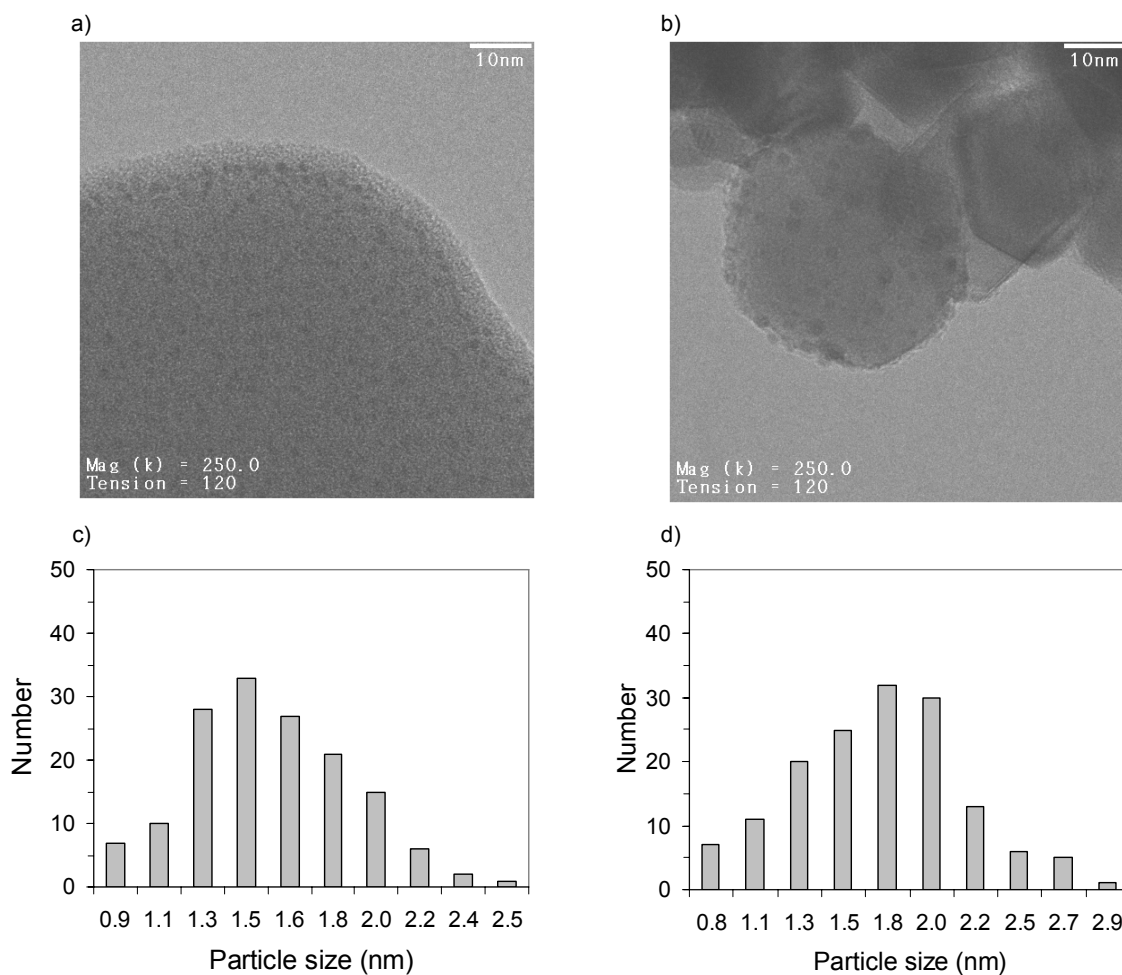


Figure 6-2. TEM pictures and particle size distribution of Au loaded on self prepared ceria supports. TEM pictures of: a) Au/CeO₂ (N600) 1 wt.-% and b) Au/CeO₂ (N100) 1 wt.-%. Particle size distribution of: c) Au/CeO₂ (N600, 1.0) and d) Au/CeO₂ (N100, 1.0).

XRD patterns of ceria supports are shown in Figure 6-3. Reflexes corresponding to cubic fluorite type ceria were observed at $2\theta = 28.6^\circ, 33.1^\circ, 47.5^\circ, 56.4^\circ, 59.1^\circ$ and 69.5° . The intensity of ceria reflexes decreased with increasing surface area, which indicates a decrease in crystallinity. Also broadening of reflexes was registered,

indicating smaller particles in case of ceria obtained by precipitation of nitrate and calcination of carbonate. The average prime particle size was determined by the Scherrer equation as described in Chapter 2, results are given in Table 6-5.

Table 6-5. Average prime particle size of ceria and self prepared ceria samples.

<i>Sample</i>	<i>CeO₂</i>	<i>CeO₂ (N100)</i>	<i>CeO₂ (N600)</i>	<i>CeO₂ (C600)</i>
<i>Particle size, [nm]</i>	456	31	22	18

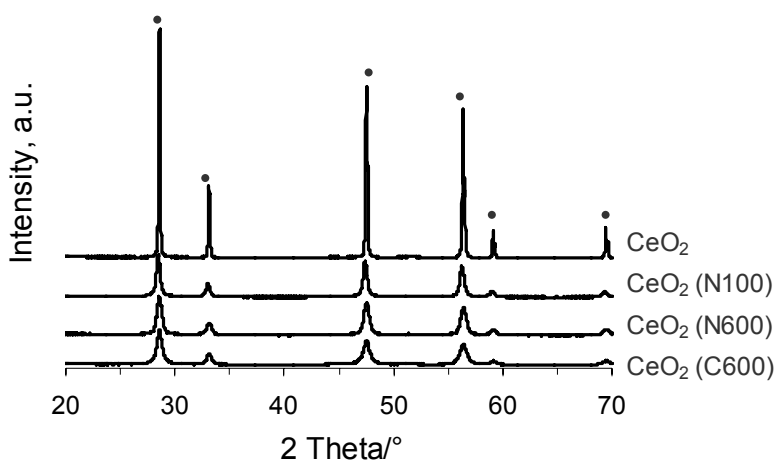


Figure 6-3. XRD patterns of ceria used as support for Au/ceria samples.

The crystal transformation by calcination from cerium carbonate to ceria was followed by in-situ XRD (see Figure 6-4). Cerium carbonate was heated from ambient temperature to 700 °C with rate of 10 K·min⁻¹ in a flow of synthetic air at 5 mL·min⁻¹. XRDs were recorded at each temperature step of 100 °C. Transformation from cerium carbonate to ceria was observed at 100 °C. Further temperature increase resulted in an increase of crystallinity. Narrowing of ceria reflexes indicated an increase of the particle sizes. The particle size was increased from 7.5 nm at 100 °C to 18 nm at 600 °C. After calcination at 700 °C the particle size increased to 50 nm.

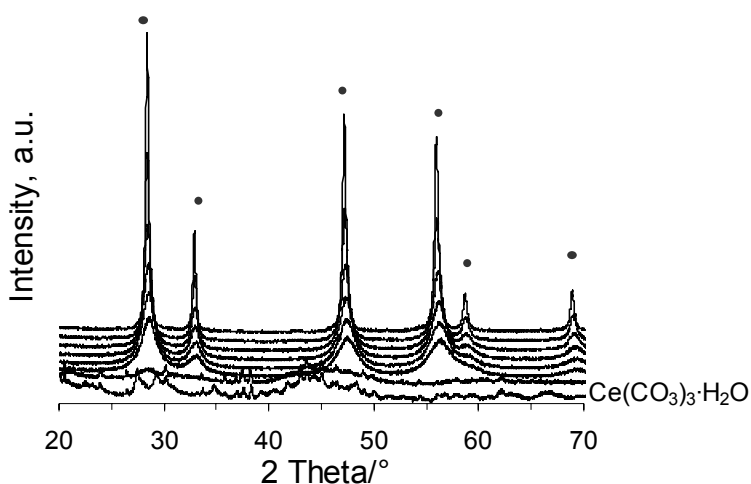


Figure 6-4. XRD patterns of $\text{Ce}(\text{CO}_3)_3 \cdot \text{H}_2\text{O}$ during heating from ambient to 700 C.

XRD patterns of ceria, urea modified ceria and Au/ceria samples are depicted in Figure 6-5 for comparison. The reflexes correspond to cubic fluorite type ceria. The characteristic reflex for crystalline Au at 38 ° did not appear, even not in the case with highest gold loading (2 wt.-%).^[9] Changes of the ceria crystal phase were not detected by the modification with urea and loading with gold.

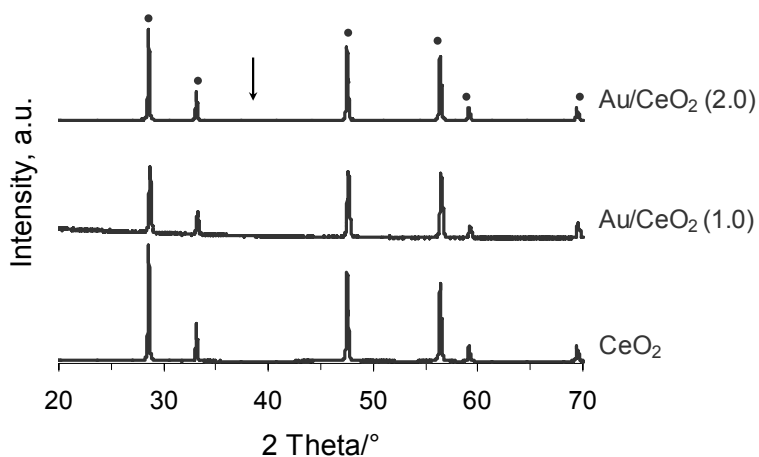


Figure 6-5. XRD patterns of ceria, Au/ceria (1.0) and Au/ceria (2.0).

Structure analysis via XRD of CeO_2 (N100) obtained from nitrate precursor in aqueous ammonia solution and Au modified samples are shown in Figure 6-6. The

deposition of Au neither with urea nor with NaOH caused noticeable changes in the structure of ceria. Calculation of particle sizes with the Scherrer method gave sizes of 31 (support) and 29 nm (Au/ceria).

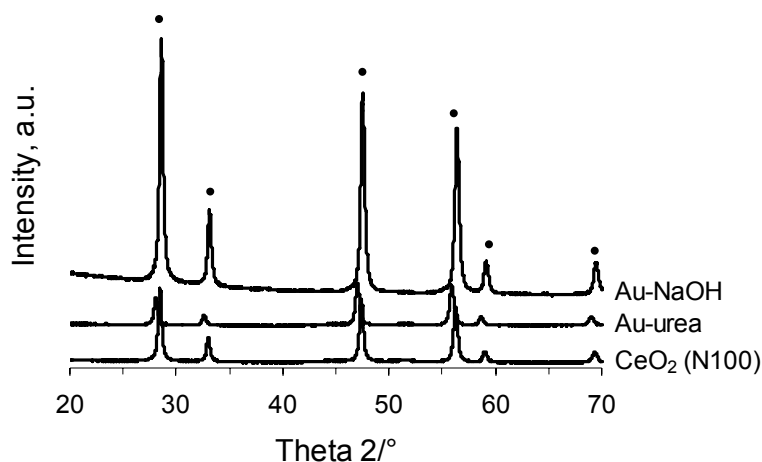


Figure 6-6. XRD patterns of CeO₂ (N100) and Au loaded CeO₂ (N100) samples by DPu and NaOH method.

XPS studies were carried out analyzing the surface structure of plain ceria and after modification with urea and precipitation of gold. The Ce 3d XP spectra obtained from the samples labeled ceria-urea, Au/CeO₂ (1.0) and for comparison of ceria are plotted in Figure 6-5. The Ce 3d spectra were dominated by a doublet at binding energies of 882.5/889 eV in all cases. An additional peak at 885.5 eV appears in case of urea and Au-ceria samples. The doublet corresponds to Ce⁴⁺ in CeO₂, while the latter energy is related to Ce³⁺ as it exists in Ce₂O₃ or in CeO₂ with oxygen vacancies.^[51]

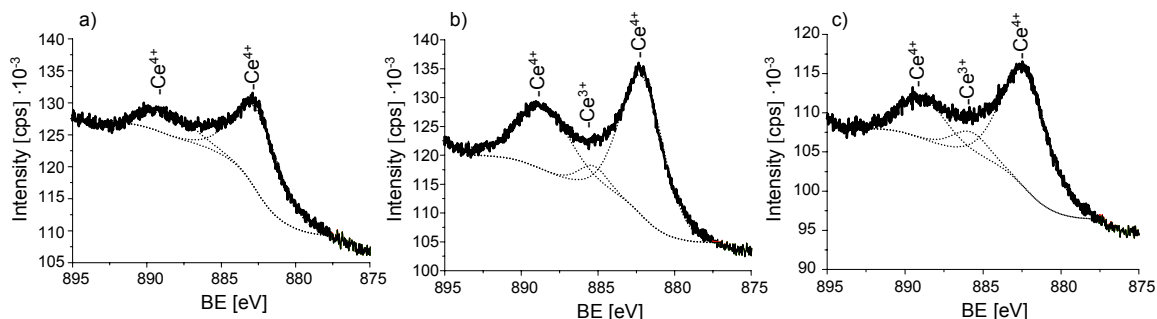


Figure 6-7. Ce 3d XPS of (modified) ceria.

a) CeO_2 , b) CeO_2 -urea and c) Au/CeO_2 (1.0)

Two different carbon peaks were observed in the C1s XP spectra for all samples (see Figure 6-8). The main peak located at 284 eV is assigned to adventitious carbon. The spectra were calibrated to this signal. The second carbon species was observed at binding energy of 288.5 eV for ceria and correlated to surface carbonates.^[52] Due to the modification of ceria with urea the intensity of the carbonate signal decreased. The intensity of carbon in the spectra of Au/CeO_2 decreased for both signals, indicating less carbonate formation on this sample.

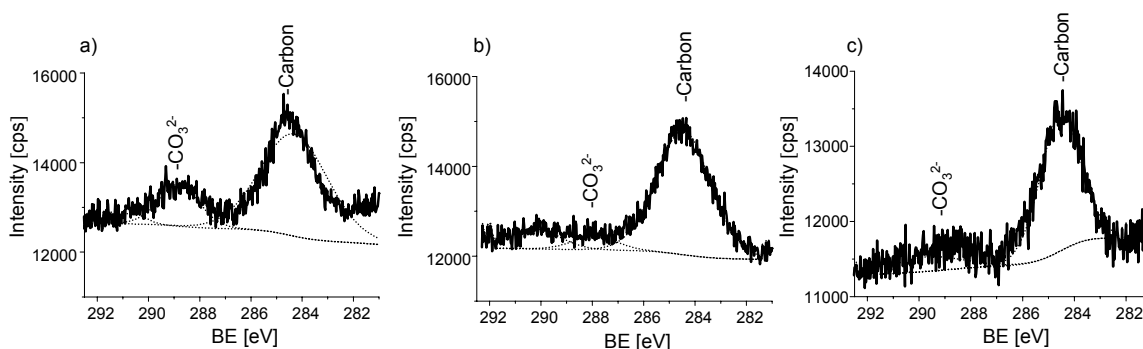


Figure 6-8. C1s XPS of (modified) ceria.

a) CeO_2 , b) CeO_2 -urea and c) Au/CeO_2 (1.0)

Surface hydroxyl- and carbonate-groups occurred with a broad signal located at 532 eV and a second signal related to lattice oxygen atoms at 529 eV was identified by O1s XP spectra for all samples (see Figure 6-9). The intensity of the signal related to OH- and CO_3^{2-} -groups was decreased by adding urea and almost completely removed by adding Au. Meanwhile, a third species developed after adding Au at 526.5 eV, which can

be assigned to basic oxygen. The shift of the O^{2-} peak to lower binding energies for CeO_2 -urea and Au/CeO_2 indicates increasing basicity, as the effective negative charge of oxygen is higher.^[53] Thus, the basicity increased in the following order: $CeO_2 < CeO_2$ -urea and Au/CeO_2 .

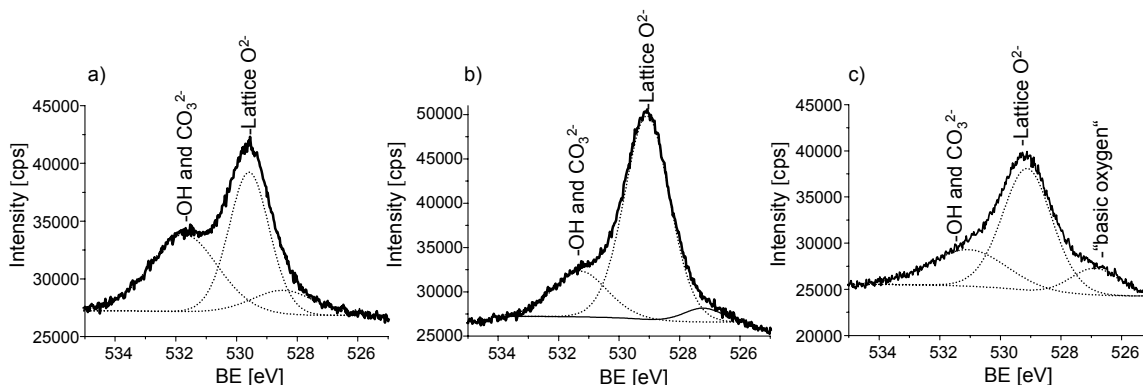


Figure 6-9. O 1s XPS of (modified) ceria.

a) CeO_2 , b) CeO_2 -urea and c) Au/CeO_2 (1.0)

The Au 4f spectrum of Au/CeO_2 (1.0) indicated the presence of two different Au species. The dominating doublet corresponding to Au^0 occurred at 83.75/87.5 eV.^[54, 55] The small peak with a binding energy of 85.05 eV (14 at-%) can be related to Au^+ ions.^[54]

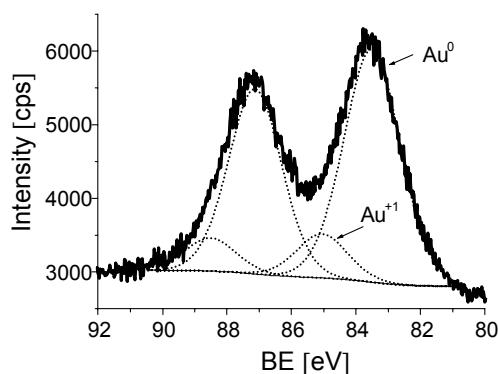


Figure 6-10. Au 4f XPS of Au/CeO_2 (1.0).

6.3.2 Thermal stability of urea modified and Au supported ceria

The thermal stability of selected samples was studied for conditions similar to the activation procedure via mass spectrometry and IR.

Figure 6-11 shows desorption profiles during heat treatment in vacuum from ambient to 500 °C. Two profiles for ceria, urea modified ceria and Au/CeO₂ were analyzed in detail, namely, for ammonia (m/e = 16) and carbon dioxide (m/e = 44). The desorption profiles of ammonia and carbon dioxide are strongly related to each other. The desorption maxima of NH₃ and CO₂ occur between 100 and 300 °C. The amount of desorbing NH₃/CO₂ decreased with the concentration of precipitated urea in the order Au/CeO₂ (1.0) > (0.8) > urea > (0.4) ≥ CeO₂.

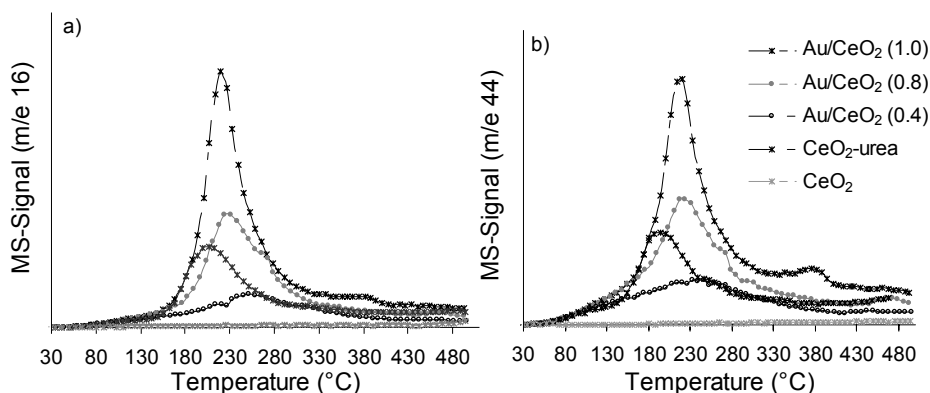


Figure 6-11. Desorption profiles for ceria, urea modified ceria and Au/ceria samples during heating from RT to 500 °C.

a) Ammonia (m/e 16) and b) Carbon dioxide (m/e 44).

No further ammonia desorption was detected after increasing temperature above 500 °C. However, in case of ceria a peak was registered at 600 °C with a maximum at 675 °C (Figure 6-12). This peak is related to oxygen desorbing from the surface.

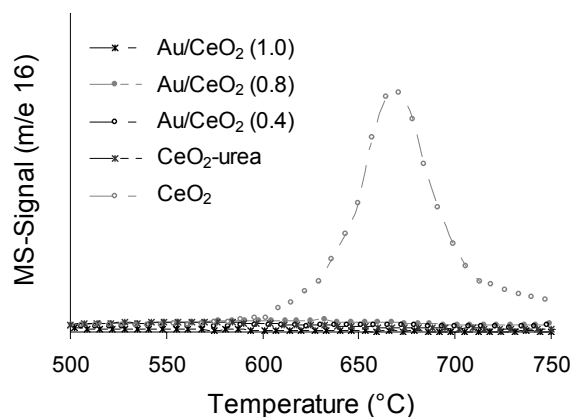


Figure 6-12. Desorption profiles of ammonia (m/e 16) for ceria, urea modified ceria and Au/ceria samples between 500 and 750 °C.

Surface modifications caused by decomposition of urea, as observed by MS during TPD, were also investigated by in-situ IR. Therefore a sample of ceria modified with urea (*CeO₂-urea*) was heated in vacuum from 50 to 500 °C with a ramp of 10 K·min⁻¹. Spectra were recorded stepwise every 100 °C and are illustrated in Figure 6-13. The characteristic bands are given in Table 6-6 and were attributed in accordance with the literature. [46, 56-60]

Table 6-6. Characterization of IR bands during thermal decomposition of *CeO₂-urea*.

Species	Frequency (cm ⁻¹)		300°C	400°C	500°C
	100°C	200°C			
v(OH) Type I	3700	3714	3718	3717	3715
v(OH) Type II	3646	3648	3640	3631	3624
v(OH) Type III	-	-	-	3485	3482
v(CO₂)	2339	2339	2339	2338	2338
v(C≡N)	-	-	2258	2248	-
v(O-C≡N)	2169	2170	2169	2168	2167
v(NO⁺)	-	1973	1971	1972	1971
v(CO₃²⁻)	1657-1584	1654-1578	1620-1500	1597-1506	-
v(C-NH)	1470	1467	-	-	-
v(N-C-N)	-	-	1457	1456	1453
v(NH-C=O)	1316	1324	1334	1335	1336
v(NH₃)	1258	1260	1264	1263	-
v(C=O)	1154	1152	-	-	-

Overall three groups of IR bands are observed between 3800 and 2800 cm^{-1} (OH-stretching vibrations), 2400-1900 cm^{-1} (triple and double carbon bands) and below 1800 cm^{-1} (region of deformation and combination vibrations)

After outgassing at 100 °C a band at 3700 cm^{-1} assigned to terminal (type I) hydroxyl groups was observed. A second band appeared at 3646 cm^{-1} which is attributed to bridging (type II) hydroxyl groups of ceria.^[61]

The broad band allocated between 3600 and 3000 cm^{-1} is assigned to water adsorbed on the surface via hydrogen bonds. As the temperature increased all hydroxyl bands decreased significantly in intensity, an additional band at 3485 cm^{-1} appeared above 400 °C. This band seemed to be covered by adsorbed water before. It is assigned as hydroxyls (type III) located in the pores, correlating to cerium oxyhydroxide phase.^[62]

Residual urea presence from the preparation procedure and decomposition products (occurring already at low temperatures from 60 °C)^[46] caused bands at 2339 and 2169 cm^{-1} . These are assigned to CO_2 and iso-cyanates, respectively, although the intensities of these bands were low compared to the bands representing carbonates (1660-1580 cm^{-1}). In addition a band at 1470 cm^{-1} was observed at 100 °C. This band is assigned to the asymmetric N-C-N stretching vibration of urea.^[59] Bands with low intensity related to biuret and ammonia were observed at 1316 and 1258 cm^{-1} , respectively.

All bands were varied in intensity and shape during the further heating process. This is attributed to the decomposition of urea and the formation of intermediate stable compounds. Three regions of bands were mostly affected by the thermal treatment (see Figure 4a). (i) The band for iso-cyanate at 2169 cm^{-1} reached a maximum in intensity at 300 °C. (ii) Between 100 and 300 °C an additional band developed at 1973 cm^{-1} (related to nitrosyl-ions NO^+)^[60] showing a higher intensity than the band at 2339 cm^{-1} . The formation of dinitrosyl complexes with a band around 1910 cm^{-1} was also described in literature after reduction of ceria surfaces and exposition to NO .^[63] The intensity of this band had a maximum at 400 °C but was still clearly visible at 500 °C. (iii) The band at 1316 was shifted to 1334 cm^{-1} after heating to 300 °C and increased in intensity by further heating and was stable at 500 °C. This band was as intensive at 400 °C as the bands at 2167 and 1973 cm^{-1} and remained with appreciable intensity at 500 °C. It is

assigned to biuret ($\text{H}_2\text{N-CO})_2\text{NH}$) formed by condensation of two urea molecules upon heating and removal of ammonia from urea, which indicates a high surface density of urea. All these bands decreased in intensity at higher temperature, and nearly disappeared at 500 °C.

The CO-bands in the region between 1700 and 1400 cm^{-1} were almost removed at 500 °C.

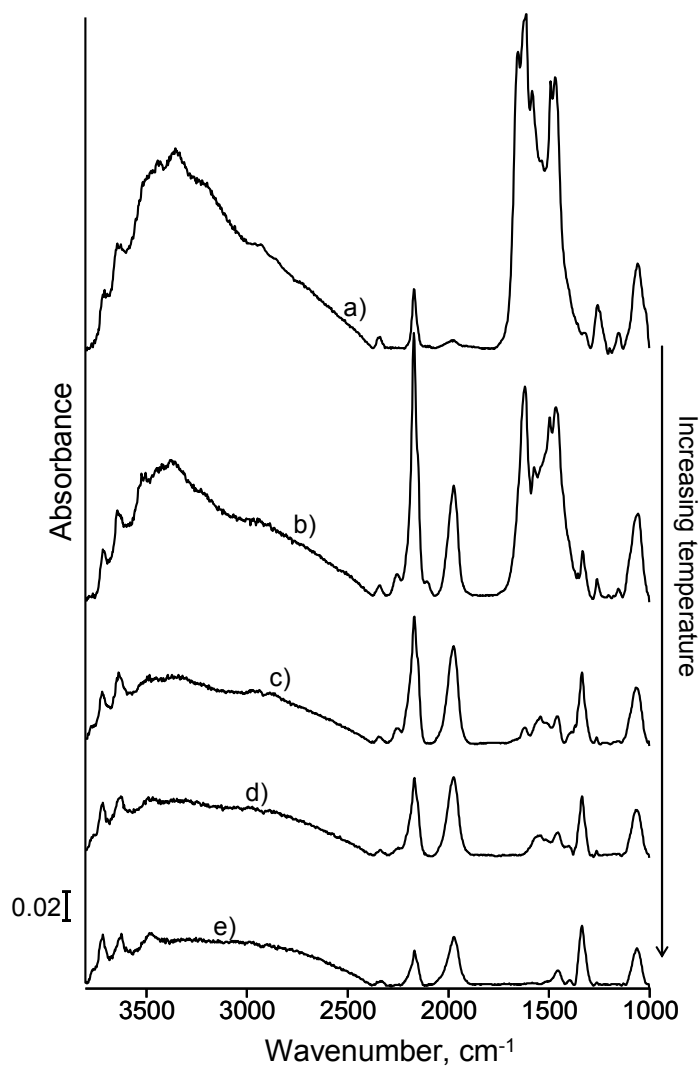


Figure 6-13. Infrared spectra of ceria-urea during heating under vacuum from 100 to 500 °C.

a) 100 °C, b) 200 °C, c) 300 °C, d) 400 °C and e) 500 °C.

The presence of remaining vibration bands at 500 °C attests that several decomposition products of urea, which contain carbon and nitrogen, were not removed by

heating to 500 °C and remain most probably on the ceria surface. Mitoraj and Kisch^[58, 64] studied the decomposition of urea over titania for photocatalysis applications and found new surface species correlating to poly-*s*-triazine containing melamine fragments.

In a similar series of experiments the thermal stability of the Au/CeO₂ (1.0) sample was tested (see Figure 6-14). Main differences to CeO₂-urea were found preferably in the OH region and in the relative intensity of the signals around 2000 cm⁻¹. After activation at 500 °C bands were observed at 3721 and 3642 cm⁻¹ indicating type I and type II hydroxyls.^[61] The bands are slightly shifted to higher wavenumbers. A pronounced shoulder at 3481 cm⁻¹ was not observed in this case indicating a loss of the type III species. The band at 2339 cm⁻¹ was not observed after evacuation at 500 °C and had only a low intensity at 100 °C. An upward shift of the cyanate band to 2173 cm⁻¹ was observed. The band at 1975 cm⁻¹ was more intense than the band at 2173 cm⁻¹. The band at 1340 cm⁻¹ on the other hand side decreased in intensity compared to the bands at 1975 and 2173 cm⁻¹ indicating less formation of biuret. Carbonate bands were still visible after activation at 500 °C as in the case of ceria with urea. The different dependencies of band positions and intensities indicate different decomposition kinetics and routes of CeO₂-urea and Au/CeO₂.

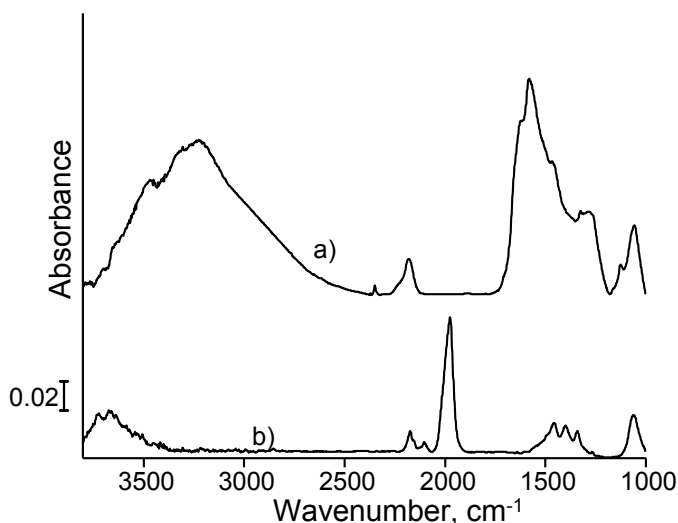


Figure 6-14. Infrared spectra of Au/ ceria (1.0) at 50 °C and after heating at 500 °C under vacuum.
a) 50 °C and b) 500 °C)

6.3.3 Infrared spectroscopy of adsorbed methanol

To identify the active surface species of ceria, urea modified ceria and Au supported ceria methanol was adsorbed. The method of adsorbing methanol as probe for basicity is discussed by Sánchez-Sánchez and Blasco^[65] for zeolites and references herein. Moreover, Binet and Daturi^[66] suggest the use of methanol as an IR probe to study the reduction process in ceria containing components. In purpose of activation the samples were heated with a ramp of $10\text{ K}\cdot\text{min}^{-1}$ from RT to $500\text{ }^{\circ}\text{C}$ for 2 h under reduced pressure. Methanol was adsorbed at 0.1 mbar for 0.5 h after cooling to $50\text{ }^{\circ}\text{C}$. After adsorption of methanol, again, the samples were heated with $10\text{ K}\cdot\text{min}^{-1}$ to 250 or $300\text{ }^{\circ}\text{C}$ for 0.5 h under reduced pressure and cooled to $50\text{ }^{\circ}\text{C}$.

6.3.3.1 Ceria – influence of modification with urea and gold

Upon methanol adsorption three characteristic bands located at 2915, 2846 and 2810 cm^{-1} were observed in the $\nu(\text{CH}_3)$ region and at 1104 cm^{-1} in the $\nu(\text{OC})$ spectral range for ceria (see Figure 9, curve a). The bands are characteristic for methoxy species formed by dissociative adsorption of methanol. The bands in the $\nu(\text{CH}_3)$ region can be assigned to different types of methoxy species. The bands located at 2915 and 2810 cm^{-1} were attributed to on-top type I methoxy species coordinated to Ce^{4+} , while the band at 2846 cm^{-1} was assigned to bridging type II methoxy species typical for reduced ceria samples.^[67] A negative band was observed around 1378 cm^{-1} due to the interaction of methanol with hydroxyl carbonate species.

A slight downward shift of the adsorption bands in the $\nu(\text{CH}_3)$ region was observed by adding urea to ceria. The band located at 2846 cm^{-1} related to Ce^{3+} was altered, however an additional band at 2838 cm^{-1} characteristic for oxidized ceria was obtained in the spectrum of CeO_2 -urea (Figure 6-15, curve b). The $\nu(\text{CO})$ band of methoxy species was shifted upward to 1109 cm^{-1} and of distinct intensity compared to CeO_2 . Whereas the negative band at 1340 cm^{-1} occurred with less intensity. But, the most important difference between the spectra of CeO_2 and CeO_2 -urea is the strong negative band at $\sim 1965\text{ cm}^{-1}$ observed due to the interaction of methanol with the new surface groups which were formed by the decomposition of urea during the activation process (described in the previous section).

The spectrum of Au/CeO₂ (Figure 6-15, curve c) observed after adsorption of methanol completely differed. The intensity of the $\nu(\text{CH}_3)$ bands was markedly decreased and the $\nu(\text{CO})$ band of the methoxy species was almost not visible. However, the negative band at 1965 cm^{-1} occurred with strong intensity and new bands arose at 1558 , 1372 and 1357 cm^{-1} , indicating the alteration of methanol. The bands can be assigned to formate which was formed during the oxidation of the methoxy species.^[68, 69]

After thermo-evacuation at $200\text{ }^{\circ}\text{C}$ the intensity of the $\nu(\text{CH}_3)$ bands related to methoxy I and II types were markedly decreased for all samples. Carbonates were formed involving surface hydroxyl carbonates (negative bands near 1340 and 1100 cm^{-1}) over CeO₂ and CeO₂-urea. In contrast carbonate formation was not observed for Au/CeO₂.

The dehydrogenation of methanol is also followed by the formation of formaldehyde or CO.^[70, 71] The formation of CO (2170 cm^{-1}) was only observed for urea and Au modified ceria. By heating to $200\text{ }^{\circ}\text{C}$ formaldehyde is decomposed into CO which interacts with surface metal cations as Ce^{4+} or Au^{+} .^[72, 73]

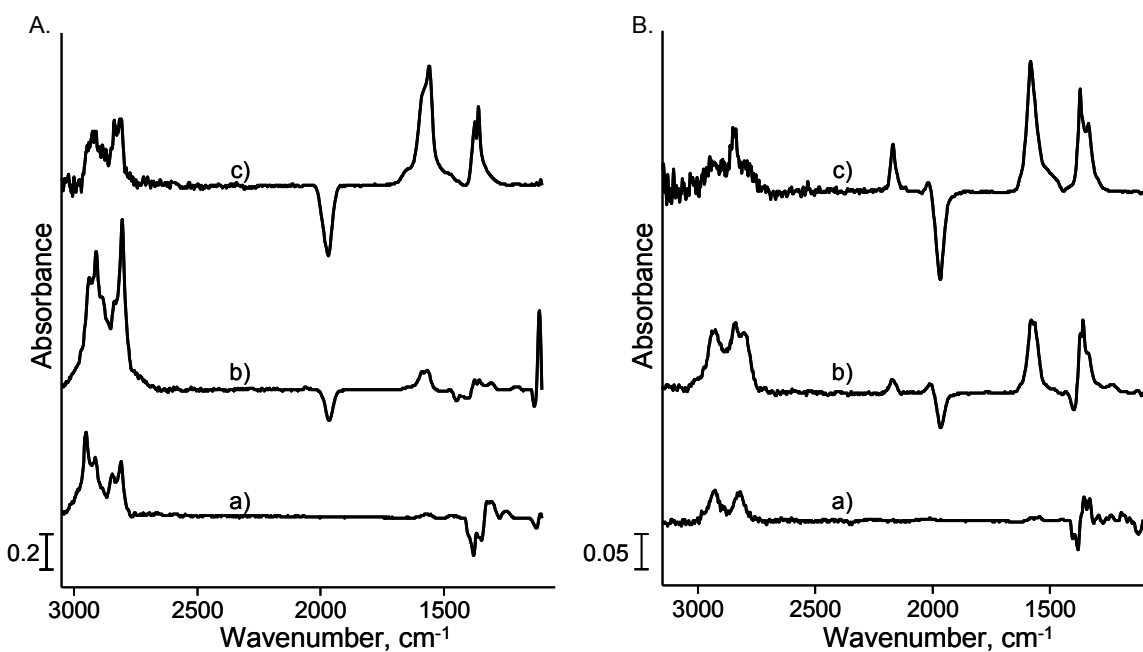


Figure 6-15. Infrared spectra after adsorption of MeOH.

A. At 0.1 mbar at $50\text{ }^{\circ}\text{C}$ and B. After thermo-evacuation at $200\text{ }^{\circ}\text{C}$.

a) CeO₂, b) CeO₂-urea and c) Au/CeO₂.

6.3.3.2 Ceria - influence of Au deposition method

The adsorption of methanol on ceria (N100) obtained by precipitation of cerium nitrate in aqueous ammonia solution was carried out as described above. For comparison methanol was adsorbed on Au loaded ceria (N100) samples prepared with DPu method and NaOH precipitation method, too.

After adsorption of methanol on ceria (N100) and Au loaded ceria samples a strong negative band was observed at $\sim 3740\text{ cm}^{-1}$ indicating that methanol interacts via H-bonding with surface OH-groups. Between $2950\text{--}2750\text{ cm}^{-1}$ adsorption bands in the C-H region were observed. Those bands are related to methoxy and formate species adsorbed on Ce^{4+} .^[68, 74] Former species are formed via deprotonation of methanol on surface basic sites. In the low frequency region bands were observed at ~ 1470 , $1370\text{--}1330$, $1196\text{--}1150$ and 1111 cm^{-1} . The adsorption band at 1571 cm^{-1} occurred only in case of urea deposited Au/ceria sample with strong intensity. The band was observed at 1582 cm^{-1} with less intensity in case of Au deposited on ceria with NaOH. This band is assigned to formate, which was formed via dehydrogenation of methanol.^[70]

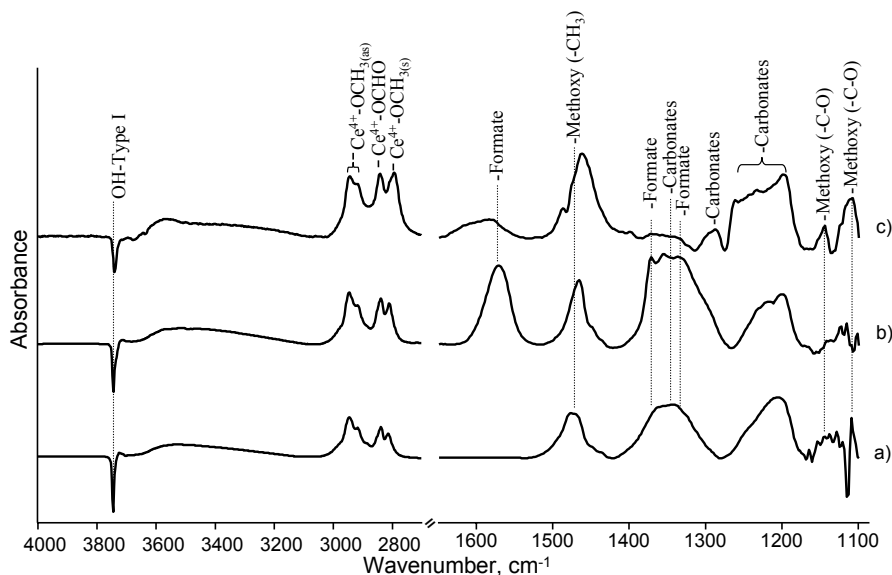
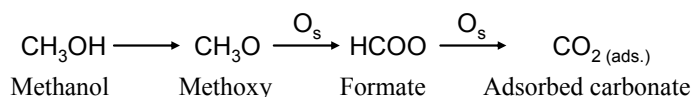


Figure 6-16. Difference spectra of adsorbed MeOH at 0.1 mbar and 50°C.

a) CeO_2 (N100), b) $\text{Au/CeO}_2\text{-urea}$ (1.0, N100) and c) $\text{Au/CeO}_2\text{-NaOH}$ (1.0, N100)

Figure 6-17 shows the difference spectra during desorption of methanol at 200 °C in vacuum for CeO₂ (N100), Au/CeO₂-urea and –NaOH (1.0, N100). The negative band at ~3740 cm⁻¹ remained with less intensity compared to the spectra at 50 °C for all samples. The adsorption bands in the CH-region (2950-2790 cm⁻¹) related to methoxy and formate species were slightly shifted to higher wave numbers. While the band at 2810 cm⁻¹ was decreased a new band at 2976 cm⁻¹ occurred for Au/CeO₂-urea (N100, 1.0), indicating that the surface methoxy groups were changed after heating to 200 °C. The band at 2792 cm⁻¹ which was observed for Au/CeO₂-NaOH (1.0, N100) indicates the interaction of adsorbed OHCO-species with Ce³⁺.^[66]

Methanol was decomposed over Au modified CeO₂ (N100) samples, as in the low frequency region a strong adsorption band at 1571 cm⁻¹ related to formate-species occurred. This band was not observed for ceria, indicating less activity of the support.



Equation 6-1. Decomposition of methanol involving surface oxygen atoms.

Further intense peaks were observed at 1466 cm⁻¹ (-CH₃), 1371 and ~1330cm⁻¹ (formate), 1360-1350 cm⁻¹ and ~1320 cm⁻¹ (carbonates), 1218-1200 cm⁻¹ (carbonates) and at ~1144 and 1102 cm⁻¹ (methoxy). The formation of carbonates was more pronounced over ceria than on the Au modified samples. An intense negative band near 1100 cm⁻¹ occurred for ceria (N100) indicating the loose of surface oxygen atoms due to the formation of carbonates.^[68]

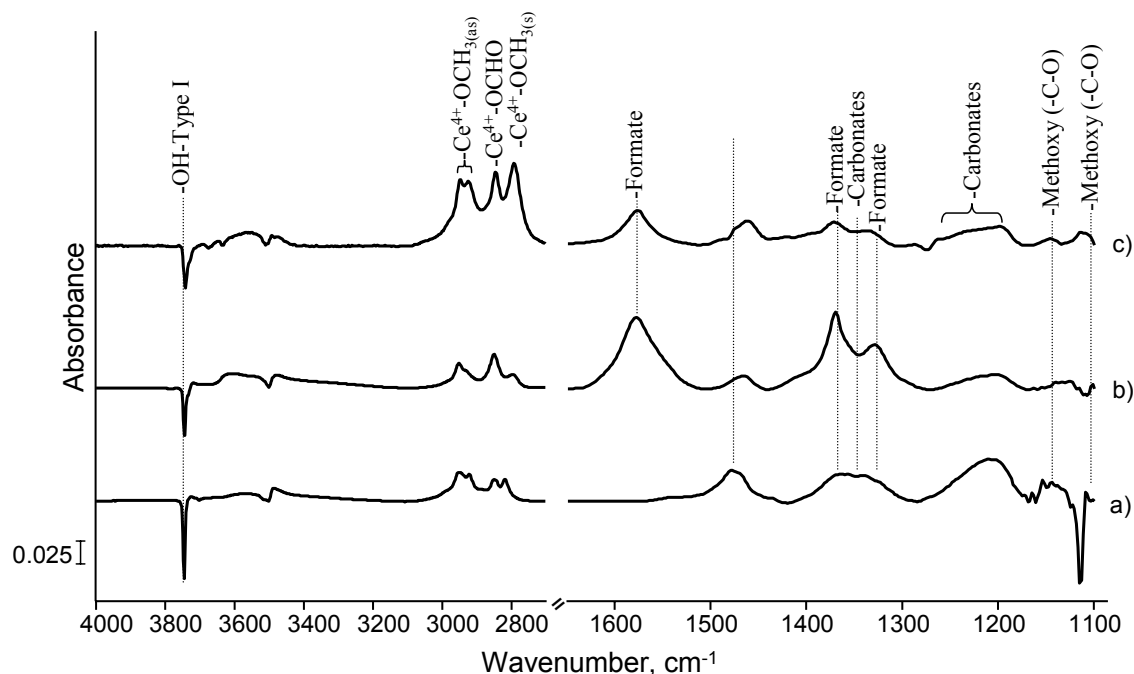


Figure 6-17. Difference spectra during desorption of methanol at 200 °C in vacuum.

a) CeO_2 (N100), b) Au/CeO_2 -urea (1.0, N100) and c) Au/CeO_2 -NaOH (1.0, N100)

Table 6-7. Characteristic adsorption bands occurred during degassing of MeOH at 200 °C for CeO_2 and Au/CeO_2 .

Species	Frequency (cm^{-1})					
	CeO_2	CeO_2 -urea	Au/CeO_2	CeO_2 (N100)	Au/CeO_2 -urea (N100, 1.0)	Au/CeO_2 -NaOH (N100, 1.0)
$\nu(\text{-OCH}_3)$	2926, 1451	2925, 1426	-	2921, 1478	1466	1462
$\nu(\text{-OCHO})$	1542	1577, 1369	1580, 1370	-	1578, 1370	1576, 1371
$\nu(\text{Me}^{\text{n+}}\text{-CO})$	-	2172	2168	-	-	-
$\nu(\text{-CO}_3)$	1352, 1329, 1291-1142	1355, 1229, 1121	1334	1362-1342, 1210-1120	1329, 1203-1126	1336, 1290-1190
$\nu(\text{-C-O})$	-	-	-	1101	1102	1113

Table 6-7 gives an overview of the characteristic adsorption bands of methanol during degassing at 200 °C in vacuum for ceria and Au modified ceria samples. While the formation of carbonates dominated for plain ceria, the formation of formaldehyde was more likely over Au/ceria. The adsorption of CO, which was formed during dehydrogenation of methanol and decomposition of formate, occurred for urea and urea/Au modified ceria with low surface area, only.

In general dehydrogenation of methanol is accelerated by adding Au to ceria.

6.3.4 Infrared spectroscopy of adsorbed propan-2-ol

For better understanding of mechanistic aspects the adsorption of propan-2-ol on ceria and Au modified ceria samples was followed by in-situ IR spectroscopy.^[37] In purpose of activation the samples were heated with a ramp of 10 K·min⁻¹ from ambient to 500 °C for 2 h under reduced pressure. Propan-2-ol was adsorbed at 0.1 mbar for 0.5 h after cooling to 50 °C. After adsorption of propan-2-ol, again, the samples were heated with 10 °C·min⁻¹ to 300 °C for 0.5 h under reduced pressure and cooled to 50 °C.

6.3.4.1 Adsorption of propan-2-ol on commercial ceria and modified ceria

After adsorption of propan-2-ol and heating to 200 °C (= reaction temperature) clearly resolved bands in the ν (CH) region located at 2971, 2936 and 2867 cm⁻¹ were observed for ceria. Together with the band at 1113 cm⁻¹ this bands are assigned to *iso*-propoxide species which are strongly adsorbed on the metal cations of ceria. The band located at 1677 cm⁻¹ can be attributed to C=O of acetone coordinated to Lewis acid sites of ceria.^[75, 76] Acetone was irreversibly adsorbed on strong Lewis acidic sites. A strong negative band occurred near 1370 cm⁻¹ indicating the interaction of propan-2-ol with hydroxyl carbonates as it was observed during IR experiments with adsorbed methanol. The interaction of propan-2-ol with surface hydroxyl carbonates was associated with the formation of bicarbonates (1325 cm⁻¹).

The intensities of the ν (CH) bands of adsorbed *iso*-propoxide are markedly decreased for CeO₂-urea. The remaining adsorption bands located near 2964, 1382 and 1124 cm⁻¹ can be assigned to un-reacted propan-2-ol.^[77] The negative band located at 1965 cm⁻¹ indicates the interaction of propan-2-ol with the new surface groups developed during the decomposition of urea.

Bands in the ν (CH) region were not observed for Au/CeO₂ indicating that the adsorbed propan-2-ol was either completely removed or converted to acetone and further products. The band at 2008 cm⁻¹ was also observed by Singh^[75] during the partial oxidation of propylene over Rh/Al₂O₃ wherein acetone is formed as intermediate and was further oxidized to CO and hydrocarbons. He assigned the band at 2008 cm⁻¹ to linearly adsorbed CO on metal sites. As for CeO₂-urea a negative band at 1964 cm⁻¹ was observed. New bands arose at 1533 and 1430 cm⁻¹ related to carboxylates.

In contrast to plain ceria the band at 1677 cm^{-1} did not appear for CeO_2 -urea and Au/CeO_2 indicating that the strength of surface Lewis acid sites was decreased by the deposition of Au with urea. The results suggest that the acetone precursor is formed over ceria, however, as it is irreversibly adsorbed on strong Lewis acid sites, thus dehydrogenation products would not occur during the conversion of propan-2-ol. Over Au/CeO_2 acetone was formed and oxidized to CO, which was linearly adsorbed on the surface. In contrast to CeO_2 and CeO_2 -urea adsorbed propan-2-ol-ol was not observed for Au/CeO_2 at 200°C . These results suggest that the modification of ceria with Au accelerates the dehydrogenation of propan-2-ol conversion.

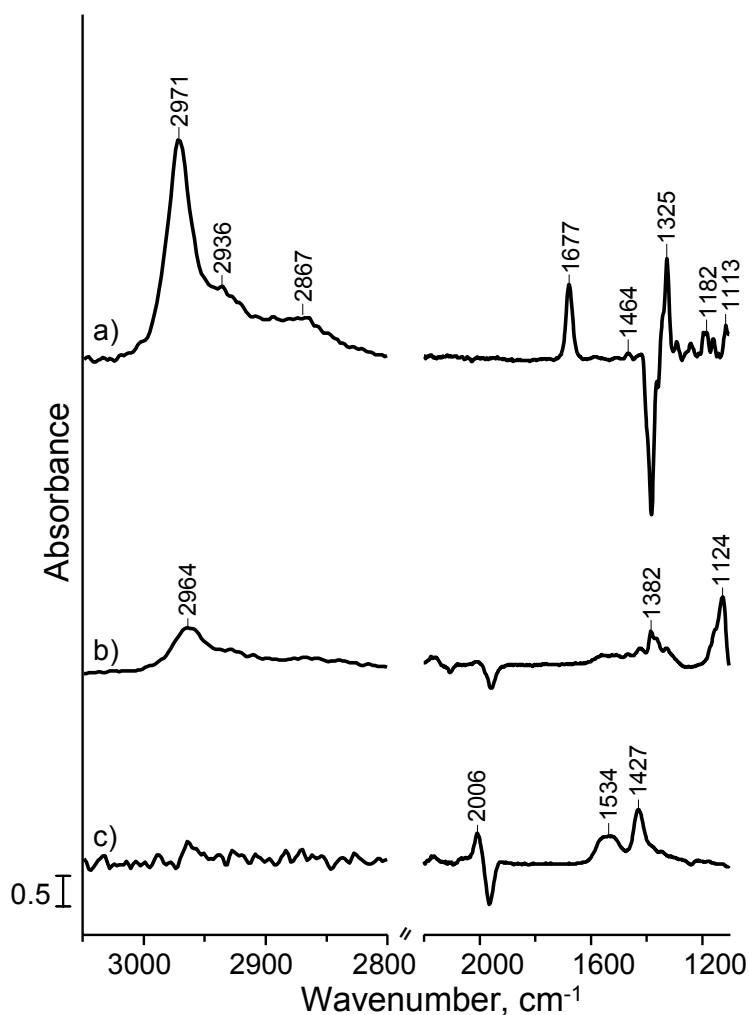


Figure 6-18. IR spectra after propan-2-ol adsorption at 200°C .

a) CeO_2 and b) CeO_2 -urea and c) Au/CeO_2 (1.0).

6.3.4.2 Adsorption of propan-2-ol on ceria (N100) and Au/ceria (N100)

The adsorption of propan-2-ol was also carried out for self prepared ceria and Au modified ceria samples, obtained by precipitation in aqueous solution with ammonia (CeO_2 (N100)). Au was deposited either via urea or NaOH. The samples were in purpose of activation, heated from ambient to 500 °C with a ramp of 10 K·min⁻¹ for 2 h under vacuum. Propan-2-ol was adsorbed at 0.1 mbar for 0.5 h after cooling to 50 °C. It was degassed at temperature steps of 100 °C from 100-300 °C.

The difference spectra of ceria (N100), Au/CeO₂-urea (1.0, N100) and Au/CeO₂-NaOH (1.0, N100) after adsorption of propan-2-ol at 50 °C are shown in Figure 6-19 (A). The adsorption bands in the C-H region had very low intensities compared to the sharp bands of the two different OH-groups (not shown here). In contrast, for Au deposited on ceria (N100) with NaOH the OH-groups occurred with very low intensities compared to the CH- adsorption bands of propan-2-ol. In case of Au loaded ceria (N100) a small band at 2118 cm⁻¹ and at 1468 cm⁻¹ were observed. The band related to acetone^[37] at ~1690 cm⁻¹ and *iso*-propoxide at ~ 1130 cm⁻¹ appeared for all samples, however with different intensities. Lowest intensity of the former band occurred for Au/CeO₂-NaOH (1.0, N100) indicating less dehydrogenation activity compared to the sample with Au deposited by urea.

Characteristic bands of carboxylates occurred between 1600 and 1350 cm⁻¹ for Au modified ceria during heating to 200 °C (see Figure 6-19 (B)). Methane was formed during the reaction of carboxylates with surface OH-groups over Au/CeO₂-NaOH (1.0, N100). In contrast, on plain ceria carbonate formation involving surface oxygen atoms occurred instead of carboxylation. The band at 1135 cm⁻¹ related to *iso*-propoxide altered by heating to 200 °C. However, it remained with remarkable intensity on Au/CeO₂-NaOH (1.0, N100). No propan-2-ol was left on the ceria (N100) and Au/CeO₂-urea (1.0, N100) surface (not shown here), as the adsorption bands in the C-H stretching region markedly decreased after degassing at temperatures higher than 200 °C.

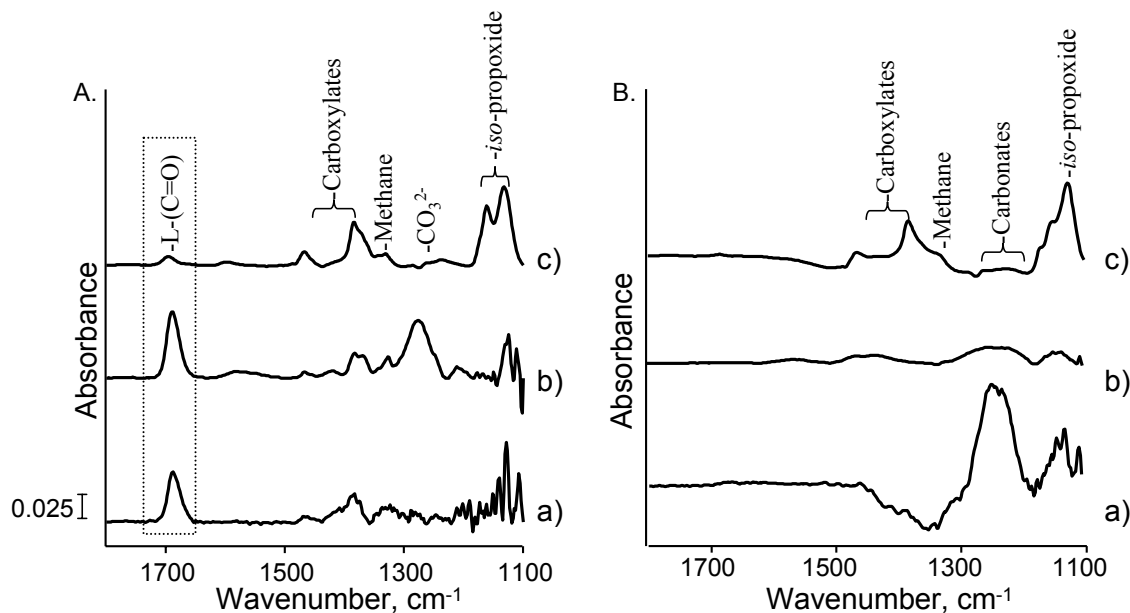


Figure 6-19. Difference spectra of adsorbed propan-2-ol.

A. 0.1 mbar for 0.5 h (50 °C) and B. after heating at 200°C in vacuum for
a) CeO₂ (N100), b) Au/CeO₂-urea (1.0, N100) and c) Au/CeO₂-NaOH (1.0, N100).

The experiments with adsorbed propan-2-ol and after degassing at 300 °C showed that acetone was formed over all samples. However, propan-2-ol was stronger adsorbed and less converted to acetone on Au/CeO₂-NaOH than on the supporting material and Au/CeO₂-urea (N100, 1.0). The results indicate that the modification with Au protects the ceria surface from carbonate formation.

6.3.5 Infrared spectroscopy of adsorbed pyridine

Pyridine was adsorbed on activated ceria samples to probe acid site properties. Pyridine acts as strong Lewis base, due to the lone pair located on the N-atom in the ring. The typical gas phase ring vibration CCN modes (8a, 8b, 19a and 19b) of pyridine are perturbed due to adsorption on the surface. The 8a mode (1587 cm⁻¹) is shifted to higher wavenumbers when pyridine interacts with the surface.^[5] In Table 6-8 the ring vibration modes of adsorbed pyridine on ceria and Au supported ceria are listed. Pyridine was adsorbed either via OH-groups or the interaction with surface metal cations.

Table 6-8. Ring vibration modes of adsorbed pyridine on CeO₂, urea and Au modified CeO₂.

Ring vibration $\nu(\text{CCN})$	Frequency (cm^{-1})				
	CeO ₂	CeO ₂ -urea	Au/CeO ₂	CeO ₂ (N600)	Au/CeO ₂ (N600)
L-Pyd	1612, 1573, 1483	1627, 1573, 1486	1573, 1483	1621, 1573, 1481	1622, 1573, 1481
H-Pyd	1445	1598, 1441	1597, 1441	1594, 1440	1595, 1440
B-Pyd	1548	-	-	-	-

Pyridine adsorption on oxidized and reduced ceria surfaces was carried out to identify the kind of acid sites. While for oxidized ceria mainly Ce⁴⁺ is expected, for reduced ceria Ce³⁺ was expected to be the dominating species. Before pyridine was adsorbed at 0.1 mbar at 50 °C the samples were activated in situ in vacuum at 300 °C to remove carbonates and water. Well resolved bands were obtained after background (spectrum of the activated sample) subtraction for all samples. The relevant part of the spectra between 1650 and 1400 cm⁻¹ is shown in Figure 3-20.

For oxidized ceria bands of pyridine vibration appeared at 1444 (ν_{19b}), 1489 (ν_{19a}), 1575 (ν_{8b}) and 1600/1628 (ν_{8a}) cm⁻¹. The occurrence of the ν_{8a} band at two different wavenumbers was ascribed by Zaki^[78] proposing Lewis acid sites with different strength. The large width at half height of the band at 1443 cm⁻¹ suggests that indeed the bands is composed of two contributions (see arrow in the Spectrum B(a) in Figure 3-20). The band at 1557 cm⁻¹ is tentatively attributed to pyridinium ions though the band is usually observed at somewhat lower wavenumbers.^[79]

On reduced ceria, the formation of bands characteristic of pyridinium ions was not observed. Only bands of pyridine coordinatively adsorbed on Lewis acid sites were noted. In comparison to oxidized ceria the ν_{19b} - and ν_{8a} -bands were shifted to lower wavenumbers indicating lower acid site strength. The shoulder at the ν_{8a} -band (1601 cm⁻¹) was not observed. One can conclude that after reduction of ceria in hydrogen the largest fraction of accessible Ce⁴⁺ cations was reduced to Ce³⁺, so that the remaining bands after pyridine adsorption at 1630, 1601, 1490 and 1442 cm⁻¹ can be assigned to Ce³⁺ in different coordination states. It should be noted, however, that the width at half height of the band at 1442 cm⁻¹ was much smaller in this sample

After evacuation at 200 °C, weakly bound and physisorbed pyridine was removed. While the intensity of the ν_{19a} -band at 1490 cm⁻¹ decreased drastically for reduced ceria, it remained with distinct intensity in case of oxidized ceria. Thus, the rather strong acidity

for the latter sample is confirmed. The downshift of the ν_{8a} -band from 1612 cm^{-1} for oxidized ceria to 1602 cm^{-1} for reduced ceria suggests clearly the different Lewis acid strength of Ce^{4+} and Ce^{3+} induced by the reduction in H_2 .

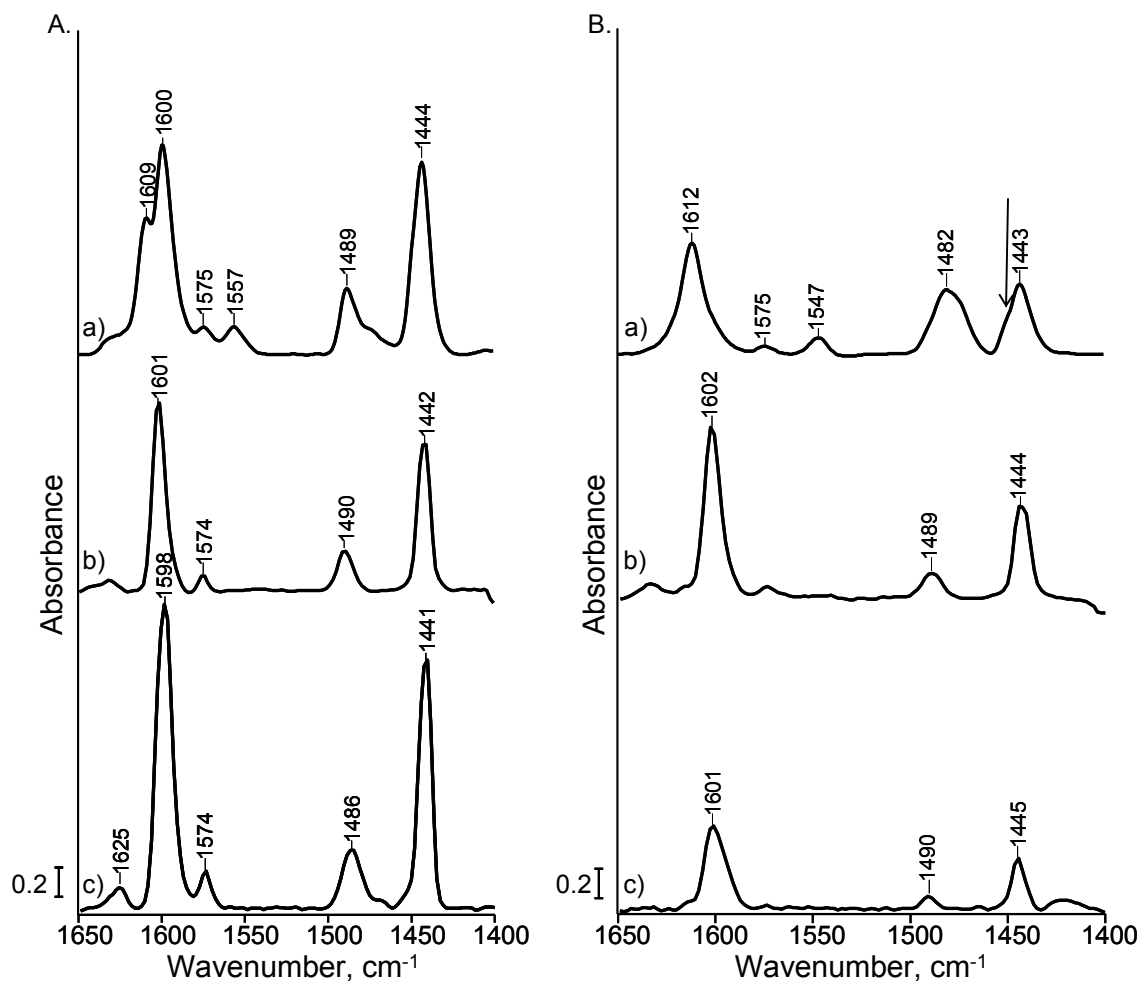


Figure 6-20. IR difference spectra obtained after pyridine adsorption at 50 °C (A) and after evacuation at 200 °C for one hour (B)

a) Oxidized Ceria, b) reduced ceria and c) Au/CeO₂.

Samples were previously activated in vacuum at 300 °C.

For Au/CeO₂ similar IR spectra as for reduced ceria were obtained after pyridine adsorption. Bands of adsorbed pyridine were found at 1441, 1486, 1573, 1598 and 1625 cm^{-1} . All bands are attributed to pyridine coordinated to Lewis acid sites. Subtle shifts in the wavenumbers, such as from 1442 to 1441 cm^{-1} for the ν_{19b} -band and from

1601 to 1598 cm^{-1} for the ν_{8a} -band indicate weakly bound, i.e., mainly physisorbed pyridine.^[80] After heating to 200 °C under reduced pressure the same bands as for reduced ceria remained indicating the dominance of Ce^{3+} for this sample.

6.3.6 Acid-base properties determined by NH_3 - and CO_2 -TPD

The acid and base site concentrations of ceria and modified ceria samples were determined via NH_3 - and CO_2 -TPD, respectively. Table 6-9 gives an overview of the resulting acid-base properties. The acid and base site concentration, correlated to the mass, of self-prepared ceria samples was higher than for low surface area ceria. However, is the acid/ base site density correlated to the specific surface area, highest concentration of active sites was observed for commercial ceria the. The basicity of bare ceria samples was slightly increased from 7 to 9 % for self-prepared samples. The modification of low surface ceria with Au via DPu was followed by an increase of active sites; however the basicity was slightly decreased. In contrast, fewer amount active sites occurred for higher surface area ceria (N600), obtained from nitrate precursor, after modification with Au. But the basicity was clearly increased from 9 to 14 %. An increase of basicity after modification with Au was also observed for ceria (C600) and ceria (N100). The more detailed analysis is described in the following sections.

Table 6-9. Acid/base properties of ceria and Au modified ceria samples determined by NH_3 - and CO_2 -TPD.

<i>Sample</i>	<i>Specific surface area</i>	<i>Acid sites</i>	<i>Basic sites</i>	<i>Basicity</i>	<i>Active sites</i>
	$[\text{m}^2\cdot\text{g}^{-1}]$	$[\mu\text{mol}\cdot\text{g}^{-1}]$	$[\mu\text{mol}\cdot\text{g}^{-1}]$	$[\%]$	$[\mu\text{mol}\cdot\text{m}^{-2}]$
CeO_2	6	16	0.5	3	1.25
CeO_2 N600	45	30	3.0	9	0.73
CeO_2 C600	49	22	2.2	9	0.49
CeO_2 N100	41	24	0.3	1	0.59
Au/ CeO_2 (1.0)	6	13	0.9	6	2.32
Au/ CeO_2 N600 (1.0)	44	19	3.20	14	0.50
Au/ CeO_2 C600 (1.0)	44	19	3.30	15	0.51
Au/ CeO_2 N100-urea	44	16	0.80	5	0.36
Au/ CeO_2 N100-NaOH	37	13	2.00	13	0.35

6.3.6.1 Ceria and Au/ceria samples obtained by commercial ceria

The desorption profiles of ammonia for various ceria catalysts hardly vary. A maximum occurred at approximately 200 °C. A second maximum was observed at temperatures higher than 550 °C for all samples except Au/ceria (1.0). Ceria showed a second strong desorption peak with maximum at 670 °C. The amount of desorbing ammonia was determined by the peak area between 100 and 500 °C (= activation temperature). The acid site concentration was slightly increased in the order ceria ($16 \mu\text{mol}\cdot\text{g}^{-1}$) < ceria-urea ($9 \mu\text{mol}\cdot\text{g}^{-1}$) < Au/ceria (0.4) ($11 \mu\text{mol}\cdot\text{g}^{-1}$) < Au/ceria (0.8) = Au/ceria (1.0) ($11 \mu\text{mol}\cdot\text{g}^{-1}$).

The second desorption peak is related to water and oxygen in case of ceria, desorbing from the bulk or surface, respectively. The amount of desorbing ammonia at temperatures less than 500 °C was increased with loading of urea/Au. Thus, a slight increase in acidity due to Au^+ species acting as weak Lewis acid sites is expected.

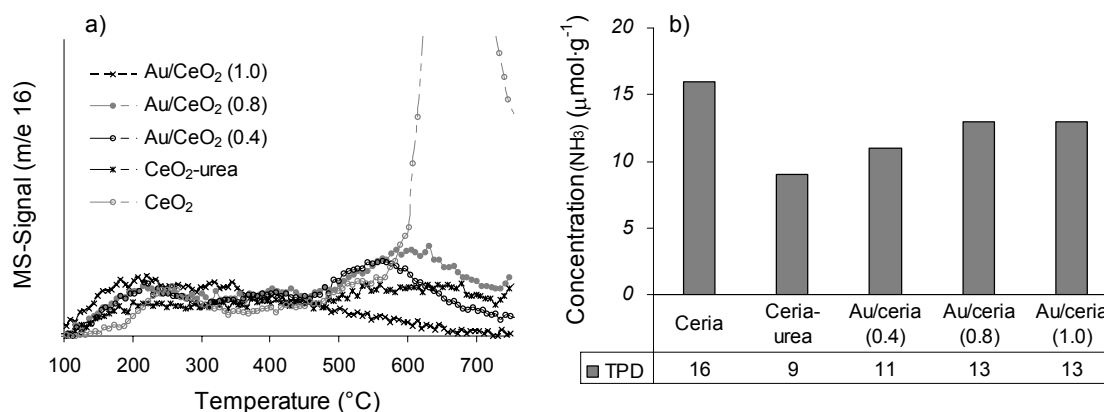


Figure 6-21. Acid site concentration of various ceria samples determined by NH₃-TPD.

a) Desorption profiles of ceria, ceria-urea and Au loaded ceria samples and b) Concentration of desorbing ammonia for ceria, ceria-urea and Au loaded ceria samples.

Desorption profiles of CO₂ for ceria and urea modified ceria samples show two main peaks. The first peak was observed at low temperatures between 40 and 250 °C, a second broader peak occurred at temperatures above 450 °C. The shapes of the second peak are quite different, compared to the first one. The low temperature peak of ceria is very small, whereas the peak maxima of the modified samples are more intense but do

not differ in shape. The high temperature peak is correlated to CO_2 formed by strongly adsorbed carbonates, those as from the bulk. In case of urea treated samples the second peak is more intense than for ceria. Indicating re-adsorption of CO_2 , this was formed during the decomposition of urea. The basic site concentration of ceria ($0.6 \mu\text{mol}\cdot\text{g}^{-1}$) was increased by modification with urea ($2.1 \mu\text{mol}\cdot\text{g}^{-1}$). The concentration of basic sites determined by the peak area from 40 to 500°C (= activation temperature) gives for ceria ($0.5 \mu\text{mol}\cdot\text{g}^{-1}$) and was increased by modification with urea ($1.4 \mu\text{mol}\cdot\text{g}^{-1}$). No linear correlation between basic sites and amount of Au was observed, as the concentration of desorbed CO_2 ($\leq 3.6 \mu\text{mol}\cdot\text{g}^{-1}$) was very low for all cases.

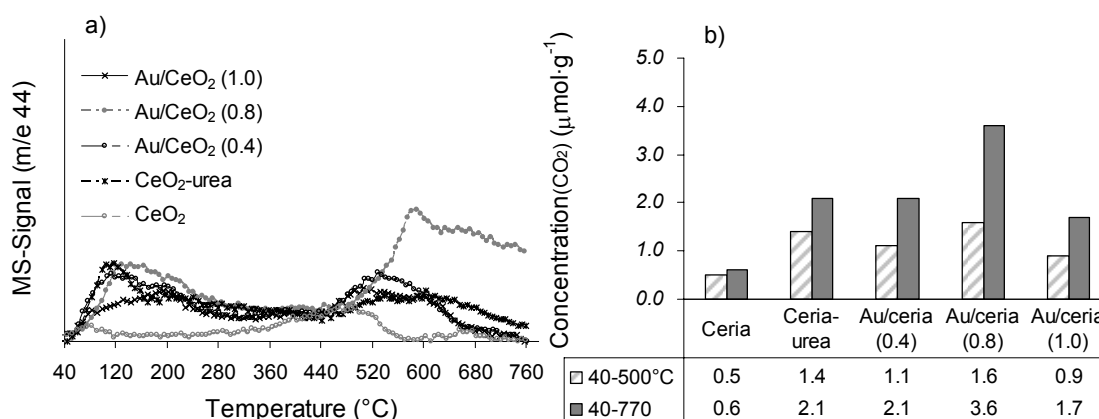


Figure 6-22. Basic site properties of ceria and modified ceria samples determine by CO_2 -TPD.

a) CO_2 -Desorption profiles of ceria, ceria-urea and Au loaded ceria samples and b) Concentration of desorbing carbon dioxide for ceria, ceria-urea and Au loaded ceria samples.

6.3.6.2 Ceria and Au/ceria samples obtained by self-prepared ceria

The acid site properties of ceria (N600) and Au loaded ceria (N600) are shown in Figure 6-23. The desorption profiles of ammonia for ceria (N600) and Au/ceria (N600) were of similar shape, however the maximum was shifted to lower temperatures, after modification with urea/Au from 254 to 219 $^\circ\text{C}$. The concentration of desorbing ammonia was decreased from 30 to 19 $\mu\text{mol}\cdot\text{g}^{-1}$ with Au modification.

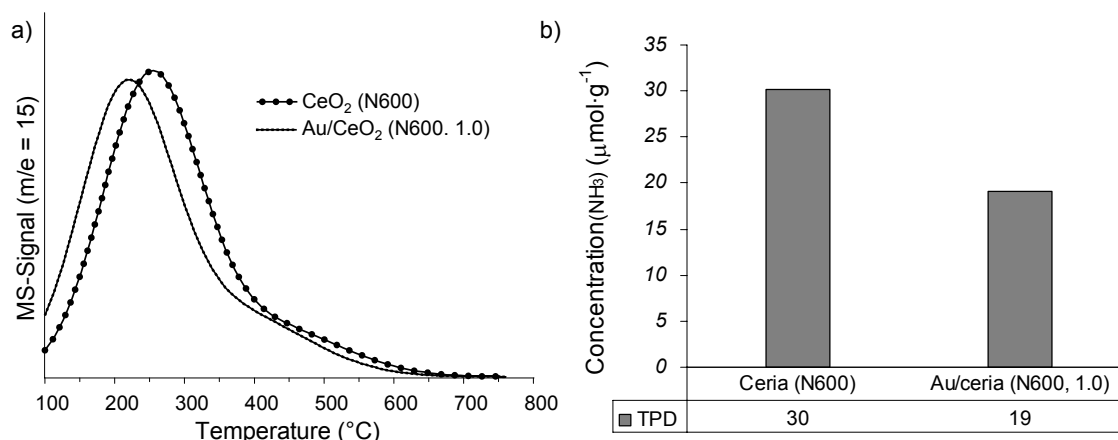


Figure 6-23. Acid site properties of CeO₂ (N600) and Au/CeO₂ (N600) determined by NH₃-TPD.

a) NH₃-Desorption profiles of CeO₂ (N600) and Au/CeO₂ (N600, 1.0) and b) Concentration of desorbing ammonia for CeO₂ (N600) and Au/CeO₂ (N600, 1.0).

The desorption profiles and acid site concentration for ceria (C600) and Au/ceria (C600) are shown in Figure 6-24.

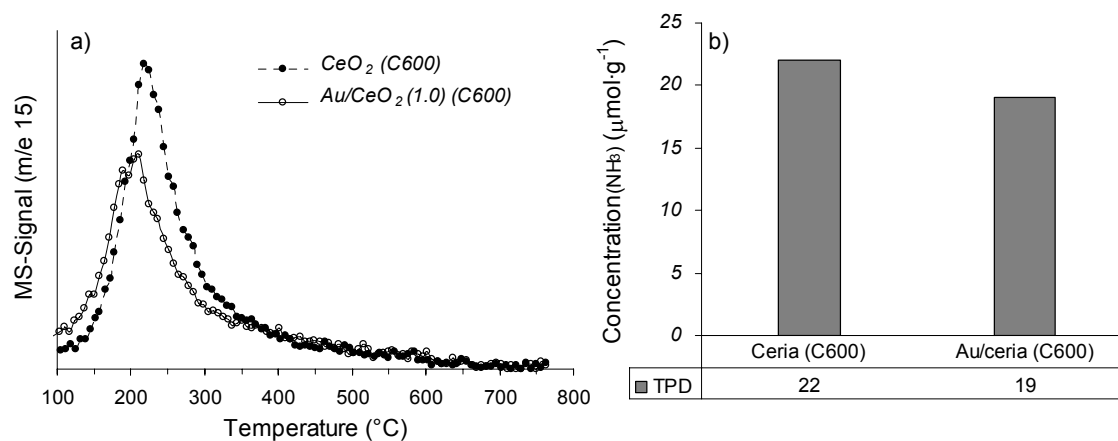


Figure 6-24. Acid site properties of CeO₂ (C600) and Au/CeO₂ (C600) determined by NH₃-TPD.

a) NH₃-Desorption profiles of CeO₂ (C600) and Au/CeO₂ (C600, 1.0). b) Concentration of desorbing ammonia for CeO₂ (C600) and Au/CeO₂ (C600, 1.0).

For both samples only one peak was observed. The peak maximum of ceria (C600) occurred at 225 °C, deposition of Au was followed by a decrease of the desorption maximum to 205 °C. Not only the desorption maximum was shifted to lower temperatures, but also the density of acid sites was decreased due to the deposition of Au. Compared to ceria (N600), ceria obtained from carbonate precursor (C600), had less acid

sites. While after modification with Au, the acid site concentration was the same in both cases.

The CO₂-desorption profiles of self-prepared ceria samples CeO₂ (N600), CeO₂ (C600) and Au modified ceria samples show one main peak at 120 °C. A second desorption maximum occurred at 370 °C in case of CeO₂ (C600) and Au/CeO₂ (C600, 1.0) and at 440 °C for CeO₂ (N600) and Au/CeO₂ (N600, 1.0). In both cases was the density of basic sites increased after modification with Au via the DPu method. The Au modified ceria samples showed a third small desorption maximum at temperatures higher than 600 °C. The concentration of desorbing CO₂ was calculated between 40 and 500 °C (= activation temperature) and for the whole temperature range between 40 and 770 °C. The amount of desorbing CO₂ was clearly increased between 500 and 770 °C. The influence of CO₂ desorbing in the high temperature range was more drastically for ceria (N600) samples than for ceria (C600) samples. In the temperature range between 40 and 500 °C the difference between support and Au modified sample was 0.2 μmol·g⁻¹ for ceria (N600) and 1.1 μmol·g⁻¹ for ceria (C600). However, the basic site concentration of Au/ceria samples hardly varied, whereas ceria (N600) was slightly more basic than ceria (C600). Due to modification with Au, the basic site concentration of ceria was increased for both samples.

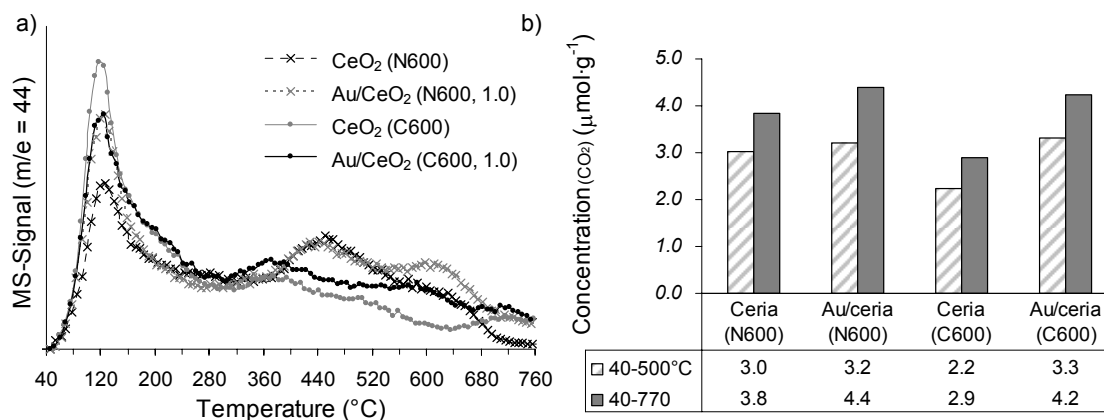


Figure 6-25. Basic site properties of CeO₂ (N600, C600) and Au/CeO₂ (N600, C600) determined by CO₂-TPD.

a) CO₂-Desorption profiles of CeO₂ (N600, C600)) and Au/CeO₂ (N600, C600, 1.0).

b) Concentration of desorbing carbon dioxide for CeO₂ (N600, C600) and Au/CeO₂ (N600, C600, 1.0).

6.3.6.3 Ceria and Au modified ceria via DPu and NaOH method

The NH_3 -desorption profiles of various ceria (N100) samples shown in Figure 6-26 a) show one maxima between 200 and 250 °C, the shape of the desorption peaks hardly vary at temperatures less than 500 °C. The peak maxima decreased in the order CeO_2 (230 °C) > $\text{Au/CeO}_2\text{-NaOH}$ (225 °C) > $\text{Au/CeO}_2\text{-urea}$ (210 °C). At temperatures higher than 500 °C, which is equal to the activation temperature, a strong peak, with maximum at 635 °C, occurred in case of $\text{Au/CeO}_2\text{-NaOH}$. This peak was not observed for ceria and Au/ceria-urea . The acid site density decreased after deposition of Au. Between 100 and 500 °C the concentration of desorbing ammonia decreased from $24 \mu\text{mol}\cdot\text{g}^{-1}$ (CeO_2), to 16 ($\text{Au/CeO}_2\text{-urea}$) and $13 \mu\text{mol}\cdot\text{g}^{-1}$ ($\text{Au/CeO}_2\text{-NaOH}$).

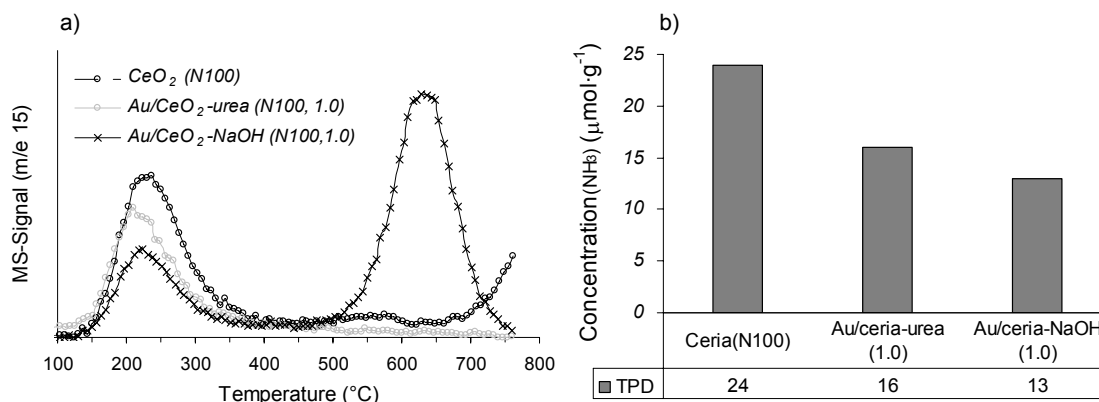


Figure 6-26. Acid site concentration of CeO_2 (N100) and Au/CeO_2 (N100) via DPu and deposition precipitation with NaOH determined by NH_3 -TPD.

a) NH_3 -Desorption profiles of CeO_2 (N100), $\text{Au/CeO}_2\text{-urea}$ and $\text{Au/CeO}_2\text{-NaOH}$.

b) Concentration of desorbing ammonia for CeO_2 (N100), $\text{Au/CeO}_2\text{-urea}$ and $\text{Au/CeO}_2\text{-NaOH}$.

The CO_2 -desorption profiles of self-prepared ceria (N100) derived by the precipitation of the nitrate with ammonia and Au modified samples are shown in Figure 6-27. One main peak occurred between 100 and 400 °C and second one between 520 and 600 °C for CeO_2 (N100) and $\text{Au/CeO}_2\text{-urea}$ (1.0, N100). The shape of the desorption profile related to $\text{Au/CeO}_2\text{-NaOH}$ (1.0, N100) differed completely in the higher temperature range compared to the other two samples. A strong intensive peak with a maximum at 660 °C was observed for $\text{Au/CeO}_2\text{-NaOH}$ (1.0, N100), whereas, for ceria

and Au/ceria-urea the desorption peaks in this temperature range were broad and occurred with low intensities.

The basic site density of CeO_2 (N100) was increased by the deposition of Au. At which the deposition with NaOH had a stronger effect on the increase than the deposition with urea.

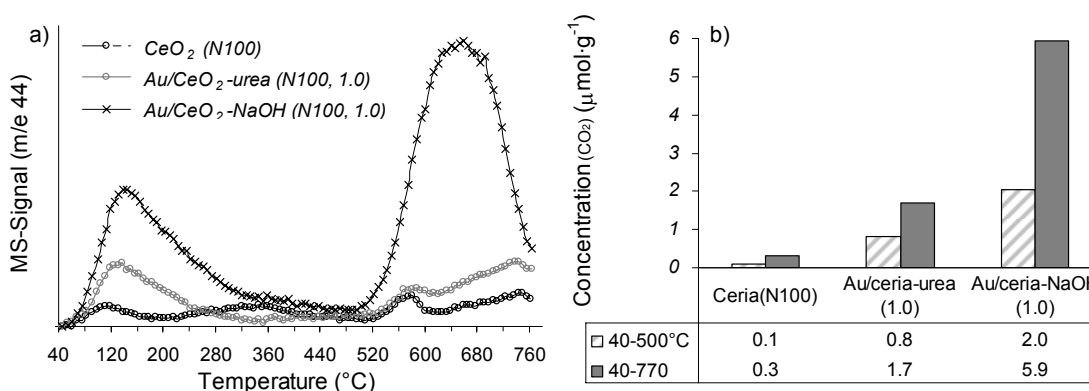


Figure 6-27. Basic site properties of CeO_2 (N100) and Au/ CeO_2 (N100) via DPu and deposition precipitation with NaOH determined by CO_2 -TPD.

a) CO_2 -Desorption profiles of CeO_2 (N100) and Au/ CeO_2 (N100, 1.0).

b) Concentration of desorbing carbon dioxide for CeO_2 (N100) and Au/ CeO_2 (N600, 1.0).

6.3.7 Conversion of propan-2-ol as catalytic test for acid-base centers

The conversion of propan-2-ol was used to test the catalytic activity and probe acid-base properties of ceria samples. The detailed mechanism of propan-2-ol conversion is described in Chapter 1. In short, over acid sites propene is formed via dehydration and over dominating basic sites acetone is formed via dehydrogenation of propan-2-ol.

6.3.7.1 Influence of Au

The influence of Au incorporation onto ceria was investigated by variation of (i) the amount of Au-loading and (ii) by changing the activation conditions (6.3.7.2). Two set-ups for experiments were established.

(i) First the samples were reduced at 300 °C in flow of 20 mL·min⁻¹ hydrogen as described above. After activation, the reaction was carried out under He-atmosphere at 150-225 °C and a constant stream of propan-2-ol. The reaction progress over time for

ceria is illustrated in Figure 6-28 a). At temperatures less than 200 °C no conversion of propan-2-ol was observed for ceria. At 200 °C propene is formed at conversion less than 0.3 %, however ceria is slightly deactivating. When temperature was increased to 225 °C propene is still formed with 100 % selectivity at low conversion. Within 80 min the activity of ceria decreased with 25 %. The conversion of propan-2-ol dropped from 0.8 to 0.6 %.

Figure 6-28 (b) illustrates the reaction progress for Au supported on ceria (1 wt.-%). Conversion of propan-2-ol occurred already at 150 °C. At all temperatures acetone was formed as main product with 100 % selectivity. Conversion increased at each temperature step from 0.9 % at lowest temperature (150 °C) to 29 % at highest temperature (225 °C). In contrast to ceria, the Au/CeO₂ (1.0) did not deactivate even not during reaction at 225 °C.

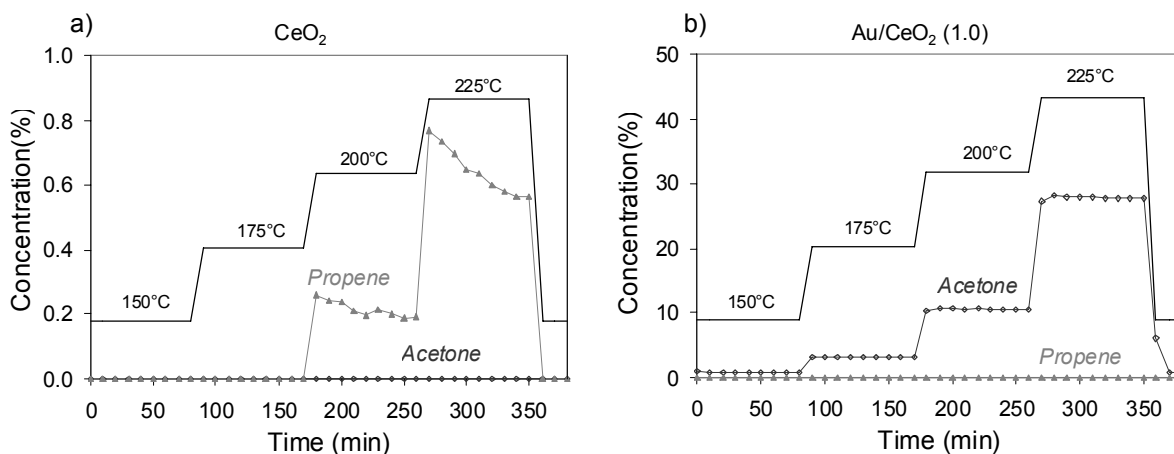


Figure 6-28. Reaction progress during conversion of propan-2-ol between 150 and 225 °C after activation of catalysts in H₂ at 300 °C.

a) Ceria and b) Au/ceria (1.0).

The rates of dehydrogenation and dehydration for ceria, urea modified and Au/ceria catalysts are illustrated in Figure 6-29. For ceria no activity in dehydrogenation was observed, while, due to deposition of urea acetone was formed with a rate of 248 $\mu\text{mol}\cdot(\text{g}\cdot\text{s})^{-1}$. Further increase of activity in dehydrogenation occurred for Au/CeO₂. The rate of acetone formation was enhanced with increasing amount of deposited Au. The highest rate of dehydrogenation (846 $\mu\text{mol}\cdot(\text{g}\cdot\text{s})^{-1}$) was observed for 1 wt.-% Au/CeO₂.

The rate of dehydration was $19 \mu\text{mol}\cdot(\text{g}\cdot\text{s})^{-1}$ for ceria. Deposition of urea without Au slightly accelerates the formation of propene to $24 \mu\text{mol}\cdot(\text{g}\cdot\text{s})^{-1}$. The comparison of the rates of acetone and propene formation for ceria-urea showed, that the dehydration was 2 orders of magnitude lower than dehydrogenation. Addition of Au to ceria suppressed the formation of propene. Only 0.1 wt.-% Au supported on ceria eliminated the dehydration of propan-2-ol.

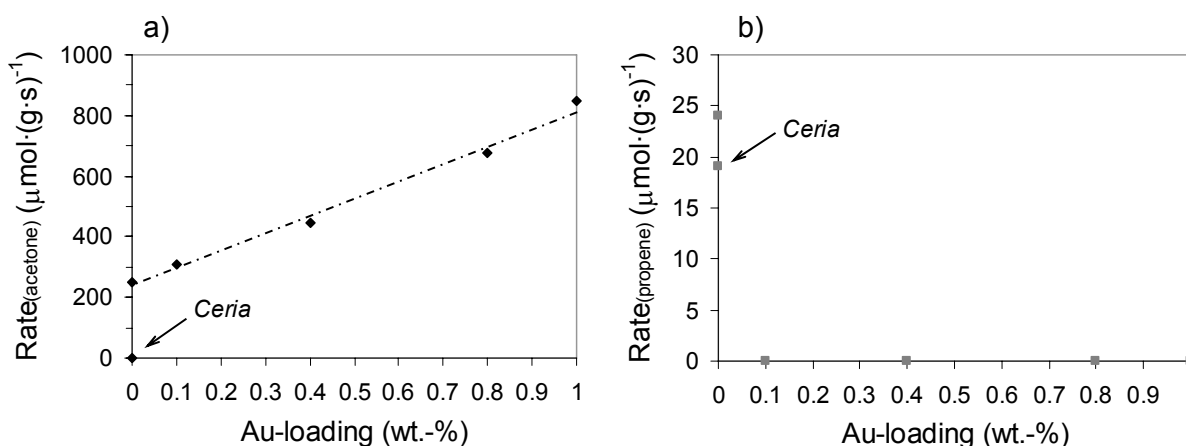


Figure 6-29. Rate of propan-2-ol conversion for ceria, urea modified ceria and Au/ceria catalysts at 225 °C and carrier-gas flow of 40 mL·min⁻¹.

a) Rate of acetone formation and b) rate of propene formation.

6.3.7.2 Influence of activation conditions

(ii) The activation conditions were changed testing the redox properties of ceria and the state of Au, whereas, the reaction conditions remain the same for all catalysts. Figure 6-30 shows reaction rates of dehydrogenation of Au/CeO₂ for temperature range from 150 to 225 °C. The rate of acetone and propene formation increased with increasing temperatures for both Au/CeO₂ catalysts and all activation conditions. The treatment in inert He-atmosphere was followed by higher activity in dehydrogenation compared to more reducing H₂-atmosphere at 300 °C. If the activation temperature in H₂-atmosphere was increased from 300 to 500 °C the activity of dehydrogenation decreased dramatically (Au/CeO₂ (0.8)). The substitution of hydrogen by helium caused a significantly increase in acetone formation at 300 °C as well as at 500 °C. These observations appear particularly at reaction temperatures higher than 175 °C.

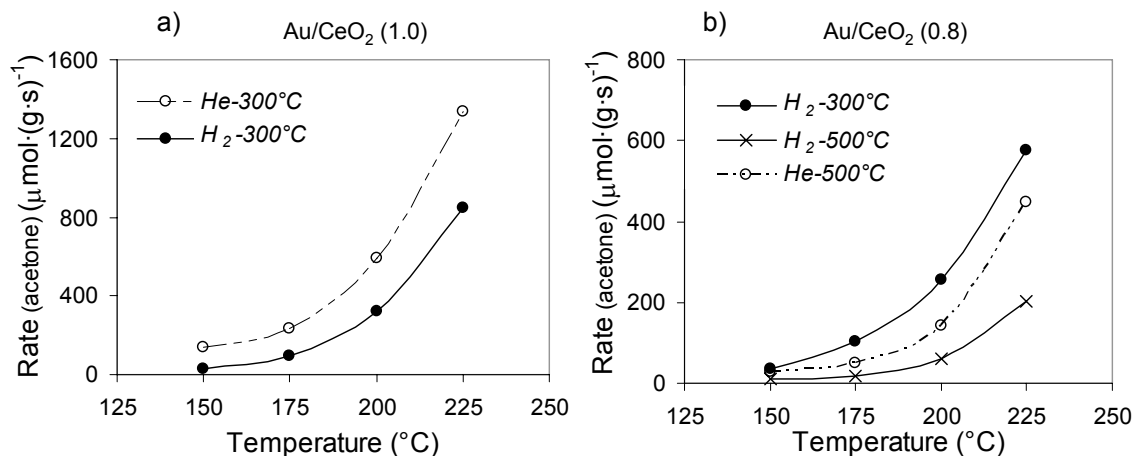


Figure 6-30. Rate of propan-2-ol conversion at 150 to 225°C for various pre-treated Au/ceria catalysts.

- a) Au/CeO_2 (1.0) pre-treated at 300°C in H_2 or He and
 b) Au/CeO_2 (0.8) pre-treated at 300 or 500°C in H_2 or He .

6.3.7.3 Influence of ceria support

To clarify the effect of ceria on the conversion of propan-2-ol, various ceria and Au/ceria materials were tested. Therefore a series of three different ceria supports obtained either from Merck or by synthesis from nitrate and carbonate precursors and supported catalysts with 1 wt.-% Au accordingly were used. The catalysts were activated in He flow of $20\text{ mL}\cdot\text{min}^{-1}$ at 500°C .

The rate for acetone and propene formation in the conversion of propan-2-ol for various ceria catalysts at temperatures between 175 and 250°C are shown in Figure 6-31. The highest activity was observed for CeO_2 obtained by Merck. The self prepared samples CeO_2 (N600) and (C600) showed almost the same activity. However, selectivity of ceria varies. While CeO_2 (N600) and (C600) exhibited similar activities in dehydrogenation and dehydration, ceria obtained from Merck was almost inactive for acetone formation at temperatures less than 225°C . The acetone formation rate for CeO_2 (Merck) was less than $0.5\text{ }\mu\text{mol}\cdot(\text{g}\cdot\text{s})^{-1}$. With increasing temperatures the rate of acetone formation for CeO_2 (Merck) was doubled. In comparison, the rate for dehydration in case of CeO_2 (Merck) was 19 times higher than for N600 and C600 at a reaction temperature of 225°C . At lower temperatures between 175 and 200°C the selectivity for acetone is 0 for CeO_2 (Merck) and 100 % for N600 and C600. The selectivity of acetone decreased at

200 °C to 75 %, while for CeO₂ (Merck) the selectivity for acetone at 250 °C still was zero and at 275 °C increased to 2 %.

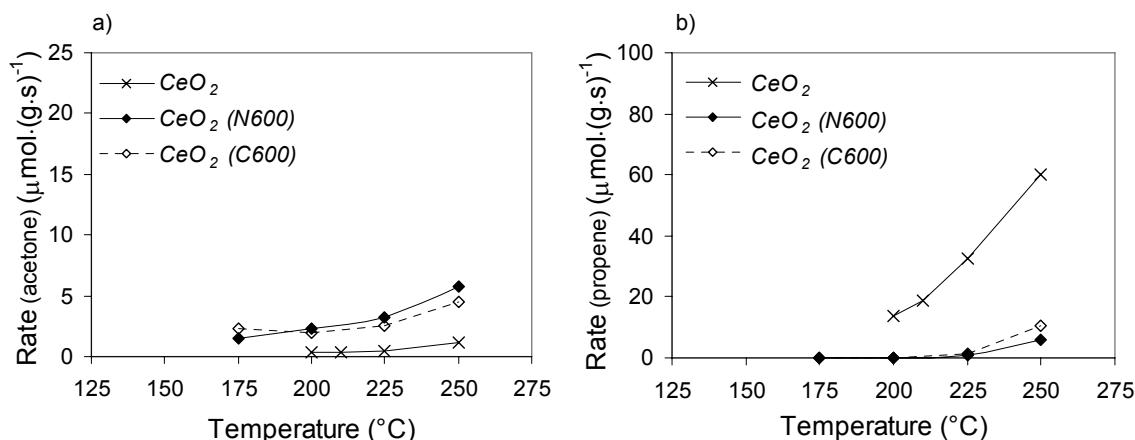


Figure 6-31. Rate of propan-2-ol conversion at 175 to 250 °C for various ceria catalysts.

a) Rate of acetone formation and b) rate of propene formation.

By adding Au to ceria the activity of propan-2-ol conversion was strongly enhanced. For all Au-catalysts acetone was the main product.

Formation of acetone was induced by deposition of Au for CeO₂ (Merck) as the rate of acetone formation was increased from 0.5 to 171 μmol·g⁻¹ at 225 °C. The formation of acetone was enhanced by a factor of 57 due to deposition of Au for CeO₂ (N600) at 225 °C. Highest rate of acetone formation (340 μmol·g⁻¹) was observed for Au/CeO₂ (C600) at 250 °C.

Dehydration did not occur at lower temperatures for Au/CeO₂ (Merck) and (N600). At 225 °C propene formation took place with low activity (< 5 μmol·g⁻¹). The rate of dehydration was increased from 2 to 18 μmol·g⁻¹ with increasing temperature from 175 to 250 °C, respectively, for Au/CeO₂ (C600)

Between 150 and 200 °C exclusively dehydrogenation was observed with 100 % selectivity for Au/CeO₂ (Merck) and (N600). At higher temperatures selectivity slightly decreased. The selectivity of acetone was almost 95 % for Au/CeO₂ (C600) at all temperatures.

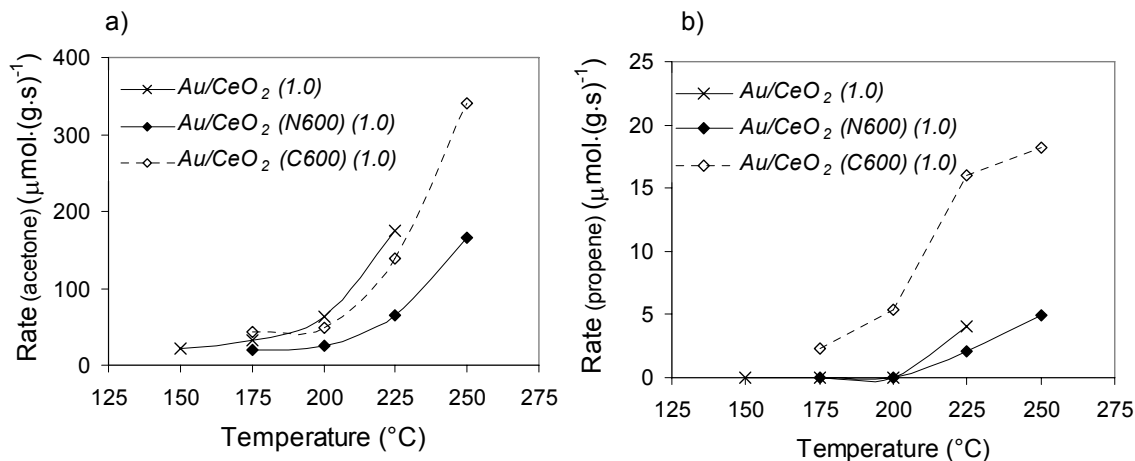


Figure 6-32. Rate of propan-2-ol conversion at 150 to 250 °C for various Au supported ceria catalysts.

a) Rate of acetone formation and b) rate of propene formation.

6.3.7.4 Influence of deposition-precipitation agent

A series of ceria and Au/ceria catalysts was prepared to test the influence of the deposition-precipitation agent on the development of acid and base properties. Ceria prepared from a nitrate precursor (N100) was incorporated with Au by using urea or NaOH. The catalysts were pre-treated in a He flow of 20 mL·min⁻¹ at 500 °C. The catalytic activity in the conversion of propan-2-ol was tested in the temperature range from 175 to 250 °C.

The yields of acetone during the conversion of propan-2-ol at 175 to 250 °C for CeO₂ (N100) and Au supported CeO₂ (N100) catalysts are shown in Figure 6-33 a). The yield of acetone was less than 0.5 % for CeO₂ (N100) at all temperatures. For Au/CeO₂-NaOH (1.0, N100) the yield of acetone was less than 1 % at 175 °C. However, with increasing temperature the yield of acetone was increased to 1.8 % at 250 °C. Below 250 °C the catalyst Au/CeO₂-NaOH (1.0, N100) was deactivating with time on stream. However, at 250 °C no deactivation was observed. Compared to CeO₂ (N100) the yield of acetone was slightly increased by precipitating Au with NaOH. The yield of acetone was 3.5 % for Au/CeO₂-urea (1.0, N100) at 175 °C. With increasing temperatures the yield of acetone increased up to 50 % at 250 °C. Below 250 °C no deactivation was observed. At 250 °C a slight decrease of acetone yield from 50 to 48 % occurred with time on stream.

Adding Au to ceria accelerates the formation of acetone only slightly in case of using NaOH as precipitation agent, whereas, the precipitation of Au on ceria with urea exhibits an apparent increase in the formation of acetone from less than 1 % to 50 % at 250 °C. But even at low temperatures (150 °C) the yield of acetone was increased with by one order of magnitude for Au/ceria-urea.

Figure 6-33 b) shows the formation of propene. At temperatures less than 200 °C, the activity in propene formation for CeO₂ (N100) and Au/CeO₂-urea (1.0, N100) appeared to be similar having yields of 0.15 to 0.6 % at 150 and 175 °C, respectively. At 200 °C the yield of propene was increased from 0.6 to 2.8 % for CeO₂ (N100) and to 2 % for Au/CeO₂-urea (1.0, N100). No propene formation occurred for Au/CeO₂-NaOH (1.0, N100) below 225 °C. A small amount (< 0.2 %) of propene was observed for Au/CeO₂-NaOH (1.0, N100) at 225 °C, however after 40 min no further propene formation could be detected.

At 250 °C yield of propene was 9 % for CeO₂ (N100) and 4.7 % for Au/CeO₂-urea (1.0, N100). Both catalysts deactivated with time on stream. The yield of propene was 0.4 % Au/CeO₂-NaOH (1.0, N100) at 250 °C. In contrast to CeO₂ (N100) and Au/CeO₂-urea (1.0, N100) Au/CeO₂-NaOH (1.0, N100) did not deactivate at 250 °C. The yield of propene decreased with almost 71 % for CeO₂ (N100) and Au/CeO₂-urea (1.0, N100) after 70 min.

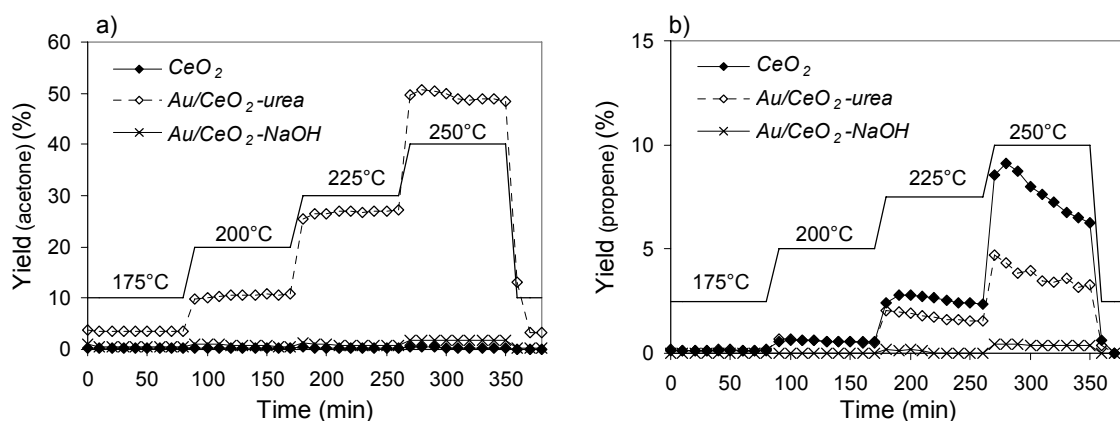


Figure 6-33. Yield of acetone and propene during propan-2-ol conversion at 175 to 250 °C for ceria (N100), Au/ceria-urea (1.0, N100) and Au/ceria-NaOH (1.0, N100).

a) acetone and b) propene.

Figure 6-34 a) shows the rates of acetone formation during the conversion of propan-2-ol at temperature range from 175 to 250 °C for CeO₂ (N100), Au/CeO₂-urea (1.0, N100) and Au/CeO₂-NaOH (1.0, N100). The rates were increased unequally with form lowest (175 °C) to highest temperature (250 °C) for all catalysts. The rate was doubled from 1 to 2 $\mu\text{mol}\cdot(\text{g}\cdot\text{s})^{-1}$ in case of ceria. While, the activity was slightly increased from 4 to 11 $\mu\text{mol}\cdot(\text{g}\cdot\text{s})^{-1}$ for Au/CeO₂-NaOH (1.0, N100), an markedly increase from 22 to 293 $\mu\text{mol}\cdot(\text{g}\cdot\text{s})^{-1}$ was observed for Au/CeO₂-urea (1.0, N100).

The rate for dehydration (Figure 6-34 b) was similar for CeO₂ (N100) and Au/CeO₂-urea (1.0, N100) but no dehydration occurred for Au/CeO₂-NaOH (1.0, N100) at temperatures less than 225 °C. However, at 250 °C the rate of dehydration was 46 $\mu\text{mol}\cdot(\text{g}\cdot\text{s})^{-1}$ for CeO₂ (N100), thus it was almost twice the number of dehydration rate for Au/CeO₂-urea (1.0, N100) and 23 times higher than the one of Au/CeO₂-NaOH (1.0, N100).

The selectivity of acetone decreased from 59 % (175 °C) to 5 % (250 °C, after 350 min) with time on stream and increasing temperature for CeO₂ (N100). Similar observations occurred for Au/CeO₂-urea (1.0, N100). The selectivity of acetone was 96 % in the beginning of the reaction, however at 250 °C and 350 min selectivity of acetone was 84 %. Au/CeO₂-NaOH (1.0, N100) showed higher stability and selectivity. Selectivity of acetone was 100 % until 250 °C and after 170 min. At 250 °C the selectivity of acetone decreased to 82 %.

At lower temperatures and in the beginning of the reaction Au/CeO₂-NaOH (1.0, N100) showed highest selectivity in the order of the CeO₂ (N100) catalysts. However, at high temperatures and in the end of the reaction selectivities for both Au loaded catalysts were almost the same, whereas the Au/ceria catalyst precipitated with urea was 27 times more active than the catalyst precipitated with NaOH. Compared to ceria support Au/CeO₂-urea (1.0, N100) was more than 140 times more active in the conversion of propan-2-ol. At 250 °C and after 350 min dehydration was the main reaction for ceria, whereas for Au loaded catalyst dehydrogenation was dominating.

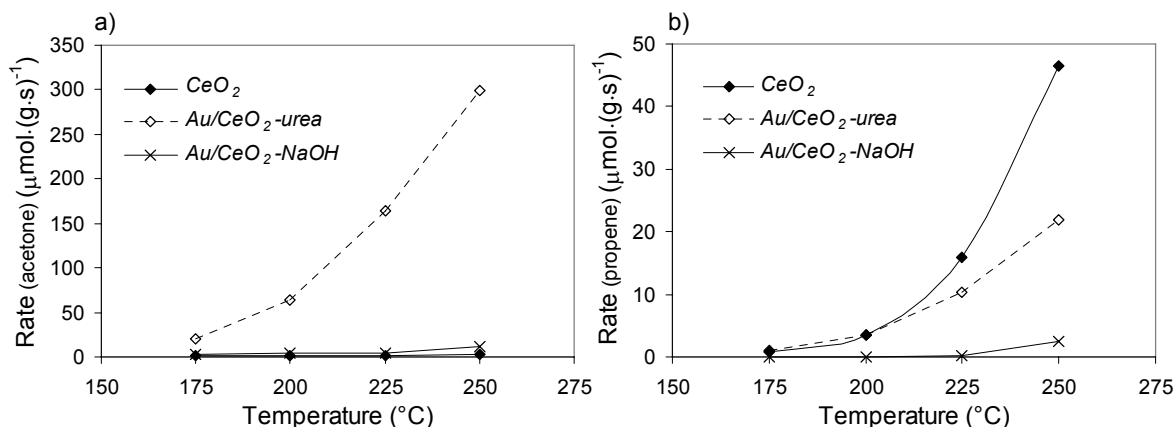


Figure 6-34. Rates of propan-2-ol conversion for ceria (N100), Au/ceria-urea and Au/ceria-NaOH.

a) acetone formation and b) propene formation.

6.3.7.5 Formation of by-products

The formation of by-products under reaction conditions as described above and reaction temperature at 225 °C occurred only for self-prepared samples. However The formation of by-products is strongly dependent on pre-treatment conditions as temperature and atmosphere. By-products (BP) are defined as di-*iso*-propylether, C₆-components and ketones (secondary products = SP). Di-*iso*-propylether is a condensation product of propan-2-ol, whereas the other products occur in a secondary reaction of propene or acetone. The detailed mechanism of the formation of by-products is described in Chapter1.

In Table 6-10 the formation of di-*iso*-propylether and secondary products (SP) is given for various catalysts and pre-treatment conditions.

Table 6-10. Formation of by-products over various self-prepared ceria samples depending on pre-treatment conditions.

Sample	Pre-treatment	[Gas]	Byproducts	
	[T, °C]		[di-iso-Propylether, %]	[SP, %]
CeO ₂ (N600)	500	H ₂	0.7	-
Au/CeO ₂ (N600, 1.0)	300	H ₂	0.4	24
CeO ₂ (N100)	500	He	0.3	-
Au/CeO ₂ -urea (N100, 1.0)	500	He	-	5

In general, the condensation of propan-2-ol to di-*iso*-propylether and side reactions was low. The formation of di-*iso*-propylether was in all cases less than 1 % and did not occur in case of Au/CeO₂-urea (N100, 1.0), which was activated in helium at 500 °C. In two cases formation of various side products occurred. Secondary products were formed with 24 % for Au/CeO₂ (N600, 1.0) activated in hydrogen at 300 °C, while only 5 % of side products occurred for Au/CeO₂-urea (N100, 1.0) activated in helium at 500 °C. The light components as methane, propane and butane as well as C₆H₁₀ and C₆H₁₂ were less dominant than ketonic species. While Haffad^[38] described the formation of secondary products over ceria mainly as C₆H₁₀ and C₆H₁₂ components, arising by either cationic dimerisation of propene or surface reduction of ceria with propene. For Au loaded catalysts ketones were observed as dominating species, which requires basic sites in order to condensation reactions of acetone.

6.4 Discussion

Ceria was either obtained by Merck or synthesized via different synthesis routes. Self-prepared ceria was derived by precipitation of the nitrate precursor as described in section 2.1.1. and by calcination of the carbonate precursor.

The samples varied in specific surface area particle size and acid-base properties. The specific surface area of commercial ceria was with 6 m²·g⁻¹ relatively low, whereas, for the self-prepared samples the surface areas increased to almost 50 m²·g⁻¹. Thus, one ceria is not equal to another one, even if they have the same stoichiometry.

The modification of ceria with Au was carried out by the deposition precipitation method with urea^[23] or NaOH.^[50] Au-particles were deposited in the nano-size range between 1 and 7 nm. Higher dispersion and loading of Au resulted via the deposition with urea than for NaOH.

Acid and base site densities were determined by NH₃ and CO₂-TPD, respectively. While, the acid site concentration was either decreased (Au/CeO₂ (1.0, N600), Au/CeO₂-urea (1.0, N100)), increased (Au/CeO₂ (1.0), Au/CeO₂-NaOH) (1.0, N100)) or not changed (Au/CeO₂ (1.0, C600)), the basic site concentration was increased by deposition of Au for all samples. Ceria is a moderately acidic material with acid site concentration

between 30 (CeO_2 N600) and $7 \mu\text{mol}\cdot\text{g}^{-1}$ (CeO_2). Adsorption of pyridine indicates the presence of Lewis and Brønsted acid sites for CeO_2 . Modification of ceria by gold via urea deposition changed the surface properties. The Brønsted acidity was completely removed as no characteristic band was observed via adsorption of pyridine. No Brønsted sites were observed for CeO_2 (N600). In contrast to low surface area ceria, the kind of acid sites were not changed by deposition of Au with urea. However, the strength and concentration were decreased by depositing Au onto CeO_2 (N600). Similar observations occurred for CeO_2 (C600) and (N100). Thus, in general the acidity of ceria is decreased by deposition of Au.

Thermal stability of urea- modified ceria was analyzed by infrared spectroscopy. The surface was markedly changed as new sites developed during heating. Urea was decomposed partially into CO_2 and ammonia during heating, which were almost removed at 500°C . However, several decomposition products of urea (1146 cm^{-1}) i.e. biuret (1334 cm^{-1}), melamine (1461 cm^{-1}), nitrosyls (1975 cm^{-1}) and cyanic acid (2169 cm^{-1}) were observed after heating to 500°C and remain most probably on the ceria surface. The formation of dinitrosyl complexes with a band around 1910 cm^{-1} was described in literature after reduction of ceria surface and exposition to NO .^[63] Mitoraj^[58] described the modification of titania with urea and suggested that the resulting surface contains poly-s-triazines of melem/melon fragments with IR bands at 1325 , 1463 and 1616 cm^{-1} . If the new surface sites were active and involved during the conversion of propan-2-ol was tested by infrared spectroscopy with adsorbed methanol and propan-2-ol, respectively.

Adsorption of methanol was used to test basic site properties. Methoxy-species ($\text{Ce}^{4+}\text{-OCH}_3$) were formed via dissociative adsorption of methanol on ceria. Those species were also identified for urea and urea/Au modified ceria samples. In addition, a strong negative band occurred at 1975 cm^{-1} for ceria-urea and Au/ceria after adsorption of methanol. Thus, the new surface sites were involved in the adsorption mechanism of methanol. Methanol was decomposed into formate involving surface oxygen atoms. Further oxidation of formate over ceria was followed by the formation of carbonates. Over Au/ CeO_2 methanol was dehydrogenated into CO (2170 cm^{-1}) during heating. Due to deposition of Au the oxidation of formaldehyde (1558 cm^{-1}) was suppressed and ceria

was prevented from oxygen release. Methanol adsorption experiments followed by FT-IR ruled out that the deposition of Au leads to a higher dehydrogenation ability of ceria and the carbonate formation was suppressed. Similar results occurred for self-prepared ceria (N100). However, formation of CO by dehydrogenation of methanol after adding Au was not observed for Au/CeO₂ (1.0, N100). This indicates that the ability of dehydrogenation for Au/CeO₂ (1.0, N100) was less pronounced compared to the low surface area Au/ceria. Also the carbonate formation was more pronounced over Au/CeO₂ (1.0, N100) than over Au/CeO₂. Therefore the surface area influenced the surface reactions of ceria.

In another set of IR-experiments the interaction of propan-2-ol with ceria samples was investigated. The main differences between ceria and Au/CeO₂ are (i) the formation of propene and water over ceria, which was not observed for Au/CeO₂, (ii) the protection of ceria from carbonate formation by Au, which prevents ceria from oxygen release, (iii) stronger adsorption of propan-2-ol on Au/CeO₂ and (iv) deactivation of ceria by the irreversible adsorption of acetone on strong Lewis acid sites. Latter one might be the most important change, which explains the high selectivity towards propene in the conversion of propan-2-ol and the strong deactivation of dehydration over ceria with time on stream.

The catalytic activity of ceria and Au modified ceria samples was performed in the conversion of propan-2-ol, which was also used as test-reaction for acid and base properties. The results observed at 200 °C and carrier-gas flow of 40 ml·min⁻¹ are listed in Table 6-11. The conversion of propan-2-ol decreased from 11 to 1 % for CeO₂ to CeO₂ (N600 and C600), respectively. The density of active sites decreased at the same time from 1.3 to 0.5 μmol·m⁻². While the dehydrogenation was dominating for CeO₂ and CeO₂ (N100), dehydrogenation was more pronounced in case of CeO₂ (N600) and (C600). This can be explained by the higher basicity of the latter catalysts. During IR studies with adsorbed propan-2-ol acetone was irreversibly adsorbed on CeO₂ which causes the high selectivity of that sample. For comparison in-situ IR experiments with adsorbed propan-2-ol were carried out for CeO₂ (N100) and Au modified samples, wherein also the influence of the deposition agent was tested. Similar results as for commercial obtained CeO₂ with low surface area were obtained, however no acetone was found for CeO₂ after heating to 200 °C. The formation of acetone of Au/CeO₂ (N100) was less pronounced for

the sample modified with NaOH than for urea. *Iso*-propoxide species formed during the dissociative adsorption of propan-2-ol remained on Au/CeO₂ (N100)-NaOH after heating to 200 °C. Thus, the activity in the conversion of propan-2-ol of this sample is expected to be less compared to Au/CeO₂ (N100)-urea. Methane was formed from carboxylates involving surface OH-groups over Au/CeO₂ (N100)-NaOH, which was not observed for CeO₂ (N100) and Au/CeO₂ (N100)-urea. Also propan-2-ol adsorption experiments followed by IR suggest that Au changes the redox properties of ceria and protects ceria from carbonate formation, which causes deactivation during reaction.

By the deposition of Au onto ceria the selectivity was changed from dominating dehydration to almost 100 % dehydrogenation. As dehydrogenation occurred with 75 % for CeO₂ (N600) and (C600) the changes were less pronounced compared to CeO₂ and CeO₂ (N100). An explanation for the change of the selectivity can be given by the decreasing acid site density, which occurred after the deposition of Au. However, metallic Au will accelerate the dehydrogenation of propan-2-ol, too. Adsorption experiments of methanol with ceria and Au/ ceria indicated that the basic site strength was increased after deposition of Au. The deposition of Au via NaOH caused a reduced concentration of Au compared to the urea deposited catalysts. Thus, the activity of dehydration was dramatically decreased, but the selectivity of dehydrogenation was 100 %. Also the formaldehyde formation during adsorption of methanol was less pronounced, which indicates less activity for Au/CeO₂-NaOH (N100, 1.0). Analysis of adsorbed propan-2-ol turned out, that acetone was strongly adsorbed on Au/CeO₂-NaOH (N100, 1.0), which causes reduced activity for dehydrogenation, too.

Table 6-11. Textural analysis and kinetics in the conversion of propan-2-ol of ceria and Au/ceria.

Sample	Specific surface area	Au-content	Au-Particle Size	Acid sites	Basic sites	Active sites	Basicity	Conversion	Rate (propene)	Rate (acetone)	Selectivity (acetone)
	[m ² ·g ⁻¹]	[wt.-%]	[nm]	[μmol·g ⁻¹]	[μmol·g ⁻¹]	[μmol·m ⁻²]	[%]	[%]	[μmol·(g·s) ⁻¹]	[μmol·(g·cat·s) ⁻¹]	[%]
CeO ₂	6			7	0.5	1.3	7	11	32	0.5	2
CeO ₂ N600	45			30	3.0	0.7	9	1	1	3	75
CeO ₂ C600	49			22	2.2	0.5	9	1	1	3	75
CeO ₂ N100	41			24	0.1	0.6	0	3	16	2	11
Au/CeO ₂ (1.0)	6	0.8	1.4	13	0.9	2.3	6	6	4	174	98
Au/CeO ₂ N600 (1.0)	44	1.0	1.6	19	3.2	0.5	14	11	2	64	97
Au/CeO ₂ C600 (1.0)	44	1.0	6.9	19	3.3	0.5	15	27	16	139	90
Au/CeO ₂ N100-urea	44	0.9	1.7	16	0.8	0.4	5	31	10	164	94
Au/CeO ₂ N100-NaOH	37	0.5	-	13	2.0	0.4	13	1	0	5	100

Catalytic results are obtained at $T_r = 225$ °C and $F_{He} = 40$ mL·min⁻¹. Catalysts were pre-treated in He-atmosphere at 500 °C

As the elimination of hydrogen can in principle also be catalyzed by metallic Au experiments with different loadings of Au were performed. The selectivity towards propene was changed from 100 to 0 % already by adding 0.1 wt.-% Au. The activity of dehydrogenation increased with increasing amount of Au. However deactivation of ceria was suppressed by modification with Au. The reverse reaction, the hydrogenation of acetone, took place at very low conversions on Au/CeO₂. At 150 °C, no propan-2-ol was formed, at 175 °C propan-2-ol was formed with 0.6 % conversion, at 200 °C with 1.6 % and at 225 °C with 3.1 % conversion. The rate of acetone hydrogenation was significantly lower than dehydrogenation of propan-2-ol. Both control experiments suggest the absence of direct Au catalyzed hydrogenation/ dehydrogenation (see Figure 6-35).

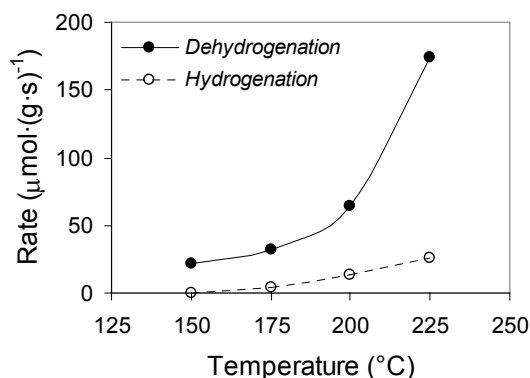


Figure 6-35. Dehydrogenation rate of propan-2-ol and hydrogenation rate of acetone for Au/ceria (1.0).

Control experiments with different pre-treatment conditions, varying the temperature between 300 and 500 °C and changing from reducing atmosphere to inert suggest, that Au⁺ ions act as weak and soft Lewis acid centers. Those stabilize the alkoxide intermediate, which also enhances the hydride abstraction. The existence of Au⁺ ions was supported by the results from XPS.

6.5 Conclusions

The high selectivity to dehydrogenation was induced for these novel basic catalysts (i) as Au and urea destroy the Brønsted acidity and blocks the access to the Lewis acid sites of the supporting material, (ii) the acetone precursor is not any longer

irreversibly adsorbed on strong Lewis acid sites, as those are eliminated, (vi) by suppressing carbonate formation, (vii) new reaction pathways are opened. NO-groups formed by decomposition of urea during the activation process afford one new route for dehydrogenation and another one are Au^+ ions. As the rate of dehydrogenation increases with increasing concentration of Au and the direct dehydrogenation of propan-2-ol on the Au particles can be almost ruled out (negligible activity for catalyzing the reverse reaction), Au particles provide weak and extremely soft Lewis acid sites at the support metal interface facilitating so the acceptance of hydride ions and accelerating dehydrogenation. However, the formation of acetone over metallic Au catalyzed dehydrogenation can not be completely excluded. The interplay of selective poisoning and formation of new and weaker acid sites, leads to a highly tuneable basic system and new class of catalysts.

Deactivation of (modified) CeO_2 is, therefore, attributed to the presence of at least moderately strong and relatively hard Ce^{4+} Lewis acid sites. Deactivation of ceria is also decreased, as carbonate formation is suppressed and strong Lewis acid sites are removed by adding urea and Au. However, this effect depends on the surface area of ceria, and is more pronounced for low surface area ceria.

Comparison of various ceria samples led to the conclusion that one ceria material is not equal to another one, even if the same stoichiometry is observed. Different synthesis methods were tested and ceria samples with almost the same surface area ($45 \text{ m}^2\cdot\text{g}^{-1}$) were obtained. However, the analysis of acid-base properties turned out different densities of acid and base sites. Also catalytic performances in the conversion of propan-2-ol resulted with different activities and selectivities. In general, the acid sites density was decreased, whereas the basic site density was increased by the modification with Au for all ceria materials.

The investigation of urea and NaOH as precipitation agent turned out that urea is more efficient regarding the Au-loading and dispersion. But using urea as deposition agent changes the oxide surface and opens new reaction pathways in catalysis may be not only in the conversion of propan-2-ol. Sodium sticks in the pores and therefore activity decreases. Nevertheless, the use of sodium increases the selectivity to acetone due to selective poisoning of acid sites.

6.6 References

- [1] W. H. Hartley, *J. Am. Chem. Soc.* **1882**, 4, 203.
- [2] S. Kodama, *Scientific Papers of the Institute of Physical and Chemical Research (Japan)* **1930**, 14, 169.
- [3] A. Trovarelli, *Catal. Rev. - Sci. Eng.* **1996**, 38, 439.
- [4] C. T. Campbell, C. H. F. Peden, *Science* **2005**, 309, 713.
- [5] C. Binet, M. Daturi, J. C. Lavalley, *Catal. Today* **1999**, 50, 207.
- [6] H. Idriss, *Platinum Metals Rev.* **2004**, 48, 105.
- [7] F. Esch, S. Fabris, L. Zhou, T. Montini, C. Africh, P. Fornasiero, G. Comelli, R. Rosei, *Science* **2005**, 309, 752.
- [8] S. Bernal, J. J. Calvino, M. A. Cauqui, J. M. Gatica, C. Larese, J. A. P. Omil, J. M. Pintado, *Catal. Today* **1999**, 50, 175.
- [9] S. Y. Liu, S. M. Yang, *Appl. Catal., A* **2008**, 334, 92.
- [10] F. Marino, C. Descorme, D. Duprez, *Appl. Catal., B* **2004**, 54, 59.
- [11] C. Milone, R. Ingoglia, L. Schipilliti, C. Crisafulli, G. Neri, S. Galvagno, *J. Catal.* **2005**, 236, 80.
- [12] A. Corma, P. Serna, *Science* **2006**, 313, 332.
- [13] T. Bunluesin, R. J. Gorte, G. W. Graham, *Appl. Catal., B* **1998**, 15, 107.
- [14] R. C. Langley, *Plating* **1967**, 54, 1347.
- [15] M. Haruta, S. Tsubota, T. Kobayashi, H. Kageyama, M. J. Genet, B. Delmon, *J. Catal.* **1993**, 144, 175.
- [16] I. N. Remediakis, N. Lopez, J. K. Norskov, *Angew. Chem., Int. Ed.* **2005**, 44, 1824.
- [17] J. T. Miller, A. J. Kropf, Y. Zha, J. R. Regalbuto, L. Delannoy, C. Louis, E. Bus, J. A. van Bokhoven, *J. Catal.* **2006**, 240, 222.
- [18] W. L. Deng, J. De Jesus, H. Saltsburg, M. Flytzani-Stephanopoulos, *Appl. Catal., A* **2005**, 291, 126.
- [19] B. H. J. Meilin, S. Yuenain, L. Yanfeng, *J. Rare Earths* **2008**, 26, 538.
- [20] L. Ilieva, J. W. Sobczak, M. Manzoli, B. L. Su, D. Andreeva, *Appl. Catal., A* **2005**, 291, 85.
- [21] C. M. J. Radnik, P. Claus, *Phys.Chem.Chem.Phys.* **2003**, 5, 172.

- [22] N. Weiher, E. Bus, L. Delannoy, C. Louis, D. E. Ramaker, J. T. Miller, J. A. v. Bokhoven, *J. Catal.* **2006**, *240*, 100.
- [23] L. Delannoy, N. Weiher, N. Tsapatsaris, A. M. Beesley, L. Nchari, S. L. M. Schroeder, C. Louis, *Top. Catal.* **2007**, *44*, 263.
- [24] B. Jorgensen, S. E. Christiansen, M. L. D. Thomsen, C. H. Christensen, *J. Catal.* **2007**, *251*, 332.
- [25] B. L. Zhu, M. Lazar, B. G. Trewyn, R. J. Angelici, *J. Catal.* **2008**, *260*, 1.
- [26] E.-Y. Ko, E. D. Park, K. W. Seo, H. C. Lee, D. Lee, S. Kim, *Catal. Today* **2006**, *116*, 377.
- [27] A. Hugon, L. Delannoy, C. Louis, *Gold Bulletin* **2008**, *41*, 127.
- [28] Q. Fu, A. Weber, M. Flytzani-Stephanopoulos, *Catal. Lett.* **2001**, *77*, 87.
- [29] A. Sandoval, A. Gomez-Cortes, R. Zanella, G. Diaz, J. M. Saniger, *J. Mol. Catal. A: Chem.* **2007**, *278*, 200.
- [30] J. A. Rodriguez, M. Perez, J. Evans, G. Liu, J. Hrbek, *J. Chem. Phys.* **2005**, *122*, 241101.
- [31] E. Iglesia, D. G. Barton, J. A. Biscardi, M. J. L. Gines, S. L. Soled, *Catal. Today* **1997**, *38*, 339.
- [32] J. A. Lercher, C. Gründling, G. Eder-Mirth, *Catal. Today* **1996**, *27*, 353.
- [33] I. Halasz, H. Vinek, K. Thomke, H. Noller, *Z. Phys. Chem. (NF)* **1985**, *144*, 157.
- [34] K. C. Waugh, M. Bowker, R. W. Petts, H. D. Vandervell, J. Omalley, *Appl. Catal.* **1986**, *25*, 121.
- [35] S. R. Blazzkowski, R. A. vanSanten, *J. Am. Chem. Soc.* **1996**, *118*, 5152.
- [36] A. Gervasini, J. Fenyvesi, A. Auroux, *Catal. Lett.* **1997**, *43*, 219.
- [37] M. I. Zaki, N. Sheppard, *J. Catal.* **1983**, *80*, 114.
- [38] D. Haffad, A. Chambellan, J. C. Lavalley, *J. Mol. Catal. A: Chem.* **2001**, *168*, 153.
- [39] D. Haffad, A. Chambellan, J. C. Lavalley, *J. Mol. Catal. A: Chem.* **2001**, *168*, 153.
- [40] M. L. Jia, H. F. Bai, Zhaorigetu, Y. N. Shen, Y. F. Li, *Journal of Rare Earths* **2008**, *26*, 528.

- [41] T. Ishida, N. Kinoshita, H. Okatsu, T. Akita, T. Takei, M. Haruta, *Angew. Chem., Int. Ed.* **2008**, *47*, 9265.
- [42] P. Haider, B. Kimmerle, F. Krumeich, W. Kleist, J. D. Grunwaldt, A. Baiker, *Catal. Lett.* **2008**, *125*, 169.
- [43] T. V. Choudhary, D. W. Goodman, *Top. Catal.* **2002**, *21*, 25.
- [44] R. Zanella, S. Giorgio, C. R. Henry, C. Louis, *J. Phys Chem. B* **2002**, *106*, 7634.
- [45] M. Mihaylov, H. Knozinger, K. Hadjiivanov, B. C. Gates, *Chem. Ing. Tech.* **2007**, *79*, 795.
- [46] P. A. Schaber, J. Colson, S. Higgins, D. Thielen, B. Anspach, J. Brauer, *Thermochim. Acta* **2004**, *424*, 131.
- [47] M. I. Zaki, G. A. M. Hussein, S. A. A. Mansour, H. M. Ismail, G. A. H. Mekhemer, *Colloids Surf., A* **1997**, *127*, 47.
- [48] A. C. Gluhoi, B. E. Nieuwenhuys, *Catal. Today* **2007**, *122*, 226.
- [49] H.-Y. Chang, H.-I. Chen, *J. Cryst. Growth* **2005**, *283*, 457.
- [50] A. Abad, A. Corma, H. Garcia, *Chem.-Eur. J.* **2008**, *14*, 212.
- [51] C. Padeste, N. W. Cant, D. L. Trimm, *Catal. Lett.* **1994**, *24*, 95.
- [52] C. H. Kim, L. T. Thompson, *J. Catal.* **2005**, *230*, 66.
- [53] A. S. Ivanova, B. L. Moroz, E. M. Moroz, Y. V. Larichev, E. A. Paukshtis, V. I. Bukhtiyarov, *J. Solid State Chem.* **2005**, *178*, 3265.
- [54] U. R. Pillai, S. Deevi, *Appl. Catal., A* **2006**, *299*, 266.
- [55] V. Matolin, M. Cabala, I. Matolinova, M. Skoda, J. Libra, M. Vaclavu, K. C. Prince, T. Skala, H. Yoshikawa, Y. Yamashita, S. Ueda, K. Kobayashi, *J. Phys. D: Appl. Phys.* **2009**, *42*, 115301.
- [56] N. B. Colthup, L. H. Dalay, S. E. Wiberley, **1990**.
- [57] S. D. f. O. C. SDBS, http://riodb01.ibase.aist.go.jp/sdbs/cgi-bin/cre_index.cgi?lang=eng.
- [58] D. Mitoraj, H. Kisch, *Chem.-Eur. J.* **2010**, *16*, 261.
- [59] M. A. Larrubia, G. Ramis, G. Busca, *Appl. Catal., B* **2000**, *27*, L145.
- [60] G. X. Li, K. Kaneko, S. Ozeki, *Langmuir* **1997**, *13*, 5894.
- [61] B. Solsona, T. Garcia, R. Murillo, A. M. Mastral, E. N. Ndifor, C. E. Hetrick, M. D. Amiridis, S. H. Taylor, *Top. Catal.* **2009**, *52*, 492.

- [62] A. Badri, C. Binet, J.-C. Lavalley, *J. Chem. Soc., Faraday Trans.* **1996**, 92, 4669.
- [63] M. Niwa, Y. Furukawa, Y. Murakami, *J. Colloid Interface Sci.* **1982**, 86, 260.
- [64] D. Mitoraj, H. Kisch, *Angew. Chem., Int. Ed.* **2008**, 47, 9975.
- [65] M. Sanchez-Sanchez, T. Blasco, *Catal. Today* **2009**, 143, 293.
- [66] C. Binet, M. Daturi, *Catal. Today* **2001**, 70, 155.
- [67] A. Badri, C. Binet, J. C. Lavalley, *J. Chem. Soc., Faraday Trans.* **1997**, 93, 1159.
- [68] C. Li, K. Domen, K. Maruya, T. Onishi, *J. Catal.* **1990**, 125, 445.
- [69] A. Abad, P. Concepcion, A. Corma, H. Garcia, *Angew. Chem., Int. Ed.* **2005**, 44, 4066.
- [70] R. Zhang, Y. H. Sun, S. Y. Peng, *Fuel* **2002**, 81, 1619.
- [71] A. Gazsi, T. Bansagi, F. Solymosi, *Catal. Lett.* **2009**, 131, 33.
- [72] C. Li, Y. Sakata, T. Arai, K. Domen, K. Maruya, T. Onishi, *J. Chem. Soc., Faraday Trans.* **1989**, 85, 929.
- [73] M. Manzoli, F. Boccuzzi, A. Chiorino, F. Vindigni, W. Deng, M. Flytzani-Stephanopoulos, *J. Catal.* **2007**, 245, 308.
- [74] T. Tabakova, F. B. Boccuzzi, M. Manzoli, D. Andreeva, *Appl. Catal., A* **2003**, 252, 385.
- [75] R. Singh, *Electrochemical and Partial oxidation of CH₄* **2008**, Dissertation (The Graduate Faculty at The University of Akron), 153.
- [76] M. I. Zaki, M. A. Hasan, L. Pasupulety, *Langmuir* **2001**, 17, 768.
- [77] J. Zawadzki, M. Wisniewski, J. Weber, O. Heintz, B. Azambre, *Carbon* **2001**, 39, 187.
- [78] M. I. Zaki, G. A. M. Hussein, S. A. A. Mansour, H. E. El-Ammawy, *J. Mol. Catal.* **1989**, 51, 209.
- [79] M. I. Zaki, G. A. M. Hussein, S. A. A. Mansour, H. M. Ismail, G. A. H. Mekhemer, *Coll. Surf. A*: **1997**, 127, 47.
- [80] C. Morterra, G. Cerrato, *Langmuir* **1990**, 6, 1810.

Chapter 7

Summary

The present dissertation includes the development and improvement of solid base catalysts and their application in liquid and gas phase reactions. The investigation of solid base catalysts is of great interest, as there are many processes in industry using base catalysis especially in the field of fine chemistry. The approach of including solid base materials for the generation of energy as an alternative to fossil fuels and decreasing the emission of greenhouse gasses i.e. CO₂ makes it an interesting objective material in the field of “green chemistry”. The use of mixed oxides derived from hydrotalcite precursors as solid base catalysts is well established; however there is still scope for development.

The influence of the Mg/Al ratio in mixed metal oxides on the acid/base properties described in the third chapter was investigated by infrared spectroscopy with adsorbed probe molecules, as pyridine, CO₂ and propan-2-ol. Further, the catalytic performance in the conversion of propan-2-ol which provides an additional test for acid-base properties of oxide catalysts was studied. Moreover, the influence on the catalytic properties by the calcination temperature and the sodium content has been investigated in detail.

High Mg/Al ratio causes high basicity, whereas the acidity decreased. Further on, sodium suppresses the dehydration reaction of propan-2-ol. However, a complete removal of sodium influences the dehydrogenation, thus, an optimal sodium content of HT4 was estimated to 1.2 wt.-%. Removing sodium during the synthesis procedure is more effective than the post synthesis via Soxhlet extraction. The optimal calcination temperature for HT4 is determined to 400 °C. Calcination at 600 °C increases the activity of the catalyst; however, the selectivity is decreased. Calcination of the commercial catalyst HT2 benefits reactivity and selectivity, an optimal calcination temperature was determined as 700 °C.

The sol-gel process is an effective synthesis method to obtain homogeneous mixed metal oxides. Special attention has to be given to factors as pH, hydrothermal treating, washing and calcination play an important role.

Chapter 4 reflects using the sol-gel process an useful method for synthesizing zinc modified Mg/Al mixed oxides. Alumina was successfully incorporated in the zinc and magnesium oxide lattice as additional tetrahedral alumina species appeared with increasing zinc content and no separate alumina phase was observed during XRD

analysis. Also the more diffuse lines related to MgO in the XRD patterns with increasing zinc content indicate an incorporation of Zn^{2+} into the MgO lattice.

A maximum of acidity was found for the sample with highest zinc-content whereas the strongest acid sites occurred for the catalyst with 46 wt.-% zinc. The strongest basic sites occurred for a zinc content of 49 wt.-%. This sample was also the most active one in dehydrogenation and dehydration. A further increase of the zinc content led to lower activity in the reaction of propan-2-ol, thus an optimum of Mg/Zn ratio, namely 1:2, was found. The higher the content of octahedral alumina species and the smaller the acid site concentration the higher the activity was. The selectivity for acetone formation was for all samples very high ($\geq 95\%$).

These results lead to the conclusion, that only small amounts of zinc in a homogeneous mixed metal ternary system are sufficient to create very highly selective dehydrogenation/basic catalysts. It is beneficial to add zinc as stabilizer, because catalyst deactivation due to coking is reduced with higher zinc contents. However, the formation of carbonates during storage remains a problem of creating stable solid base catalysts.

The activity in the reaction of 1,2-epoxy-octane with hexanol decreased with increasing acid site concentration of zinc modified Mg/Al mixed oxides. Thus, the ring-opening of 1,2-epoxy-octane with hexanol in the presence of oxide catalysts is more likely a base than acid catalyzed reaction. However, the selectivity to 1-(hexyloxy)octane-2-ol increased with increasing zinc content. Highest selectivity occurred for MgZnAl (1-2), which was also most active in dehydrogenation of propan-2-ol.

In chapter 5 the impact on basic properties by the modification of Mg/Al mixed oxides derived from LDH precursors with fluorine was established. The fluorination led to higher basicity (determined by conversion of propan-2-ol). The combination of high acid site concentration and base site strength benefits the dehydrogenation of propan-2-ol.

Depending on the precursor material, the modification of Mg/Al mixed oxides with fluorine turned out different influences on structure, surface areas and acid-base properties. A marked correlation between basic site strength and the activity of fluorinated catalysts for dehydrogenation was found. Also an influence of the Al-F bond polarization and the type of the Mg-F structure on the dehydration-dehydrogenation

activity was found. The optimal degree of fluorination was 14 to 18 wt.-% fluorine. The reaction of 1,2- epoxy octane with hexanol to 1-(hexyloxy)octane-2-ol decreased with decreasing medium basic site concentration. Thus, the ring-opening reaction of 1,2-epoxy-octane with hexanol in the presence of oxide catalysts is more likely a base than acid catalyzed reaction. This is supported by the results obtained with MgZnAl mixed oxide catalysts. In comparison of fluorine modified Mg/Al mixed oxides HT4 is the most appropriate catalyst system for the ring-opening reaction leading to the alkoxyated product with high activity.

The investigation of Au supported on ceria as a new type of basic catalysts was described in chapter 6. The high selectivity to dehydrogenation was induced for these novel basic catalysts by (i) Au and urea which destroy the Brønsted acidity and block the access to the Lewis acid sites of the supporting material, (ii) Au^+ acting as promoter for the hydride abstraction during dehydrogenation of the alcohol, (iii) Au suppressing the formation of carbonates from hydroxyl carbonates existing on ceria surface and (iv) new basic sites. Latter sites, i.e. NO-groups formed by decomposition of urea during the activation process afford one new route for dehydrogenation. As the rate of dehydrogenation increases with increasing concentration of Au and the direct dehydrogenation of propan-2-ol on the Au particles can be almost ruled out (negligible activity for catalyzing the reverse reaction), Au particles provide weak and extremely soft Lewis acid sites at the support metal interface facilitating so the acceptance of hydride ions and accelerating dehydrogenation. However, the formation of acetone over metallic Au catalyzed dehydrogenation can not be completely excluded. The interplay of selective poisoning and formation of new and weaker acid sites, leads to a highly tuneable basic system and new class of catalysts.

Deactivation of (modified) CeO_2 is, therefore, attributed to the presence of hydroxyl carbonates and at least moderately strong and relatively hard Ce^{4+} Lewis acid sites. Deactivation of ceria is also decreased, as carbonate formation is suppressed and strong Lewis acid sites are removed by adding urea and Au. However, this effect depends on the surface area of ceria, and is more pronounced for low surface area ceria.

Comparison of various ceria samples led to the conclusion that one ceria material is not equal to another one, even if the same stoichiometry is observed. Different

synthesis methods were tested and ceria samples with almost the same surface area ($45 \text{ m}^2 \cdot \text{g}^{-1}$) were obtained. However, the analysis of acid-base properties turned out different densities of acid and base sites. Also catalytic performances in the conversion of propan-2-ol resulted with different activities and selectivities. In general, the acid sites density was decreased, whereas the basic site density was increased by the modification with Au for all ceria materials.

The investigation of urea and NaOH as precipitation agent turned out that urea is more efficient regarding the Au-loading and dispersion. But using urea as deposition agent changes the oxide surface and opens new reaction pathways in catalysis may be not only in the conversion of propan-2-ol. Sodium sticks in the pores and therefore activity decreases. Nevertheless, the use of sodium increases the selectivity to acetone due to selective poisoning of acid sites. This was also observed in the Mg/Al mixed oxide catalyst system.

The work contributes the field of solid base materials in the production, development and investigation of solid base catalysts. The new materials catalyze dehydrogenation of secondary alcohols with high efficiency.

Curriculum Vitae

Manuela Bezen was born in Munich on August 11th, 1980. She visited the Gymnasium Bad Aibling until June 2001, when she graduated and received her Abitur (general qualification for university entrance). Afterwards she took up chemistry studies at the Technische Universität München, majoring in material science. In 2006, Manuela Bezen joined the group of Johannes Lercher (Chair for technical chemistry II) for her Diploma thesis entitled “Monometallic and bimetallic catalysts for the reductive amination of aldehydes”. After graduation as “Diplom-Chemiker” (master degree) in August 2006, she stayed in the group of Johannes Lercher as a PhD student at the Technische Universität München. Her work was focused on synthesis and characterization of solid base catalysts.

List of Publications

Kinetic investigations on the polymerization of 2-oxazolynes using pluritriplate initiators, (Publication), R. Luxenhofer, M.C.I. Bezen, R. Jordan, *Macromolecular Rapid Communications*, 29, **2008**, 1509

Mischmetalloxide und deren Verwendung als Katalysatoren für die Alkoxylierung, (Patent), M.C.I. Bezen, T.E. Müller, J.A. Lercher, H.-C. Raths, *Offenlegungsschrift EP09014032.8*. submitted to the European Patent Office on 10.11.2009

Selective modification of the acid-base properties of ceria by supported Au, M.C.I. Bezen, C. Bretkopf, N. El Kolli, J. M. Krafft, C. Louis, J.A. Lercher, submitted to *Chemistry - A European Journal*

Impact of fluoride modification on the acid - base properties of Mg/Al mixed oxides, M.C.I. Bezen, C. Bretkopf, J.A. Lercher, submitted to *Physical Chemistry Chemical Physics*

On the acid base properties of Zn-Mg-Al mixed oxides, M.C.I. Bezen, C. Bretkopf, J.A. Lercher, ready for submission

List of Presentations

Mono- and bimetallic noble metal clusters supported on multiwall carbon nanotubes and their application in the reductive amination of carbonyl compounds, (Oral presentation), A. Suppan, M.C.I. Bezen, T.E. Müller, J.A. Lercher, *40. Jahrestreffen Deutscher Katalytiker*, 2007, Weimar, Deutschland

Mono- and bimetallic metal clusters supported on multi-wall carbon nanotubes for the reductive amination of carbonyl compounds, (Poster presentation), A. Suppan, M.C.I. Bezen, T.E. Müller, A. Jentys, J.A. Lercher, *Europacat VIII*, 2007, Turko, Finnland

Solid base catalysts for the conversion of *iso*-propanol, (Poster presentation), M.C.I. Bezen, T.E. Müller, J.A. Lercher, *41. Jahrestreffen Deutscher Katalytiker*, 2008, Weimar, Deutschland

Synthesis and application of fluorinated hydrotalcites, (Poster presentation), M.C.I. Bezen, J.A. Lercher, *42. Jahrestreffen Deutscher Katalytiker*, 2008, Weimar, Deutschland

Au supported on ceria – A new basic catalyst, (Oral presentation), M.C.I. Bezen, N. El Kolli, C. Louis, C. Bretkopf, J.A. Lercher, *6th World Congress on Catalysis by Acids and Bases*, 2009, Genua, Italien

Au supported on ceria – A new basic catalyst, (Poster presentation), M.C.I. Bezen, N. El Kolli, C. Louis, C. Bretkopf, J.A. Lercher, *The 5th International Conference on Gold Science, Technology and its Applications*, 2009, Heidelberg, Deutschland